HIGH-SENSITIVITY DETECTION WITH TUNABLE DIODE LASERS

By

© DANIEL THOMAS CASSIDY, B.Eng., M.Sc.(Eng.)

A Thesis

Submitted to the School of Graduate Studies

in Partial Fulfilment of the Requirements

for the Degree

Doctor of Philosophy

McMaster University

October 1982

HIGH-SENSITIVITY DETECTION WITH TUNABLE DIODE LASERS

DOCTOR OF PHILOSOPHY (1982)
(Physics)

McMASTER UNIVERSITY
Hamilton, Ontario

TITLE: High-Sensitivity Detection with Tunable Diode Lasers

AUTHOR: Daniel Thomas Cassidy, B.Eng. (McMaster University)
M.Sc. (Queen's University at Kingston)

SUPERVISOR: Professor J. Reid

NUMBER OF PAGES: xxi, 156

ABSTRACT

This thesis describes methods for high-sensitivity detection of trace gases using tunable diode lasers (TDL). TDL absorption spectrometers have been widely used to acquire infrared spectra since 1970. However, high-sensitivity measurements have been limited mainly to the detection of low-pressure gases by harmonic techniques. The detection of atmospheric-pressure gases and the development of a rapid sweep technique for the accumulation of weak-absorption data over ~0.4 cm^{-1} spectral regions are emphasized in this thesis. The results of this work may be divided into four areas where major accomplishments have been realized.

Optical interference fringes generated by scattered light often limit the sensitivity of measurements performed with TDL spectrometers. The effect of fringes can be minimized by applying a jitter modulation. An investigation was undertaken to understand and quantify the effects of the jitter on the fringe and absorption signals. Simple analytic expressions describing the effects of the jitter modulation are derived and compared to experiment. Good agreement between theory and experiment is found.

The limiting noise sources of a TDL spectrometer were carefully investigated and identified. Detection methods insensitive to the noise were developed. Application of these methods leads to sensitivity limits equivalent to detecting an absorption of ~10^{-2}% for atmospheric-

pressure gases and $\sim 10^{-3}$% for low-pressure gases over path lengths $\leq$ 200 m. This represents a substantial improvement over previous work.

A rapid-sweep technique capable of detecting absorptions due to low-pressure gases of $\sim 10^{-3}$% over path lengths $\leq$ 200 m is described. Data accumulation by the rapid-sweep technique allows direct determinaton of line shapes and linewidths from the measurements.

An investigation of the TDL output power and frequency stabilitiy was performed as these laser characteristics directly affect the achievable sensitivity. The development of a new method to determine the TDL linewidth is reported. This technique permits the linewidth of any tunable laser to be quickly and easily measured.

Throughout this thesis, the sensitivity of the various detection techniques is demonstrated by the detection of pollutants and trace gases. Whenever applicable, techniques for further increasing the sensitivity are discussed.

ACKNOWLEDGEMENTS

I wish to express my appreciation to my supervisor, Dr. J. Reid, for his guidance and support in this work.

I wish also to thank the personnel at the Jet Propulsion Laboratory, California Institute of Technology, Pasadena, California, for providing the use of their facilities. The data for Fig. 4.5 and the heterodyne measurements reported in Chapter 6 were recorded at JPL.

TABLE OF CONTENTS

LIST OF FIGURES

LIST OF TABLES

CHAPTER 1

INTRODUCTION

1.1 Introduction

The study of infrared molecular spectra has long been an active and rewarding area of research as it leads to an understanding of many of the chemical and physical properties of the molecule under investigation. The geometric arrangement of nuclei and internuclei distances may be determined from measured vibrational and rotational frequencies. The existence of molecules previously unknown and the composition of planetary atmospheres, interstellar gas, comets, and stars can be deduced by comparing detailed laboratory spectra with spectra charcteristic of the system being studied. Line shapes and fine structure reveal the interactions of the molecule with its environment.

Advances in the resolution and sensitivity of recorded spectral data enhance the amount and quality of information on structure, interaction, and composition which can be gleaned from the system.

The advent of lead-salt diode lasers in 1964 [1] and the subsequent development of tertiary compounds which cover the 3- 30 μm region so rich in characteristic rotational and vibrational absorption lines has lead to significant advances in spectral resolution and sensitivity in the recording of infrared molecular spectra. The inherent lead-salt laser properties such as brightness, wavelength tunability, and large power spectral density give an infrared spectrometer based on lead-salt lasers significant advantages in achievable resolution and sensitivity

over grating and Fourier transform spectrometers. Tunable diode laser spectrometers have been widely used since the first demonstration of Doppler-limited spectra by Hinkley [2] in 1970.

For simple linear spectroscopy line broadening due to Doppler effects represents the ultimate resolution one can hope to attain. This ultimate resolution is, in general, easily achieved with a tunable diode laser spectrometer. However, the ultimate sensitivity of a tunable diode laser spectrometer is still an area of much interest. High sensitivity is desired to enable detection of weak signals in short time intervals. Potential areas of application include: studies of molecular ions [3], free radicals [4], and chemical reactions [5]; pollution monitoring, both remote and in situ, and trace gas detection [6].

High-sensitivity, high-resolution spectroscopy is used to probe the dynamics of chemical reactions [5]. Photons prepare reactants in specific quantum states and identify intermediates and reaction products. Ion-molecule reactions [3] dominate the chemistry of the upper atmospheres of planets, interstellar gas, and plasmas. Comprehension of the dynamics of these reactions requires the knowledge of the shape and electronic states of the reactants and products. High-sensitivity spectroscopy is needed to detect minute quantities on a fast time scale.

An immediate and practical application of high-sensitivity spectroscopy is the detection and monitoring of atmospheric trace gases and pollutants. Atmospheric constituents can be identified by their absorption-emission spectra, while the concentration may be determined from the strength of the spectroscopic signature. In most circumstances the concentration of the gases is small, thus high sensitivity is

required.

In view of the potential applications of infrared high-sensitivity spectroscopy it seems appropriate to study the sensitivities which can be attained. This thesis is concerned with the development of methods for high-sensitivity detection of trace gases using tunable diode lasers and resonance absorption.

Many optical techniques exist for the recording of infrared spectra, but because the cross section for infrared resonance absorption can be many orders of magnitude larger than for Raman scattering or infrared resonance fluorescence, resonance absorption is considered the most sensitive optical technique [7,8]. Resonance absorption occurs when the frequency of the electromagnetic radiation probe beam coincides with a characteristic absorption of the species under investigation.

Lead-salt lasers provide a versatile source of tunable, spectrally pure, infrared radiation with which to probe molecules. The lasers can be manufactured to operate anywhere in the 3 - 30 μm "finger print" region, may be tuned to be resonant with absorption lines by changing the operating conditions, and give output powers of ~0.5 mW in modes which are substantially narrower than the room temperature Doppler linewidth of a molecular gas.

1.2 Comparison of Techniques

There are many techniques and configurations for the recording of infrared spectra, among which are resonance absorption, resonance fluorescence, Raman scattering, optoacoustic effect, Stark and laser magnetic resonance. The first three techniques listed can be applied to

in situ measurements, while the last three techniques require specialised cells and conditions.

Resonance fluorescence is potentially a very sensitive technique. Single atoms are detected by applying resonance fluorescence detection in the visible and ultraviolet regions of the spectrum [9,10]. Due to the enhanced spontaneous lifetime of the excited state at longer wavelengths, collisional quenching dramatically reduces the fluorescent yield. Detection by infrared fluorescence is less sensitive by several orders of magnitude than detection by fluorescence from electronic transitions of atoms and molecules [7]. The cross section for Raman scattering is typically smaller than the cross section for quenched fluorescence [11] and hence detection by Raman scattering is usually inferior in sensitivity.

Optoacoustic techniques are used to measure line centre absorption coefficients as small as 10^{-8} m^{-1} [12]. Detection is performed in a special cell fitted with microphones. Photons resonant with a transition excite the molecule into vibrational states. The vibrational motion is quenched by collisions creating a pressure wave which is sensed by the microphones. For a fixed number of absorbing molecules in the cell, the optoacoustic signal is independent of pressure for pressures above 15 Torr and decreases rapidly for pressures below 15 Torr [12].

Stark [13] and laser magnetic resonance spectroscopy [14], although very sensitive (detection of absorption coefficients of ~3 x 10^{-9} m^{-1}), are limited in applicability. These techniques use strong, external electromagnetic fields to tune the transition into resonance with a fixed frequency CO_2 or N_2O laser. The molecules to be studied

must possess dipole moments or be paramagnetic and have transition frequencies within about 1% of the laser frequency. Since the Stark, laser magnetic resonance, and optoacoustic techniques require the gas to be in specialized containers they can not be applied to in situ measurements.

Infrared resonance absorption techniques may be applied successfully to the high-sensitivity spectroscopy of many molecules. Measurements can be performed in situ over path lengths through the open atmosphere or in specialized cells in laboratory environments. With tunable lead-salt diode lasers as the source of energy, any transition in the 3 - 30 μm region can be investigated. Although the detection methods described in Sec. 1.2 have advantages in specific cases, they do not compare in versatility with resonance absorption techniques employing tunable lead-salt diode lasers.

1.3 Scope of this Thesis

The material covered in this thesis deals with the development of methods for high-sensitivity detection of trace gases using lead-salt diode lasers and resonance absorption. Emphasis has been placed on two aspects of the detection process -- atmospheric pressure detection and the development of a rapid-sweep technique for the fast acquisition of absorption data over a ~0.4 cm^{-1} spectral region. To achieve high sensitivity we investigated in detail the noise sources of a tunable diode laser spectrometer and implemented detection schemes which exhibit immunity to the experimental noise. We also analysed the harmonic response of the system to optical fringes and two-tone modulation. The mathematical analysis provides insight into the effects of optical

fringe noise and the minimization of this noise. The mathematical analysis is contained in Chapter 3 while the atmospheric pressure work is discussed in Chapter 4 and the rapid-scan technique in Chapter 5. The contents of the chapters are summarized in greater detail in Sec. 1.4.

This thesis emphasizes the development of methods for high-sensitivity detection with tunable diode lasers. To illustrate the sensitivity we applied the techniques to the detection of atmospheric pollutants and trace gases.

1.4 Outline of this Thesis

Chapter 2 is intended to familiarize the reader with the acquisition of resonance absorption data using tunable diode lasers. The operating characteristics of tunable diode lasers are reviewed in the first section of Chapter 2. Since the determination of pollutants and trace gases is an important and practical application of resonance absorption spectroscopy, the connection between the strength of an absorption and the concentration of absorbing molecules is made in Sec. 2.2. Harmonic detection techniques are used in conjunction with tunable diode lasers to improve sensitivity. The connection linking the harmonic signal and the transmission is not obvious, thus the relationship between the harmonic signal and absorption is developed in the latter sections of Chapter 2. Measurements by harmonic techniques are reported extensively in Chapters 3, 4 and 5.

The minimum absorption detectable by a tunable diode laser spectrometer utilising harmonic methods is often limited by interference

fringes generated by scattered light. The sensitivity of the spectrometer to absorption can be increased by applying a second, or jitter modulation. In Chapter 3 the theory of harmonic response for single- and two-tone modulation over optical fringes and Lorentzian absorption lines is developed and compared to experimental measurements. A simple analytical expression for the two-tone harmonic line shape is derived. The expression provides a physical understanding of the effects of the second modulation and a means to unravel the effects of the second modulation on the linewidth and line shape. It is found that for a specific choice of the jitter frequency and phase it is possible to simultaneously minimize the fringe signal and increase the harmonic absorption signal.

Tunable diode laser spectrometers are extensively used for the monitoring of trace gases in the atmosphere. In many of these instruments the gas to be sampled flows at reduced pressure through a multipass optical cell, and detection is carried out by observing infrared resonant absorption lines. Low-pressure absorption lines can be detected with very high sensitivity using second harmonic techniques; Reid et al. [15] reported the detection of absorptions as small as 10^{-3}% over path lengths of 40 m in multipass cells. However, for many applications it is advantageous to monitor gases in situ, i.e., through open-path configurations at atmospheric pressure. This is a more difficult problem as one must contend with much broader and possibly overlapping absorption lines, interferences from other molecular species, and perturbations due to the turbulent atmosphere. As a result the sensitivities achieved with open-path monitors have been

significantly less than the sensitivities reported for low-pressure monitors. Ku et al. [16] reported a noise level equivalent to a 0.7% absorption in the first demonstration of open-path atmospheric monitoring employing tunable diode lasers, and there have been no major improvements in sensitivities in recent years [17,18]. Chapter 4 reports on high-sensitivity measurements of trace gases at atmospheric pressure.

We identified the factors which limit the sensitivity of tunable diode laser open-path monitors. At present our sensitivity limit corresponds to an optical absorption of 0.01% over path lengths as long as 250 m. This sensitivity is a substantial improvement over previous work performed at atmospheric pressure. In Chapter 4 we describe the phenomena which limit the achievable sensitivity, discuss techniques which lead to better sensitivity, and suggest some system improvements.

A rapid-scan technique for the detection of small absorptions over wide spectral regions is the principal subject of Chapter 5. Jennings [19] described a measurement technique which he called sweep integration. Jennings was able to detect absorptions as small as 2.5 x 10^{-2}% over path lengths of 10 cm using the sweep integration method. We modified his sweep integration technique to enable the detection of absorptions as small as 10^{-3}% over path lengths up to 200 m long. This new method, sweep integration using presubtraction, is discussed in Chapter 5. Direct determinations of the absorption line shape and linewidth, and rapid searches over ~0.4 cm^{-1} spectral regions are possible using the sweep integration technique.

The sensitivities which can be attained with tunable diode laser absorption spectrometers are influenced by the properties of the laser.

The properties of a lead-salt laser such as linewidth and output power are affected by the external environment. Chapter 6 examines the laser linewidth and output power stability as a function of the operation of a closed-cycle cooler. The cooler maintains the cryogenic temperatures necessary for the continuous-wave operation of the lead-salt lasers. A method of determining the linewidth of any tunable laser is presented in this chapter. Using the method reported the linewidth can be determined with only an etalon and rms voltmeter. A rapid and easy determination of the laser linewidth is important since the linewidth of lead-salt lasers varies dramatically from device to device and with operating temperature and current. Intensity fluctuations or noise on the laser beam due to the closed-cycle cooler is also investigated in Chapter 6. The magnitude of the laser beam noise has a direct bearing on the sensitivity which can be achieved.

The contents of Chapters 3-6 are summarized in publications by Cassidy and Reid [20-23] and Reid, Cassidy, and Menzies [24].

Chapter 7 summarizes the important contributions of this work to the field of high-sensitivity detection with tunable diode lasers and lists recommendations for the improved performance of tunable diode laser spectrometers employing resonance absorption.

CHAPTER 2

MEASUREMENTS WITH TUNABLE DIODE LASERS

2.1 Introduction

The purpose of this chapter is to familiarize the reader with some of the equipment and techniques used to perform the measurements reported in this thesis. Section 2.2 is concerned with the basic properties of lead-salt lasers. Section 2.3 contains a practical example indicating how measured absorptions are related to the concentration of absorbing molecules in the beam. Harmonic detection is often used to enhance the detectivity of weak signals. The connection between the harmonic signal and the transmission is not obvious. The material of Sec. 2.4 provides the link between the observed transmission and the harmonic signal. An important quantity -- the background signal -- is defined in Sec. 2.4. An analytic expression for the harmonic line shape and several graphs of harmonic line shapes calculated using this expression are presented in Sec. 2.5. Familiarity with the various harmonic line shapes is assumed in the following chapters. The expression for the harmonic line shape is treated in more detail in Chapter 3 and Appendix A where the theory of harmonic line shapes is extended to cover two-frequency modulation. Section 2.6 is a brief summary of the material covered in Chapter 2.

2.2 Lead-Salt Diode Lasers

Diode lasers are fabricated by forming a p-n junction in a

semiconductor crystal and then cleaving the crystal into small, reactangular parallelepipeds. Under forward bias the diode emits broadband spontaneous emission centred about a wavelength determined by the energy of the bandgap. Lasing occurs at wavelengths λ_q which satisfy the Fabry-Perot condition

$$q\lambda_q = 2nL \tag{1}$$

and for which net optical gain exists. In Eq. (1) n is the refractive index of the chip, L is the length of the chip and q is an integer. Single-mode lasing occurs when only one of the resonant wavelengths λ_q falls within the spontaneous emission curve and experiences net gain[a]. Conversely, multimode operation happens when more than one wavelength experiences gain. Mode hops occur when, under an external influence, the lasing wavelength shifts discontinuously from λ_q to λ_r where r is some integer not equal to q. For ease of interpretation of absorption data it is preferable to operate the laser in a single mode far from mode hops.

For the lead-salt family of semiconductor compounds the band gap energy is an almost linear function of the mole fraction x [26]. Members of the lead-salt family include $Pb_{1-x}Sn_xTe$, $Pb_{1-x}Sn_xSe$, $PbS_{1-x}Se_x$, and $Pb_{1-x}Cd_x$ S. The choice of compound and mole fraction dictate in which part of the spectral region between 3 and 30 μm the laser will operate [26-28]. The optical frequency of the lead-salt

---

[a] It is generally accepted that semiconductor lasers are homogeneously broadened spectrally. However, since the holes and electrons are distributed over a range of energies within their respective bands there will be a limit imposed by relaxation mechanisms on how much energy can be extracted at a fixed photon energy. If the excitation level exceeds this limit then other modes will experience net gain [25].

laser can be tuned during operation by varying any of the parameters on which the band gap energy or refractive index depend. Of the three tuning methods, thermal [27,28], magnetic [29,30], and pressure [31-33], thermal tuning is by far the easiest to implement. The band gap energy of the lead-salt compound, and hence the frequency of emission, is tunable ~ 50-200 cm^{-1} by varying the temperature of operation from 10 K to ~ 70 K. The maximum operating temperature of the laser determines the overall tuning range. The maximum operating temperature is thought to depend on material purity, carrier concentration, minority carrier mobility, and the p-n junction profile, but the effects are not well understood [28].

The lead-salt laser tunes quasi-continuously as the temperature is varied. Usually there is continuous coverage of spectra regions of ~1 cm^{-1} followed by a mode hop and a discontinuous jump in the laser frequency of a similar magnitude [26]. Coarse tuning of the laser frequency is performed by selecting the heat sink temperature. Fine tuning of the optical frequency is accomplished by controlling the injection current. Varying the injection current changes the amount of joule heating across the junction and hence the temperature of the p-n junction. For small temperature changes, the dominant effect is a change in the refractive index of the semiconductor crystal [26-28]. From Eq. (1) it can be seen that a change in the index of refraction changes the resonant frequency of the optical cavity and hence tunes the laser frequency.

The tunable diode lasers used for the work reported in this thesis are commercially available lead-salt lasers [34,28]. These

lasers typically operate single mode for currents < 10-20% above threshold, give output powers < 1mW, possess linewidths of the order of 5 MHz, and operate in the temperature range 10 to 70 K. Representative tuning rates of the optical frequency for changes in the operating temperature and injection current are 70 MHz/mK and 300 MHz/mA.

The lasers are mounted on a copper heat sink, enclosed in a vacuum jacket, and kept at cryogenic temperatures by a closed-cycle He refrigerator. The temperature of the lasers is controlled to within 10^{-3} K (over time periods of seconds) by a closed loop temperature sensor-stabilizer. The injection current is supplied by a stable DC power supply. This ancillary equipment was also obtained from the laser manufacturer [34]. Figure 2.1 is a photograph of the laser cold head, refrigeration system, temperature and current control units, and the detection electronics.

Recently there has been interest in improving the operating characteristics of lead-salt lasers. Studies indicate that magnetic and pressure tuning offer the possibility of almost complete spectral coverage of regions hundreds of cm^{-1} large [29,30,32,33]. Distributed feedback structures which possess single-mode, continuous, temperature tuning over regions of 20 cm^{-1} [35,36] and the properties of diffused homojunction lasers with temperature tuning over a 300 cm^{-1} range [37] have been reported. Improvements in the operation of lead-salt lasers will increase the number of applications for the lasers.

2.3 Concentration Measurements

In this section the operation of a tunable diode laser spectro-

Figure 2.1

Photograph of the laser support equipment and detection electronics. Components which are identified are:

a - cold head

b - compressor

c - temperature sensor - stabilizer

d - laser power supply

e - oscilloscope

f - lock-in amplifier

g - X-Y recorder.

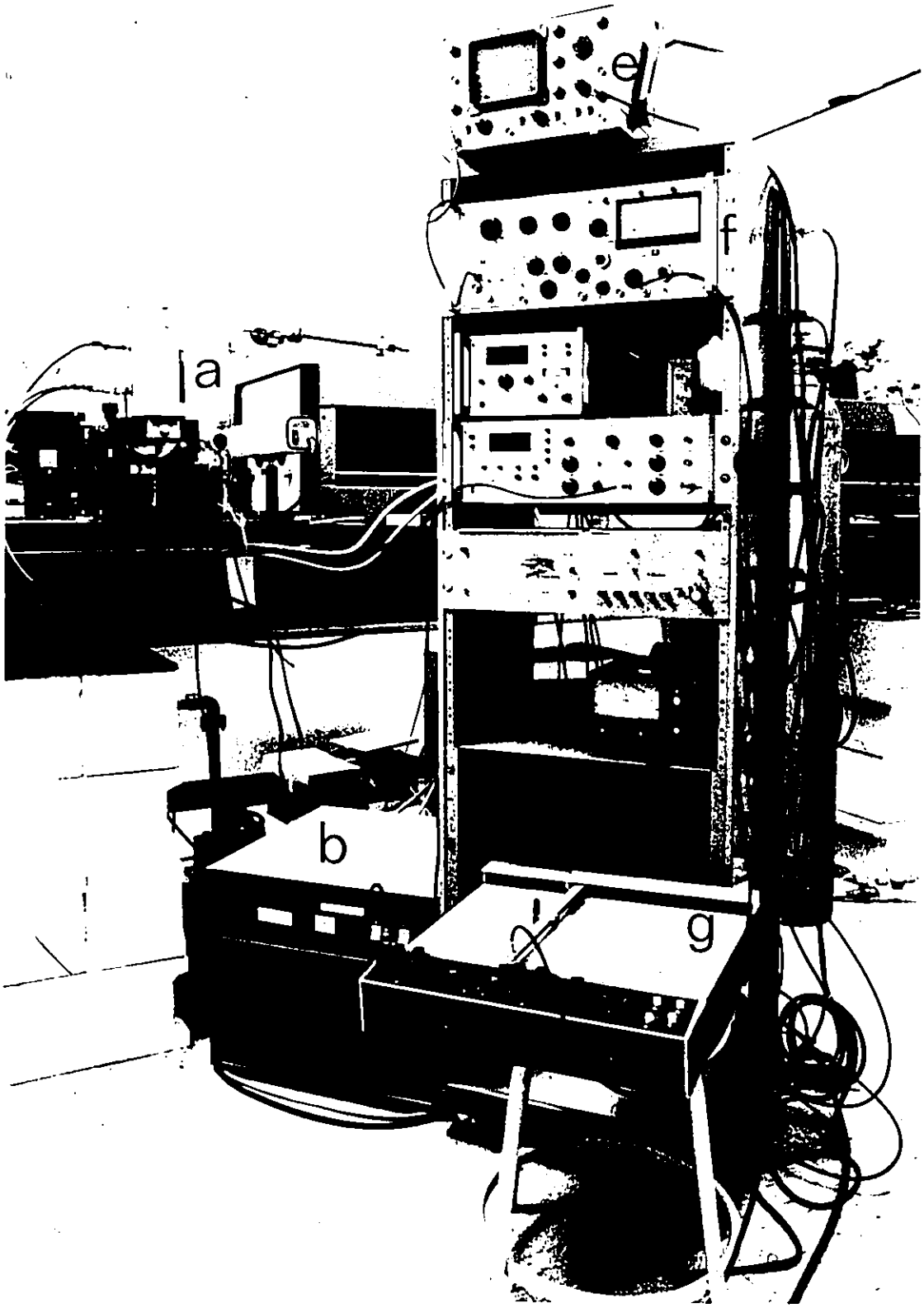
a
b
e
f
g

meter is illustrated. Many applications of a tunable diode laser require the measurement of trace gas concentrations. The gas concentration can be related to the measured transmission in a straightforward manner.

The transmission $T(\nu)$ at an optical frequency ν in the vicinity of an isolated resonant transition centred at ν_o may be expressed as

$$T(\nu) = \exp[-\alpha(\nu)\ell] \tag{2}$$

where the extinction or absorption coefficient $\alpha(\nu)$ equals

$$\alpha(\nu) = CS^o pL(\nu,\nu_o,\Delta\nu) \tag{3}$$

and

C is the average concentration of molecules over the path length ℓ

p is the pressure of the gas (total pressure)

S^o is the line strength [38]

$L(\nu,\nu_o,\Delta\nu)$ is the line shape function

ν_o is the line centre frequency and

$\Delta\nu$ is the linewidth[a].

In the limit of negligible collisional broadening $L(\nu,\nu_o,\Delta\nu)$ is a Gaussian [38] while for collision broadened lines $L(\nu,\nu_o,\Delta\nu)$ is a Lorentzian [38], vis.

$$L(\nu,\nu_o,\Delta\nu) = \frac{1}{\pi}\left[\frac{\Delta\nu}{(\nu-\nu_o)^2 + \Delta\nu^2}\right] . \tag{4}$$

For a specified line centre transmission $T(0)$, the concentration of molecules may be determined by inverting Eq.(2). Explicitly,

---

[a] In the event it is necessary to distinguish the linewidths in terms of the broadening mechanisms, a subscript L will be added to indicate the collision braodened width and a subscript D to indicate the Doppler broadened width. Unless otherwise explicitly stated, we take linewidth to mean linewidth half-width half-maximum.

Figure 2.2

Plot of normalized line centre absorption coefficient versus the scaled pressure a. The line centre absorption coefficient is normalized to unity for a pure Lorentzian absorption. The pressure p is given in terms of the parameter a. For an N_2O transition at 1140 cm^{-1} and temperature T = 300 K, p = 12a Torr. The Doppler linewidth is a function of the absolute temperature T, the mass M of the molecule in amu, and the optical frequency ν of the transition as indicated on the figure.

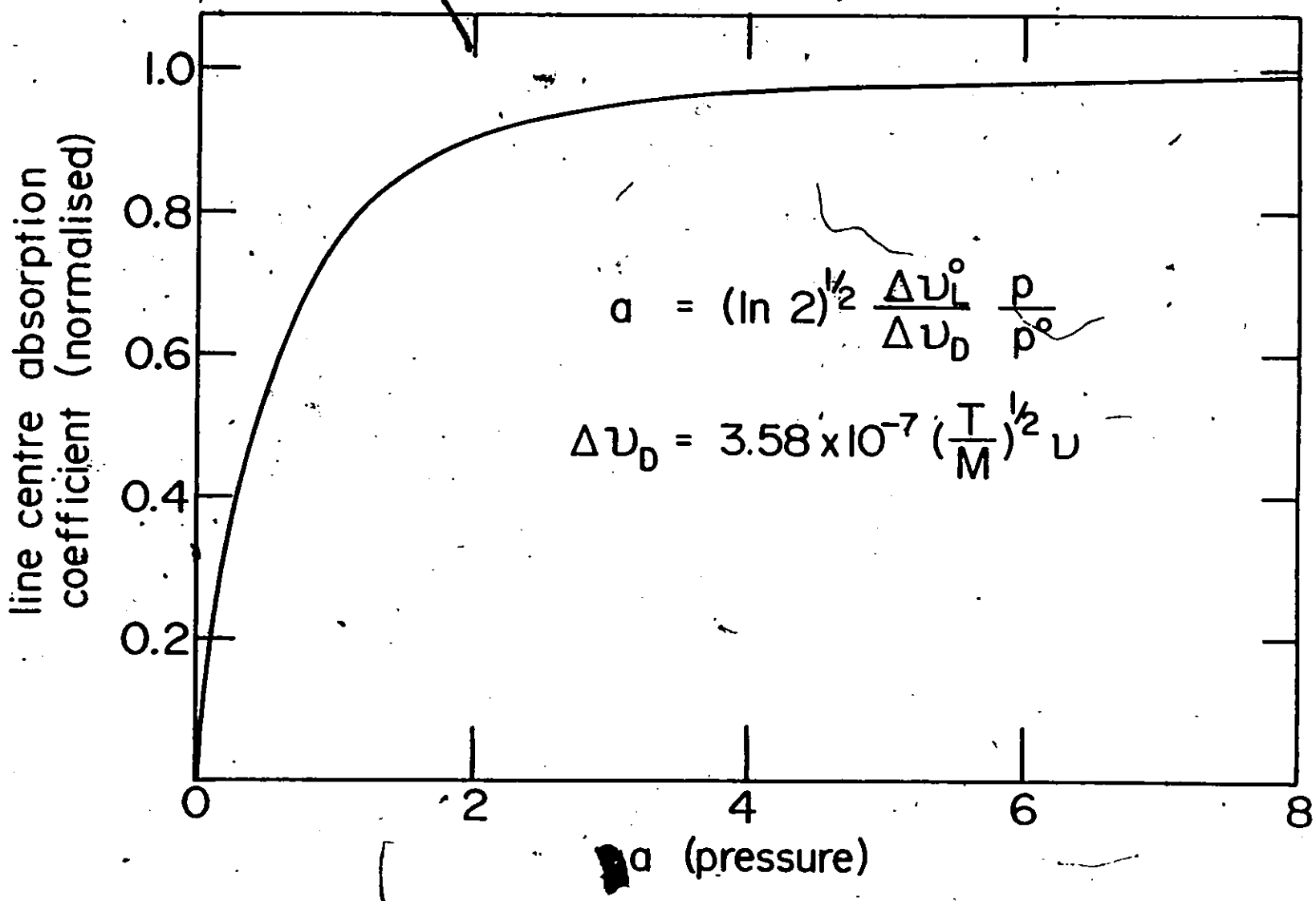
line centre absorption coefficient (normalised)
1.0
0.8
0.6
0.4
0.2
0
2
4
6
8
a (pressure)
$a = (\ln 2)^{1/2} \frac{\Delta\upsilon_L^o}{\Delta\upsilon_D} \frac{p}{p^o}$
$\Delta\upsilon_D = 3.58 \times 10^{-7} \left(\frac{T}{M}\right)^{1/2} \upsilon$

$$C = -\frac{\pi\,\Delta\nu\,\ln[T(0)]}{S^{o}\ell p}\,. \tag{5}$$

A numerical value for the concentration C can be computed once the spectroscopic constants are known. Thus to determine the concentration of molecules one need only measure the line centre absorption. In deriving Eq. (5) we have assumed a Lorentzian absorption profile.

The assumption of a Lorentzian absorption profile is one that shall be made frequently through this work. For high-sensitivity detection of trace gases the quantity of interest is the magnitude of the line centre absorption 1-T(0). Figure 2.2 is a plot of the calculated line centre absorption coefficient as a function of the scaled pressure a [39]. The parameter a is related to the pressure p of the absorbing gas by the ratio of the Lorentz linewidth $\Delta\nu_L$ to the Doppler linewidth $\Delta\nu_D$ as shown below:

$$a = (\ln 2)^{1/2}\,\frac{\Delta\nu_L^{o}}{\Delta\nu_D}\,\frac{p}{p^{o}}\,. \tag{6}$$

$\Delta\nu_L^{o}$ is the Lorentz linewidth measured at a reference pressure p^{o}. The absorption coefficient, plotted as a function of pressure in Fig. 2.2, is normalised to unity for a pure Lorentzian absorption profile.

There are at least two advantages to using a Lorentzian line shape. First, for pressures greater than a ≈ 3, the line centre absorption is close to its maximum value and approximately independent of pressure. In the pressure broadened regime (a > 3) the line centre absorption coefficient is $CS^{o}p^{o}/\pi\Delta\nu_L^{o}$ for all pressures. Second, an <u>analytic</u> expression for the harmonic line shape can be derived for modulating over Lorentzian lines. The closed-form, analytic expression for the harmonic line shape reveals the dependence of the harmonic signal on the

line shape parameters much easier than nonanalytic expressions. This fact makes analysis of any data recorded by harmonic techniques easier to interpret.

If, in an experiment, one has control of the pressure, then to achieve maximum absorption and sensitivity, the pressure should be picked based on Fig. 2.2. On the other hand, at atmospheric pressure, the lines are Lorentzian in shape. Consequently, for high-sensitivity detection the feature of interest is Lorentzian absorptions for almost all applications. Thus there is little loss in generality by emphasizing Lorentzian absorptions. If required, the line centre absorption coefficient for Voigt and Doppler profiles can be calculated using Fig. 2.2.

In the limit of small absorption,

$$C \approx \frac{\pi \, \Delta\nu_L^o}{S^o \ell p^o} [1 - T(0)][1 - (\frac{1 - T(0)}{2}) + \ldots] \qquad (7)$$

and the concentration is linearly proportional to the absorption, neglecting terms of order $[1 - T(0)]^2$.

Figure 2.3 illustrates the mechanics of determining the average concentration of gas molecules along the path from an experimental measurement of transmission. To record the transmission as shown in Fig. 2.3, the laser heat sink temperature was adjusted so that the laser operated single mode in the vicinity of an absorption line, and the current was slowly ramped. The output of the laser was collected by a lens and directed through a cell of known length containing the absorbing gas and then onto a HgCdTe photoconductive detector. A

Figure 2.3

Determination of the transmission from a direct detection scan.

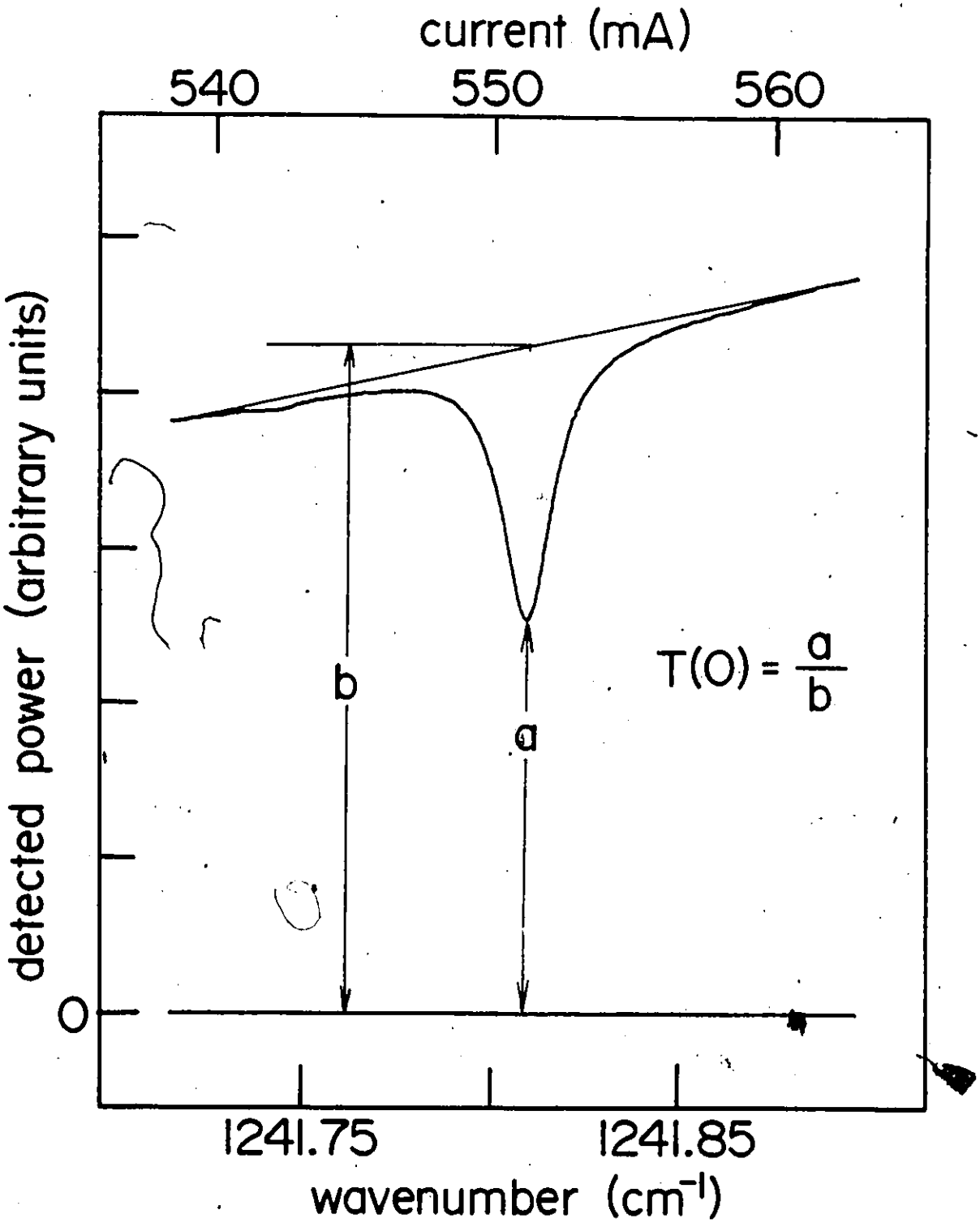
current (mA)
540
550
560
detected power (arbitrary units)
0
b
a
T(0) = a/b
1241.75
1241.85
wavenumber (cm⁻¹)

mechanical chopper was used to periodically interrupt the beam to establish the zero transmission level and provide an ac signal for the ac coupled detector. The detector output was processed by a lock-in amplifier and the detected power displayed along the ordinate and the current supplied to the laser along the abscissa of an X-Y recorder. A calibration scan with a Ge etalon in the beam was used to convert the current scale into a relative frequency scale. We refer to scans made in this manner as direct detection. Fig. 2.4 is a schematic diagram of the apparatus and Fig. 2.5 is a photograph of the optical table. Single-mode operation of the laser and the lasing wavelength are determined by placing a 0.5 m monochromator in the beam. The spectroscopic constants needed to determine the concentration of molecules in the cell may be looked up in the literature or experimentally measured.

Strongly absorbing molecules such as H_2O, CO_2, NH_3 absorb ~5 x 10^{-3}% of the incident power per ppb per metre of path length. For laboratory measurements, path lengths of ~100 m using multipass (White) cells [40-42] are easily attained. The far-field pattern of the tunable diode lasers employed in this study limits retroreflector based measurements to path lengths < 1 km. Thus to detect trace amounts (~1 ppb) of weakly absorbing molecules it is necessary to be able to detect absorptions of the order of 10^{-3}%. With direct detection technology it is very difficult to detect absorptions of such a small magnitude. With direct detection the absorptions are displayed on a large, sloping baseline and the detection scheme is very vulnerable to any type of power fluctuation on the laser beam. Reid et al. [43] have shown that a

Figure 2.4

Schematic diagram of the apparatus used to record direct detection scans.

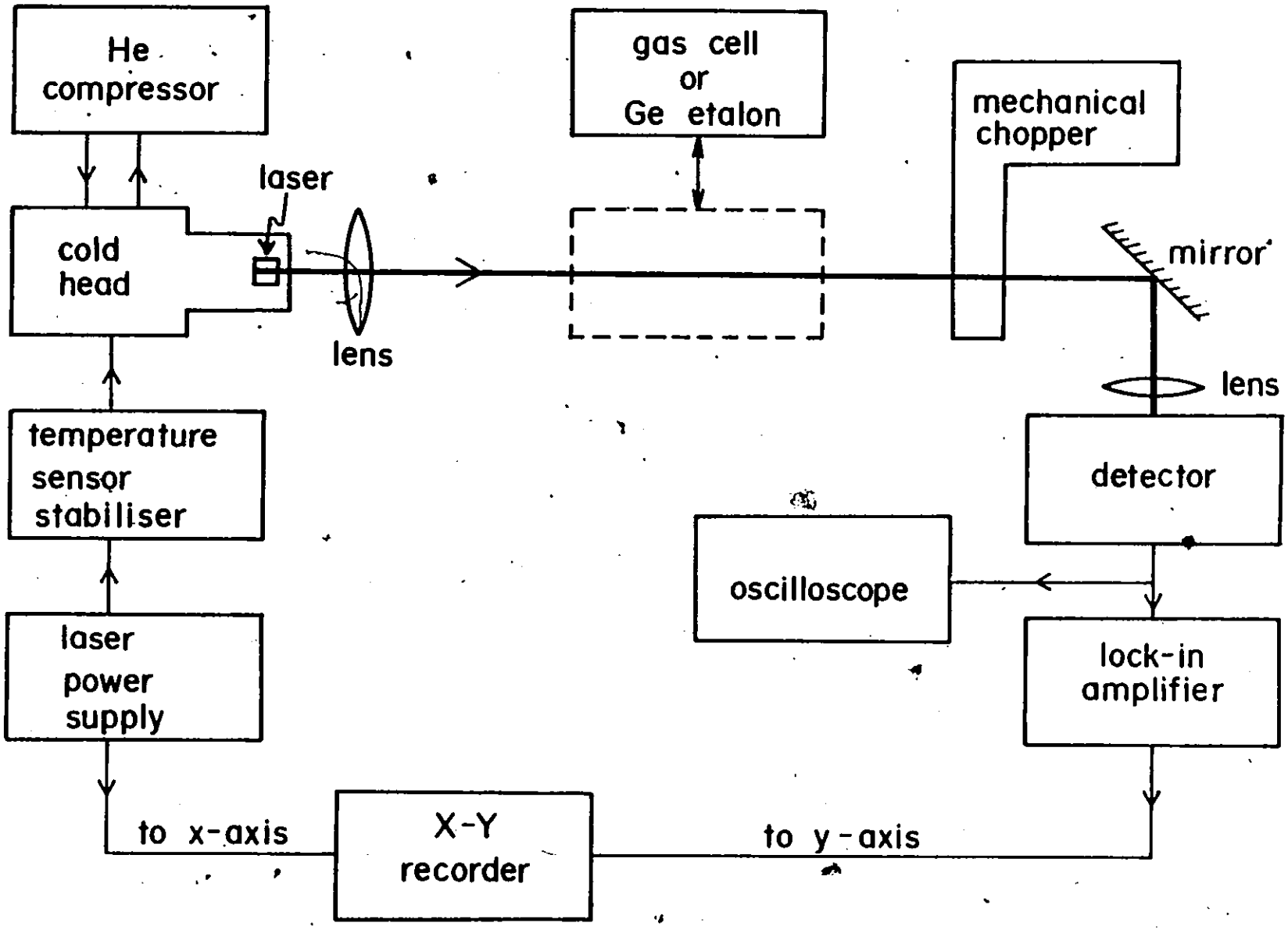
He compressor
cold head
laser
lens
gas cell or Ge etalon
mechanical chopper
mirror
lens
detector
temperature sensor stabiliser
oscilloscope
laser power supply
lock-in amplifier
to x-axis
X-Y recorder
to y-axis

2cb

Figure 2.5

Photograph of the optical table. Elements which are identified are:

a - cold head

b - lens

c - gas cell

d - etalon

e - mechanical chopper

f - mirror

g - detector.

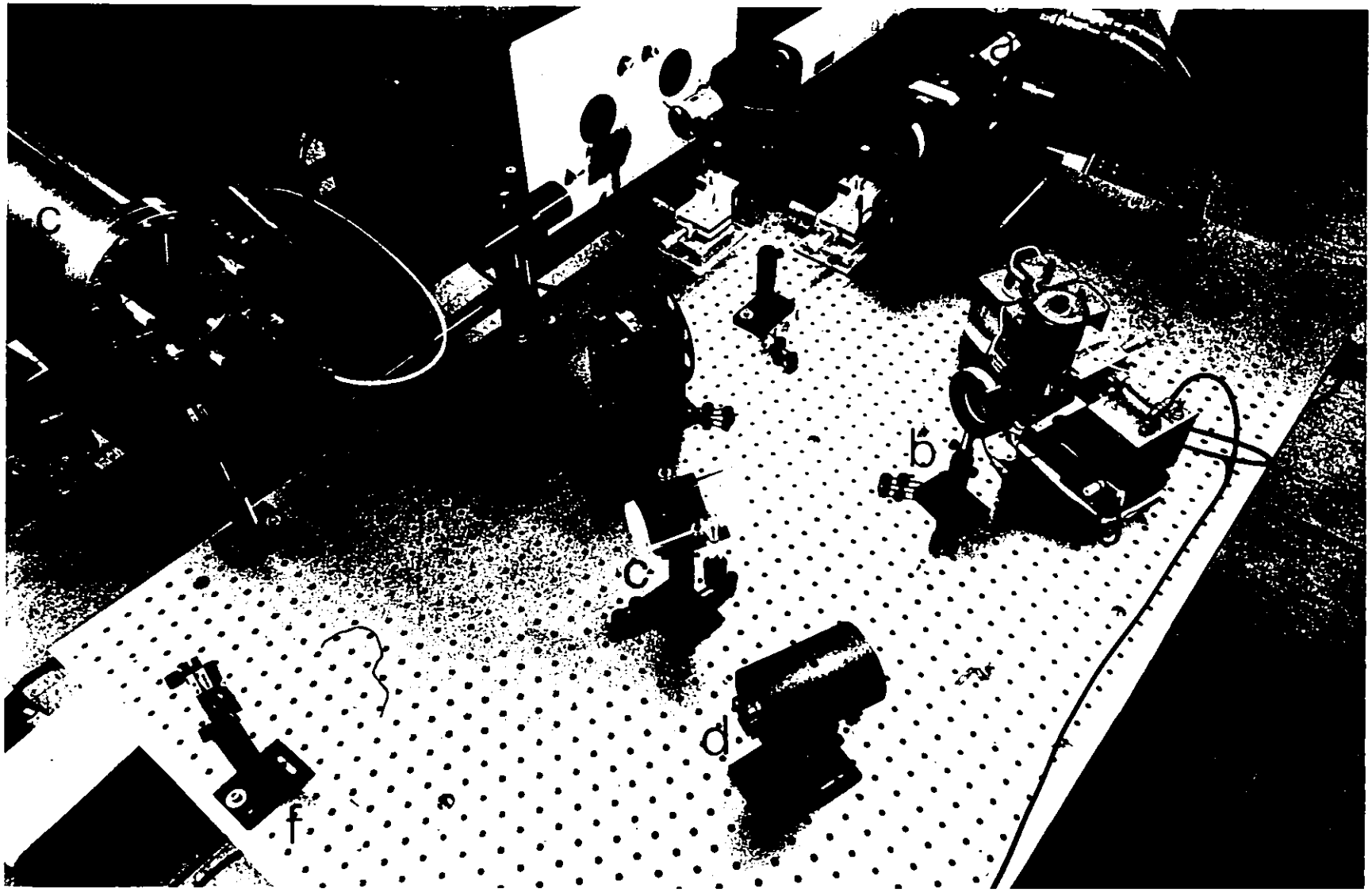
c
b
c
d
f

significant improvement in the signal-to-noise ratio is possible by employing harmonic detection. Harmonic detection is considered in Sec. 2.4.

2.4 Harmonic Detection

If one considers sinusoidally modulating the optical frequency ν of the laser (by modulating the injection current) at an audio frequency ω, such that

$$\nu = \bar{\nu} + M\cos \omega t \tag{8}$$

then the transmission $T(\nu)$ can be expanded in a Taylor series about the steady state optical frequency $\bar{\nu}$. t is the time and M is the depth of (optical) frequency modulation. Expressed as a power series the transmission is

$$T(\nu) = 1 - \alpha(\bar{\nu})\ell + M\alpha'\cos\omega t + \frac{M^2}{4}\alpha''(1 + \cos 2\omega t) \tag{9}$$

where

$$\alpha' = CS^{o}p\ell\, L'$$

$$\alpha'' = CS^{o}p\ell\, L''$$

and in the spirit of detecting small absorptions terms of order $[1 - T(\nu)]^2$ have been ignored. L' is the first derivative of $L(\nu, \nu_o, \Delta\nu)$ with respect to ν evaluated at $\nu = \bar{\nu}$ and L" is the second derivative. By detecting at the nth harmonic of the modulating frequency ω, the amplitude of the signal is proportional to the product of the concentration of molecules times the nth derivative of the line shape. Provided that the depth of wavelength modulation M is $\lesssim 0.1\ \Delta\nu$, then the demodulated signal is an accurate representation of the derivative [44].

A very substantial increase in harmonic signal may be obtained by increasing the depth of modulation M until M is of the order of several $\Delta\nu$. Under this operating condition the Taylor series expansion is invalid. Although the series expansion is invalid, the harmonic line shapes look similar to the derivatives and it is convenient to still think in terms of derivative line shapes. Arndt [45] and Walquist [46] derived analytic expressions for the harmonic line shapes obtained by modulating over Lorentzian absorption profiles. Reid and Labrie [47] compared the theory to experimental measurements of second harmonic detection of absorption lines. Excellent agreement was observed.

The relationship between the observed transmission and the second harmonic signal is shown in Fig. 2.6. The upper trace was recorded using direct detection methods. To record the lower trace the chopper was removed and the optical frequency modulated as described by Eq. (8) by applying a sinusoidal ripple to the injection current. A lock-in amplifier, referenced to the second harmonic of the modulating frequency, was used to process the detector output. We refer to scans made in this fashion as harmonic detection. Note that the second harmonic absorption signal is similar to the second derivative of the transmission. The second harmonic signal is a maximum at line centre, passes through zero near the inflection points of the Lorentzian absorption, and tends to zero far from line centre.

In practice the normalised transmission $T(\nu)$ is not measured, but rather the detected power P

$$P = P(\nu) \exp[- \alpha(\nu) \ell] \tag{10}$$

Figure 2.6

Comparison of the line shape for direct detection and second harmonic detection of an isolated, Lorentzian absorption. For the harmonic signal the sensitivity was increased ten times.

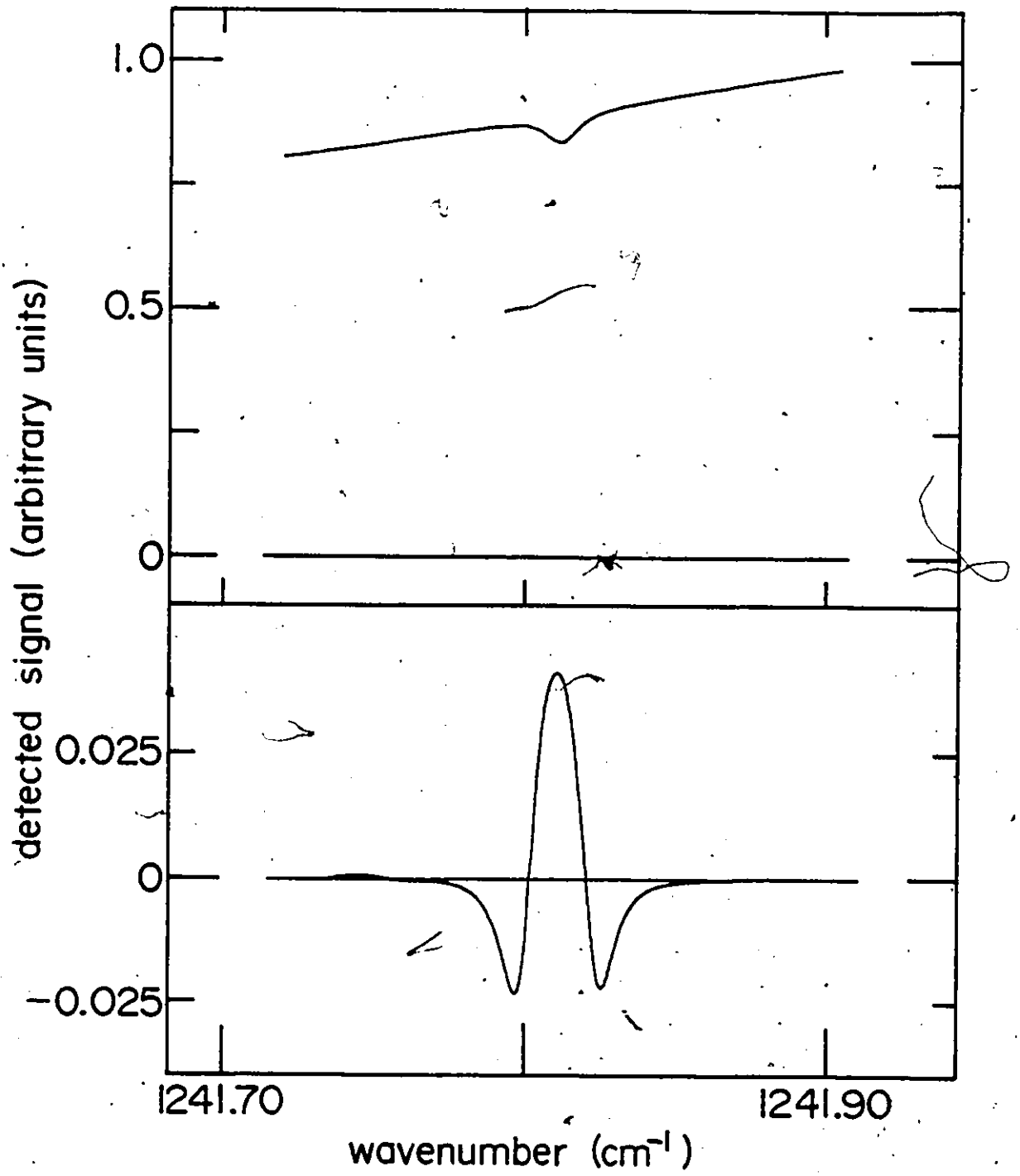
1.0
0.5
0
0.025
0
−0.025
detected signal (arbitrary units)
1241.70
1241.90
wavenumber (cm⁻¹)

where $P(\nu)$ is the output power of the laser. In the derivative approximation the detected power can be expressed as

$$
\begin{aligned}
P = {} & P(\bar{\nu})[1 - \alpha(\bar{\nu})\ell] \\
& + M\{P'(\bar{\nu})[1 - \alpha(\bar{\nu})\ell] - P(\bar{\nu})\alpha'\}\cos\omega t \\
& + \frac{M^2}{4}\{P''(\bar{\nu})[1 - \alpha(\bar{\nu})\ell] - 2P'(\bar{\nu})\alpha' \\
& \quad - P(\bar{\nu})\alpha''\}[1 + \cos 2\omega t] + \ldots \qquad (11)
\end{aligned}
$$

where again the laser frequency is given by Eq. (8) and a prime indicates differentiation with respect to ν. One of the difficulties with tunable diode lasers is that the power of a tunable diode laser is a function of wavelength. As Eq. (11) indicates, the wavelength dependent power leads to harmonic signals even in the absence of an absorption coefficient. We define background signals to be the harmonic signals which are derived only from the laser power variations.

Typical harmonic absorption signals and background signals are indicated in Fig. 2.7. The necessary wavelength modulation required for harmonic detection is provided by modulating the injection current. With tunable diode lasers, modulating the wavelength produces a simultaneous modulation of the laser power. This can be observed in traces 1(a) and 2(a) of Fig. 2.7. The large sine wave observed at the detector output is due to the laser intensity modulation, while the small dips in trace 1(a) are caused by the wavelength tuning over an isolated line. The challenge is to detect the absorption line in the presence of the laser intensity modulation. Traces 1(b) and 1(c) show the first and second harmonic signals as the laser is slowly tuned past the absorption line. These signals are the sum of the harmonic

Figure 2.7

First and second harmonic background and absorption signals. The upper series of traces were recorded with a reference cell containing an absorbing gas in the beam. The detector output is shown for a 1 kHz modulation sweeping symmetrically about line centre. The other traces display the lock-in amplifier output as the tunable diode laser is swept slowly over the position of the line.

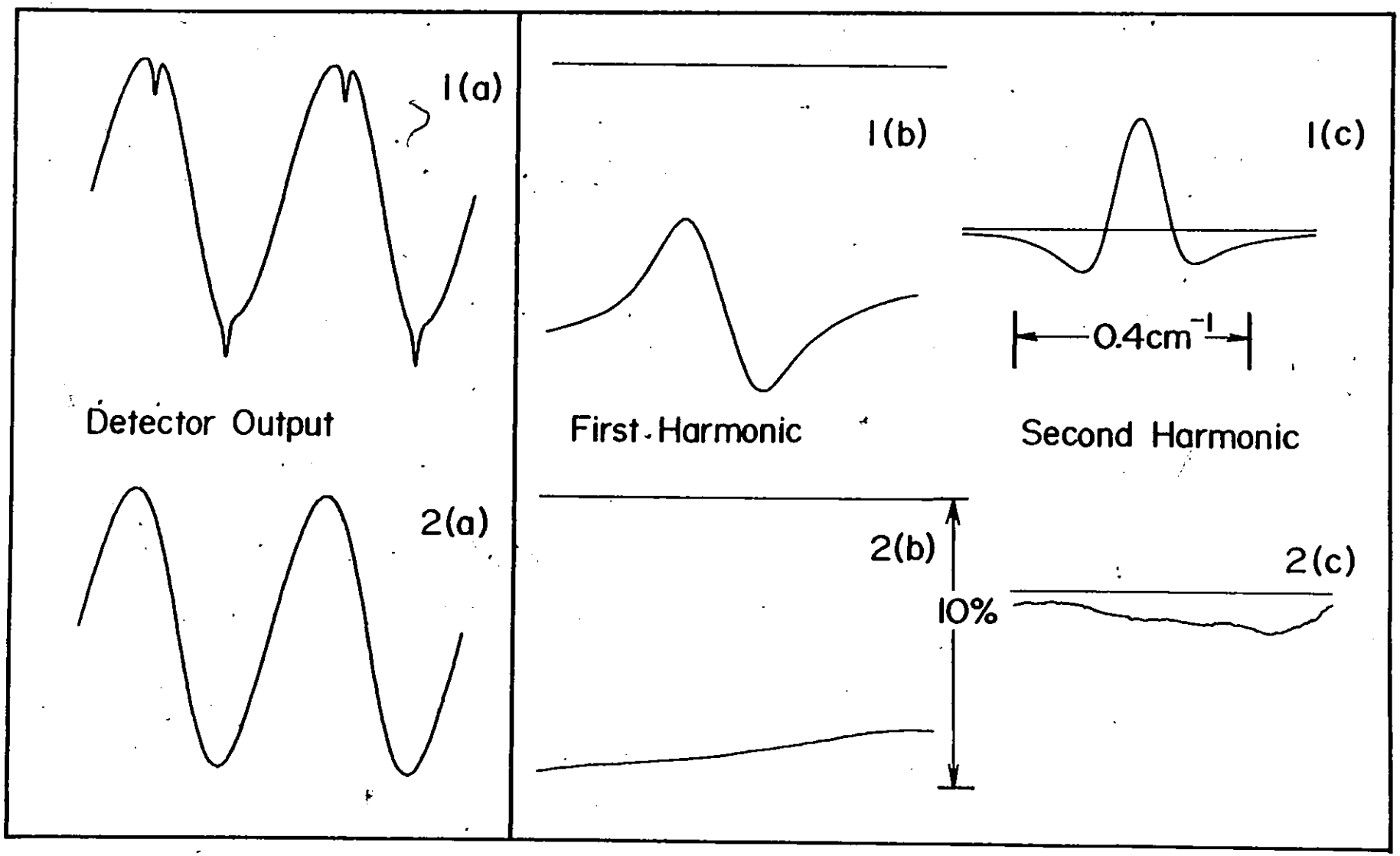
1(a)
1(b)
1(c)
0.4cm^{-1}
Detector Output
First Harmonic
Second Harmonic
2(a)
2(b)
2(c)
10%

contributions from the wavelength and laser intensity modulations. Traces 2(b) and 2(c) are taken with the absorbing gas removed and show the signals due to the intensity modulation alone. It is the harmonics of the intensity modulation which we term background signals. As shall be discussed in Chapter 4, the background signals often limit the sensitivity which can be attained.

From Eq. (11) it is clear that the harmonic absorption signal depends on the depth of modulation M, the power $P(\nu)$, and the modulation-broadened derivative of the line shape function in addition to the path length, line strength, and concentration of molecules. To remove the dependence of concentration measurements on the depth of modulation and line shape derivative it is customary to calibrate the harmonic signal in terms of percent absorption. Calibration of the harmonic signal is performed by introducing sufficient gas into the measurement path that an absorption of ~10% is observed. This absorption is then measured by both direct detection and harmonic detection methods. A comparison of the two signals quickly calibrates the harmonic signal in terms of percent absorption. The concentration of molecules along the path length is deduced by noting that the harmonic signal is equivalent to a certain percentage absorption. The concentration can be determined from Eq. (7) once the absorption is known. This procedure eliminates the need for a precise knowledge of the laser power and depth of modulation.

2.5 Harmonic Line Shapes

This section presents the harmonic line shapes for various depths

of modulation. The material covered in this section will be used in later chapters.

Arndt [45] calculated the harmonic line shape for modulating over Lorentzian absorption lines. The nth harmonic line shape S_n in terms of the normalized distance x from line centre

$$x = \frac{\nu - \nu_o}{\Delta\nu} \tag{12}$$

and normalized depth of modulation m

$$m = \frac{M}{\Delta\nu} \tag{13}$$

is

$$S_n = \varepsilon_n \, \mathrm{Re}\, i^n \frac{\{[(1 - ix)^2 + m^2]^{1/2} - (1 - ix)\}^n}{m^n \, [(1 - ix)^2 + m^2]^{1/2}} \tag{14}$$

where,

$$\varepsilon_n = 1 \quad n = 0, \quad \varepsilon_n = 2, \quad n \neq 0 \, .$$

For the nth harmonic, n an even number, the harmonic signal is a local maximum at line centre. The harmonic signal is zero at line centre for the odd harmonics. There exists an optimum depth of modulation m_{opt} such that the harmonic signal is a maximum. For the nth harmonic, n an even number, m_{opt} satisfies the equality

$$2m_{opt}^2 = n^2 + [n^2(n^2 + 4)]^{1/2}. \tag{15}$$

Equation (15) indicates that the optimum depth of wavelength modulation m_{opt} is $\sim n\Delta\nu$ for detection at the nth harmonic. As one detects at the higher harmonics increasingly larger depth of modulations are required.

Figure 2.8 shows plots of Eq. (14) as a function of x for various values of m and n. In addition to displaying the form of the various

harmonic signals, Fig. 2.8 is of use in evaluating the possible interferences from adjacent absorption lines. This point is discussed in more detail in Chapter 4. Since the absorption is assumed to be symmetric about line centre the ordinates are mirror planes. The ordinates are scaled such that a Lorentzian absorption measured by direct detection methods with a mechanical chopper of 50% duty cycle has a line centre absorption of one. The linewidth of the Lorentzian is one in the normalised units used for the abscissa, and the absorption in the tails of the Lorentzian is < 0.01 for $x > 10$. The distance from line centre for which the harmonic signal remains below 1% of the line centre harmonic signal (for that particular depth of modulation m) is indicated by a triangle.

In addition to the characteristic shape for each harmonic signal there are several points of interest in Fig. 2.8. As the depth of modulation m is decreased from the optimum value, the harmonic signal decreases in magnitude and falls to $< 1\%$ of the line centre value much nearer to line centre. The magnitude of the harmonic signal is always less than the magnitude of the absorption measured by direct detection methods. In spite of this loss of signal we experimentally find that detection by harmonic techniques is still more sensitive than direct detection. The last point we wish to emphasize here is that the (line centre) harmonic signal decreases by approximately a factor of two as the harmonic number n increases by two.

2.6 Summary

This chapter describes the experimental apparatus and introduces

Figure 2.8

Theoretical harmonic lineshapes for various depths of modulations and harmonics. The triangle indicates the distance from line centre at which the harmonic signal drops to 1% of the line centre value. The inset traces show experimentally measured harmonic signals.

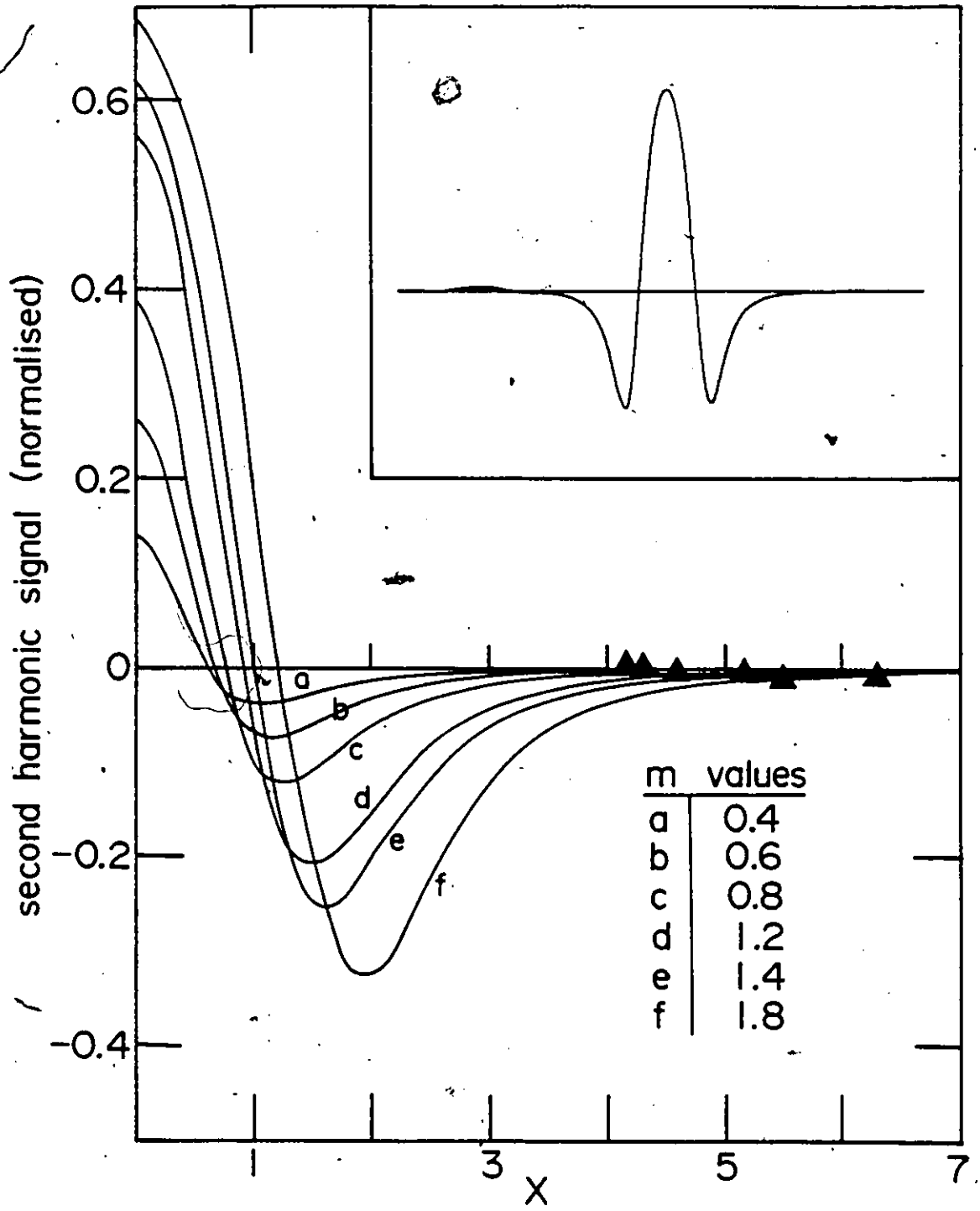
0.6
0.4
0.2
0
-0.2
-0.4
second harmonic signal (normalised)
1
3
5
7
X
a
b
c
d
e
f
m values
a 0.4
b 0.6
c 0.8
d 1.2
e 1.4
f 1.8

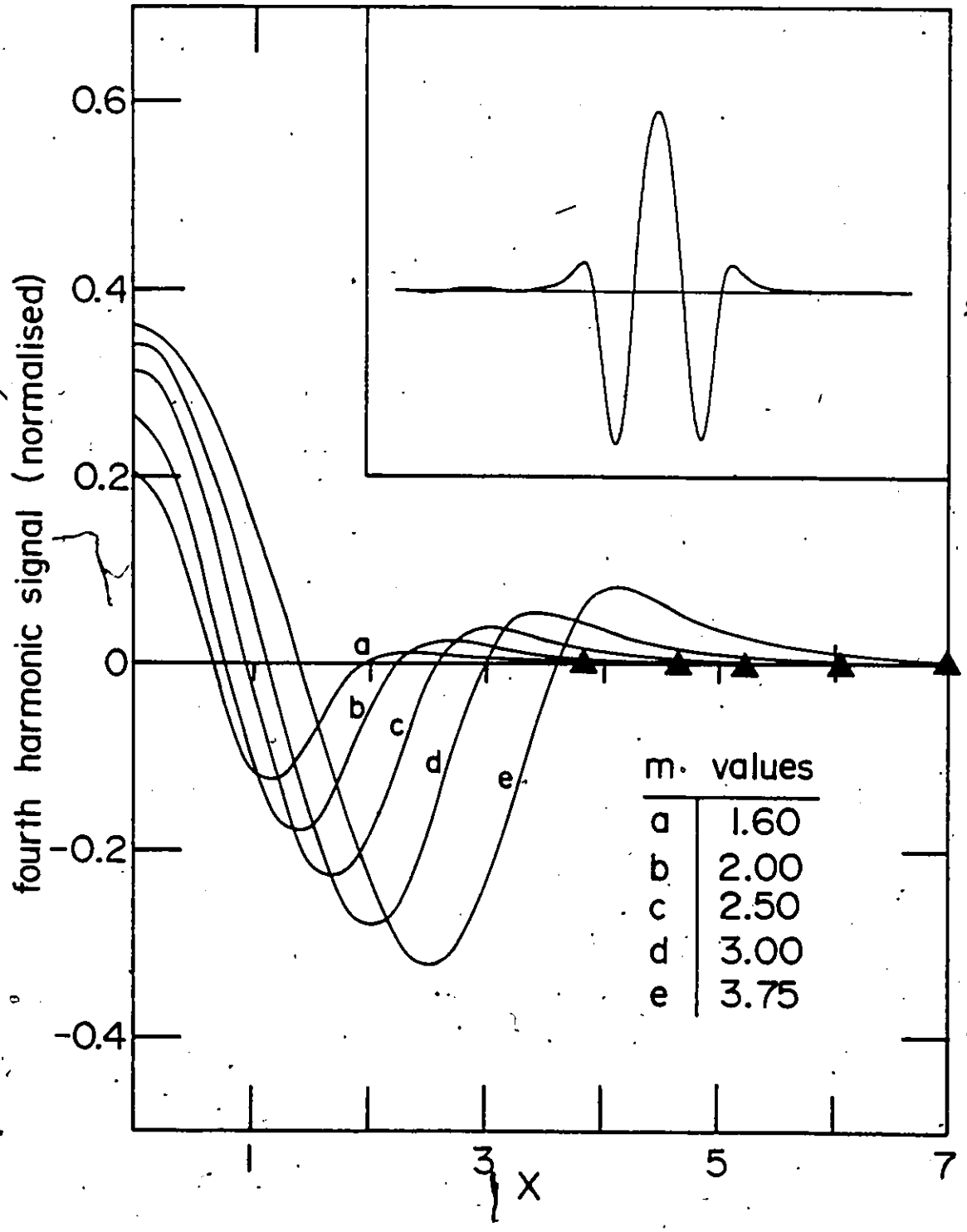
0.6
0.4
0.2
0
-0.2
-0.4
fourth harmonic signal (normalised)
1
3
5
7
X
a
b
c
d
e
m values
a 1.60
b 2.00
c 2.50
d 3.00
e 3.75

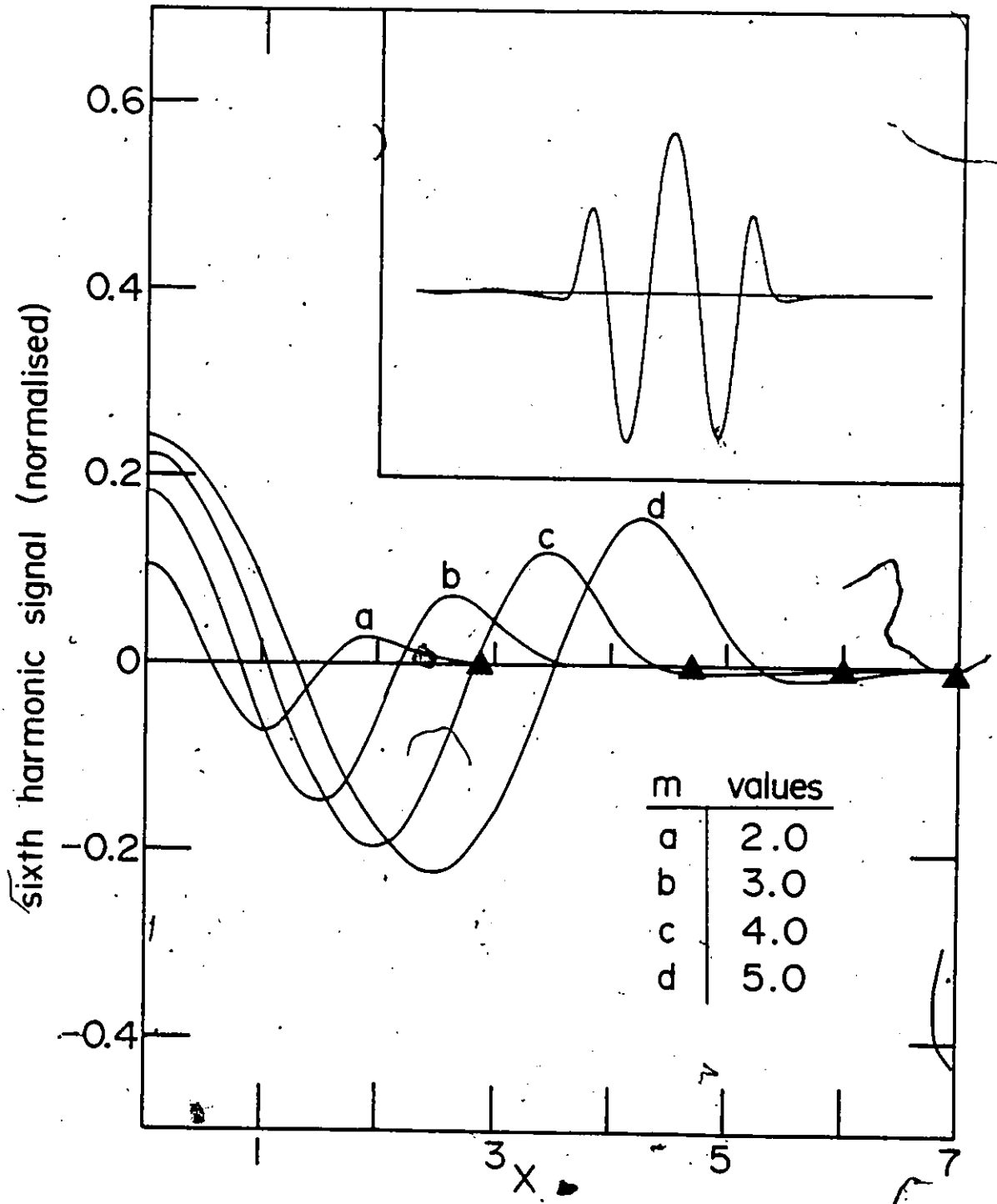
0.6
0.4
0.2
0
-0.2
-0.4
sixth harmonic signal (normalised)
a
b
c
d
m values
a 2.0
b 3.0
c 4.0
d 5.0
1
3
5
7
X

the idea of derivative line shapes obtained by modulation techniques. The shape of a Lorentzian absorption as observed in harmonic detection and an important quantity -- the background signal -- are discussed. Concepts introduced in the chapter are used in subsequent chapters. The next chapter, Chapter 3, considers harmonic detection in more detail.

CHAPTER 3

HARMONIC DETECTION WITH TUNABLE DIODE LASERS

-- TWO-TONE MODULATION

3.1 Introduction

Harmonic detection is an experimental technique for recovering weak signals masked by a strong baseline or background. In recent years harmonic techniques have been used in conjunction with tunable diode lasers to measure infrared absorptions as small as 10^{-3}% [43,48]. For this application, a sinusoidal modulation is impressed on the wavelength of the tunable diode laser while the mean value of the wavelength is slowly ramped over the absorption feature of interest. A phase sensitive detector referenced to a specific harmonic of the modulating waveform processes the detector output. In a recent paper Reid and Labrie [47] compared theory and experiment of second harmonic detection as a function of the absorption line shape. Very good agreement between theory and experiment was observed.

In this chapter we extend the analysis of harmonic detection to include two-frequency modulation. Such two-tone modulation is used to improve the sensitivity of tunable diode laser absorption spectrometers [49,15]. The second modulation is selected to minimise the effect of optical interference fringes (Fabry-Perot fringes) which usually dominate high-sensitivity absorption measurements [15]. Section 3.3 of this chapter is concerned with the harmonic response from low-finesse

Fabry-Perot fringes. Excellent agreement between theory and experiment is found. Theoretical expressions for the two-tone harmonic line shape observed by modulating over an isolated Lorentzian line are presented and compared with experimental measurements in Sec. 3.4. The usual effects of the second modulation are a broadening of the detected line shape and a reduction in the magnitude of the signal, although by a judicious choice of the second modulation frequency and phase, an enhancement of 50% in the detected signal may be realised. The exact expression for the two-tone harmonic line shape is an integral which is amenable to computer solution. An approximate expression which is valid for most modulations of experimental significance is also presented. This expression provides a physical understanding of the effect of the additional modulation on the detected line shape. Agreement between the exact calculation and experiment is within the estimated experimental uncertainty of 2%.

The calculations and experiments described in this chapter provide a detailed understanding of two-tone harmonic detection. This knowledge should assist in improving the detectivity of very weak infrared absorptions.

3.2 Experimental Apparatus

Figure 3.1 is a schematic diagram of the apparatus. The output from the tunable diode laser is focussed into a one metre base path length White cell and then onto a HgCdTe detector. Reference gas cells or a 7.62 cm Ge etalon can be placed in the laser beam. The modulation

Figure 3.1

Schematic diagram of the apparatus.

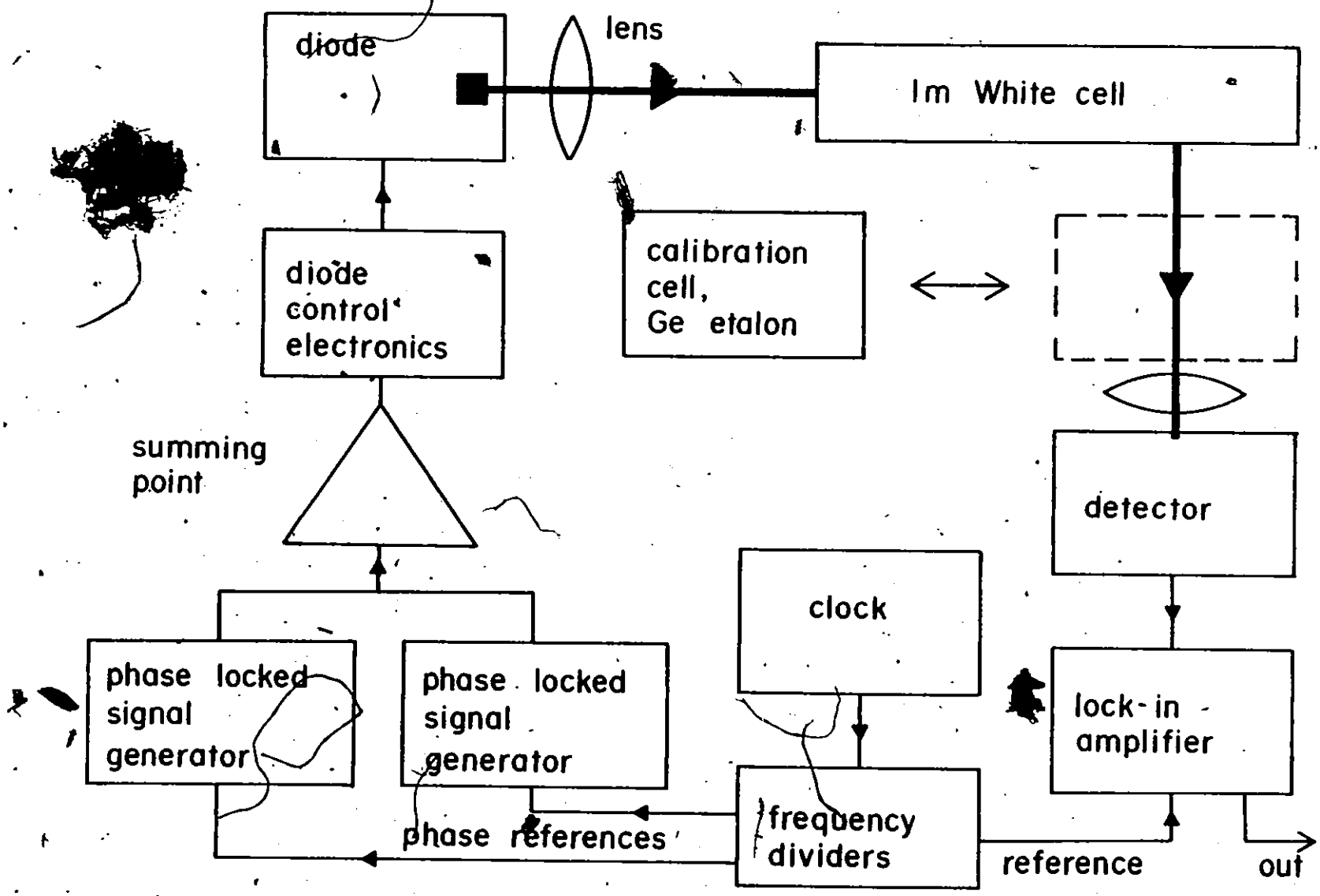
diode
lens
1m White cell
calibration cell, Ge etalon
diode control electronics
summing point
detector
clock
phase locked signal generator
phase locked signal generator
lock-in amplifier
frequency dividers
phase references
reference
out

electronics are designed to allow simultaneous modulation at two distinct frequencies, ω_1 and ω_2, while synchronous detection is performed with a lock-in amplifier referenced to $|p\omega_1 \pm q\omega_2|$, where p,q are integers. Further details of the apparatus may be found in Chapter 2 and the literature [15,20].

3.3 Harmonic Response to Etalon Fringes

Second harmonic signals from two distinct sources are shown in Fig. 3.2. The upper trace is the second harmonic signal from an isolated, pressure-broadened line of NO_2 at 1604.1 cm^{-1}. The lower trace of Fig. 3.2 is the second harmonic signal due to modulating over Fabry-Perot fringes. The fringes are caused by optical interference between adjacent focal spots on the field mirror of the multipass cell [15]. Fringes of the type illustrated in the lower trace of Fig. 3.2 limit the overall sensitivity of a tunable diode laser absorption spectrometer. Since the interferences are almost impossible to eliminate by even the most careful optical alignment, we have studied and developed modulation techniques to minimize their effect. The varying envelope of the fringes shown in the lower portion of Fig. 3.2 is due to a change in the depth of wavelength modulation of the source as the wavelength is ramped. Figure 3.2 clearly demonstrates that certain modulation amplitudes minimize the harmonic response to fringes. It is possible to minimize the harmonic response to fringes over a

Figure 3.2

Typical second harmonic signals. The upper trace is obtained by scanning over an isolated line of NO_2. A mixture of NO_2 in N_2 at 40 Torr was used to give a 10% line centre absorption. For the lower trace, the absorbing gas was removed and the sensitivity increased by 100. One now observes fringes of spacing 0.0025 cm^{-1} due to interference between adjacent spots on the field mirror of the multipass cell.

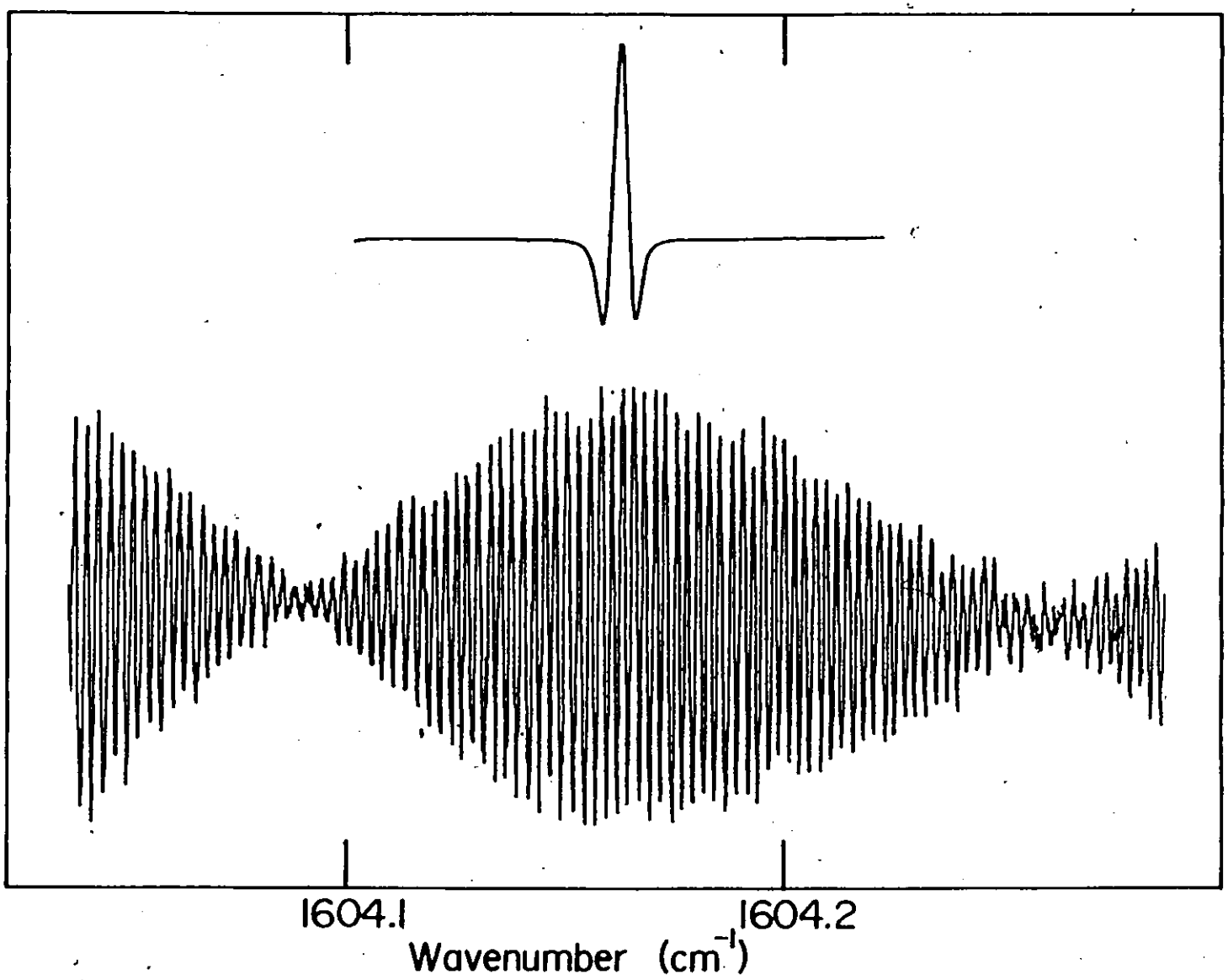
1604.1
1604.2
Wavenumber (cm^{-1})

greater spectral range by adding a second or jitter modulation[a]. In the following paragraphs we derive the response of harmonic detection to low-finesse Fabry-Perot fringes for one- and two-frequency sinusoidal modulation of the laser wavelength, and compare these predictions with experimental measurements.

The transmission through two partially reflecting surfaces separated by an optical distance of L/2 is given as a function of wave number ν by [50]

$$\frac{1}{1 + F\sin^2(\pi L\nu)} . \tag{16}$$

For fringes of low-finesse, i.e., F a small number, the transmission to first order in F is

$$1 - F[1 - \cos(2\pi L\nu)]/2. \tag{17}$$

For two-tone harmonic detection, the lasing frequency ν is modulated at two frequencies, thus

$$\nu = \nu_0(t) + M_1\cos\omega_1 t + M_2\cos\omega_2 t . \tag{18}$$

$\nu_0(t)$ is the average laser output frequency, and is written with an explicit time dependence to indicate that it is slowly ramped to cover the spectral region of interest. M_1 is the amplitude of the fundamental modulation at angular frequency ω_1 and M_2 is the amplitude of the jitter modulation at frequency ω_2. For convenience we define a dimensionless

[a]Although the change in tuning rate affects both modulations equally when measured as a percentage change, the absolute change of the jitter modulation is small in terms of the number of fringes modulated over. This feature renders the minimum of the two-tone harmonic response less sensitive to changes in the tuning rate.

depth of modulation

$$m_i' = M_i L \; ; \; i = 1,2 \; . \tag{19}$$

m_i' simply defines the amplitude of modulation in terms of the number of fringes modulated over. The harmonic content of Eq. (17) may be evaluated by using the Jacobi-Anger relation [51]. This procedure gives the amplitudes of the harmonics in terms of $J_n(x)$, the Bessel functions of the first kind of integral order n. Explicitly,

$$\cos(2\pi L\nu) =$$

$$\cos[2\pi L\nu_0(t)]\{ \sum_{r,s=0}^{\infty} \varepsilon_r \varepsilon_s (-)^{r+s} J_{2r}(2\pi m_1') J_{2s}(2\pi m_2')$$

$$\times \cos(2r\omega_1 t)\cos(2s\omega_2 t)$$

$$- 4 \sum_{r,s=0}^{\infty} (-)^{r+s} J_{2r+1}(2\pi m_1') J_{2s+1}(2\pi m_2')$$

$$\times \cos[(2r+1)\omega_1 t]\cos[(2s+1)\omega_2 t]\}$$

$$\sin[2\pi L\nu_0(t)]\{ 2 \sum_{r,s=0}^{\infty} \varepsilon_s (-)^{r+s} J_{2r+1}(2\pi m_1') J_{2s}(2\pi m_2')$$

$$\times \cos[(2r+1)\omega_1 t]\cos(2s\omega_2 t)$$

$$+ 2 \sum_{r,s=0}^{\infty} \varepsilon_r (-)^{r+s} J_{2r}(2\pi m_1') J_{2s+1}(2\pi m_2')$$

$$\times \cos(2r\omega_1 t)\cos[(2s+1)\omega_2 t]\} \tag{20}$$

where $\varepsilon_p = 1 \quad p = 0, \quad \varepsilon_p = 2 \quad p \neq 0,$

To keep the problem tractable we specialize to detection at twice the

fundamental modulation frequency and assume that ω_1 and ω_2 are not harmonically related. The second harmonic response for a system for which the modulation is described by Eq. (18) and the transmission is given by Eq. (17) is

$$F \cos[2\pi L\nu_0(t)]\ J_2(2\pi m_1')\ J_0(2\pi m_2') \ . \tag{21}$$

Evidently, the magnitude of the harmonic response to the fringes is controlled by the Bessel functions and the finesse F, while the cosinusoidal term provides the oscillating behaviour observed in the lower trace of Fig. 3.2. The period of the oscillations is equal to the free spectral range of the Fabry-Perot resonator which forms the interference fringes.

For single-frequency modulation M_2 equals zero, $J_0(0)$ equals one, and the second harmonic response follows the second order Bessel function. To check this prediction we used a tunable diode laser with a fairly constant tuning rate and a 7.62 cm Ge etalon. This etalon produces stable fringes with a spacing of 0.016 cm^{-1} and thus is much more suited to a comparison of theory and experiment than an etalon produced by a multipass cell. The results of this check are presented as Fig. 3.3. Experimentally, the second harmonic signal was observed to be a maximum for $m_1' = 0.5$ fringes, and all experimental values are normalised to this point. The abscissa was calibrated in a separate series of measurements by observing the etalon transmission on an oscilloscope and counting fringes as a function of the amplitude of the sine wave modulation applied to the diode laser. A linear least squares fit to this data enabled us to measure the wavelength tuning rate, and

Figure 3.3

Comparison of theoretical and experimental second harmonic fringe response as a function of the wavelength modulation amplitude m_1'. The peak-to-peak fringe height is normalized to unity at $m_1' = 0.5$ for both theory and experiment. The theoretical curve is the second order Bessel function $J_2(2\pi m_1')$. Experimental data points are indicated by triangles.

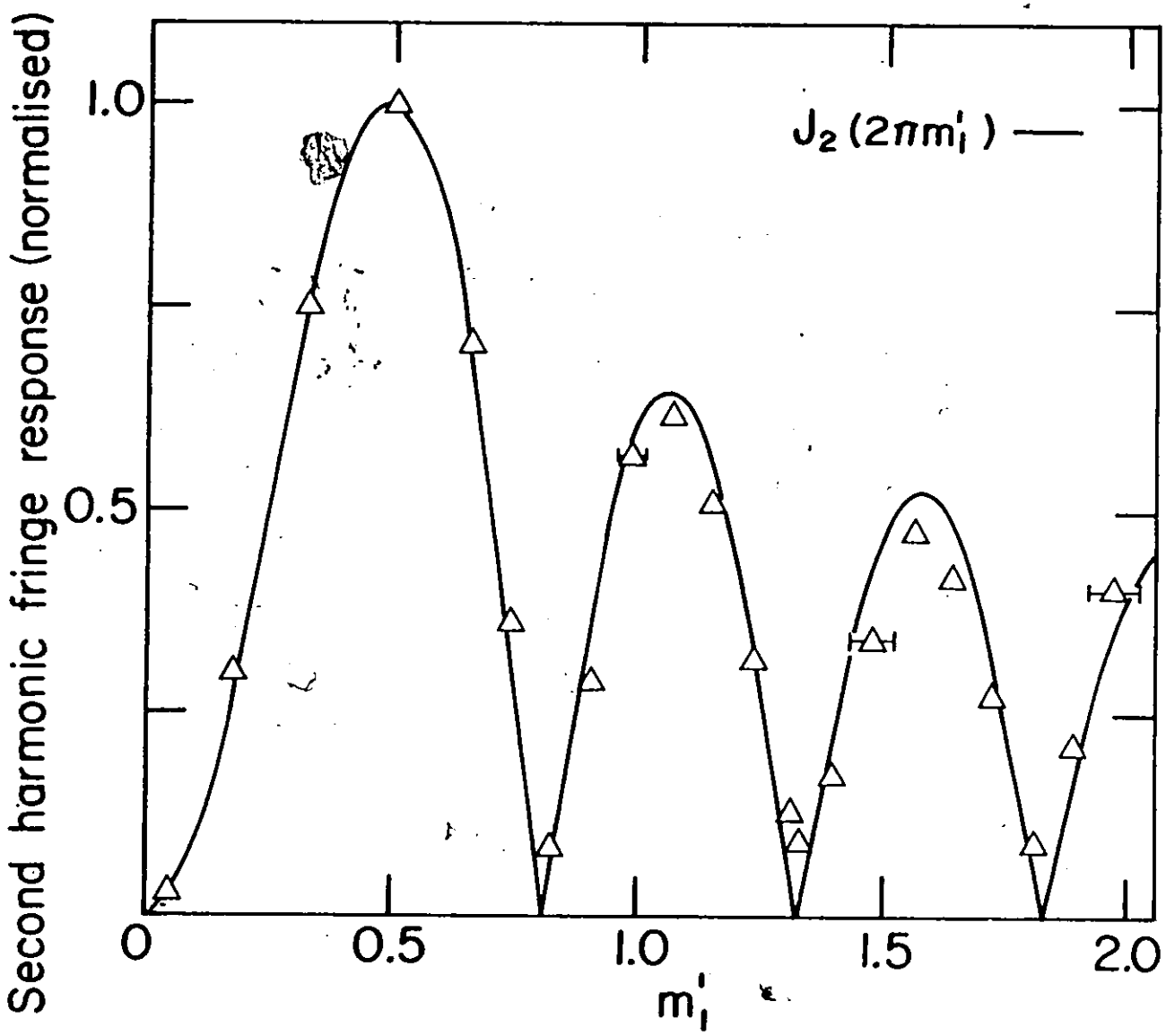
Second harmonic fringe response (normalised)
1.0
0.5
0
0.5
1.0
1.5
2.0
m_1'
$J_2(2\pi m_1')$

hence the abscissa, to $\pm 2.5\%$. Within this accuracy, the agreement between theory and experiment is excellent, as shown in Fig. 3.3. The zeros of $J_2(2\pi m_1')$ occur for $m_1' = 0.817$, 1.340, 1.849 fringes.

As expected, the envelope of the fringes can be minimized by adjusting the amplitude of modulation M_1 to correspond to a zero of $J_2(2\pi m_1')$. However, this is not a very effective technique as the absorption line signal also depends on M_1 [47] and the tuning rate varies as the laser is scanned over the region of interest (compare Fig. 3.2). A much more effective technique in reducing the harmonic response to fringes is to introduce a jitter modulation M_2 which is independent of the fundamental modulation. One can adjust M_1 to maximize the absorption line signal, and then add M_2 to reduce the effects of fringes. If the free spectral range of the fringes is much less than the linewidth of the absorption, then $M_2 \ll M_1$, and it is possible to minimize the fringes over a large spectral region.

An experiment to check the validity of Eq. (21) for non-zero M_2 was performed. The Ge etalon was placed in the beam as before, ω_1 was set to 1 kHz and M_1 adjusted for the first maximum of the response (with $M_2 = 0$). Detection at 2 kHz, i.e., the second harmonic of ω_1 was used. A jitter modulation at $\omega_2 = 370$ Hz was then added to the tunable diode laser, and the peak-to-peak second harmonic response recorded as the amplitude of modulation M_2 was varied. The results of this experiment are shown in Fig. 3.4. The abscissa of Fig. 3.4 was measured to an accuracy of $\pm 2.5\%$ as previously described. Note that the experimental results are the same, to within the experimental uncertainty, as the

Figure 3.4

Comparison of theoretical and experimental second harmonic fringe response for two-tone modulation. Experiment and theory are both normalised to unity at $m_2' = 0$. The theoretical curve is the first order Bessel function $J_0(2\pi m_2')$. Typical fringe patterns for two different values of m_2' are shown. Experimental data points are indicated by triangles.

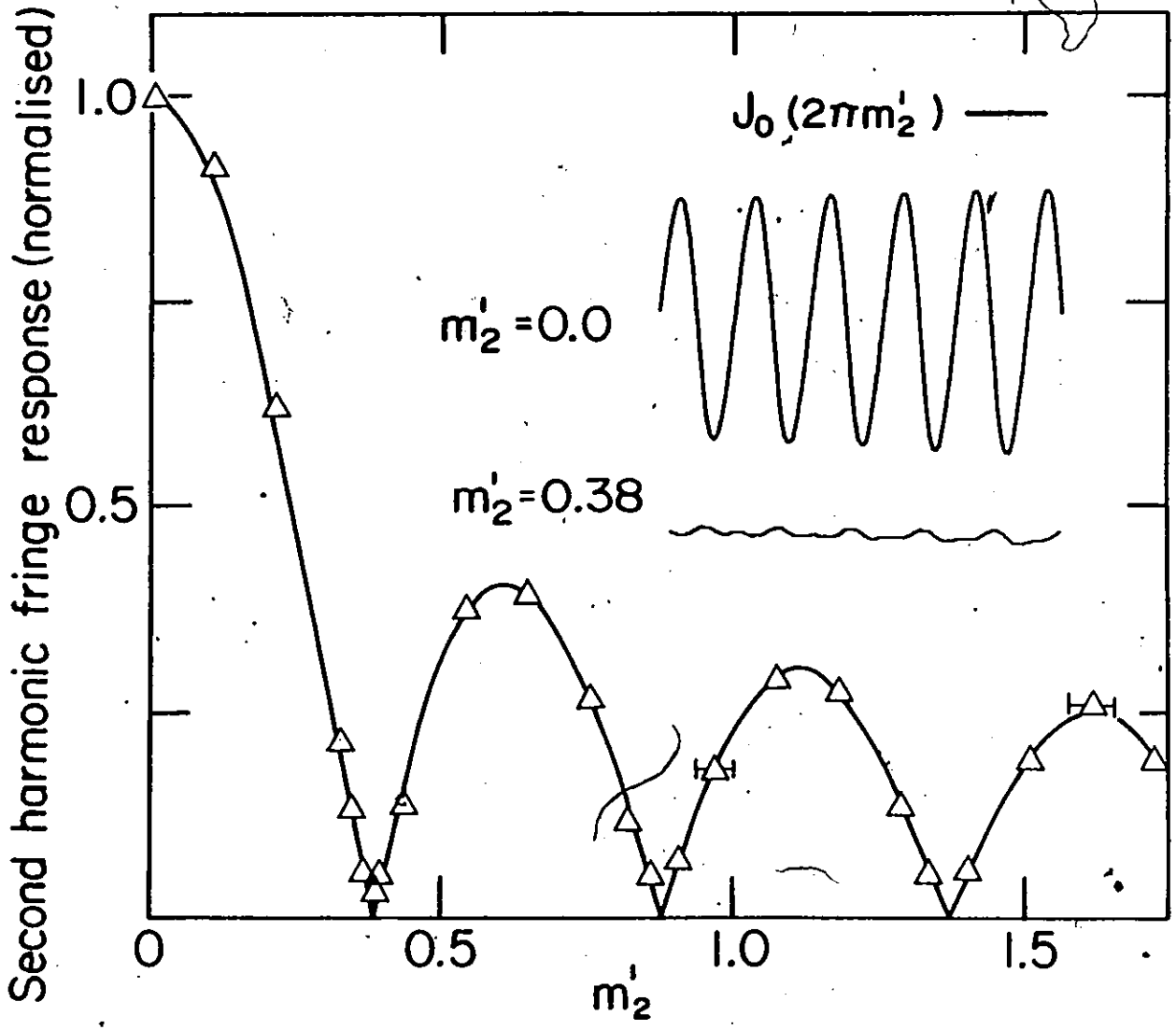
Second harmonic fringe response (normalised)
1.0
0.5
0
0.5
1.0
1.5
m_2'
$J_0(2\pi m_2')$
$m_2' = 0.0$
$m_2' = 0.38$

relationship predicted by Eq. (21). The zeros of $J_0(2\pi m_2')$ occur for m_2' = 0.383, 0.879, 1.377 fringes. The results shown in Fig. 3.4 can be used to optimise sensitivity in experiments using tunable diode lasers. The first step is to adjust the magnitude of M_1 until the absorption signal is a maximum [47]. The jitter modulation is then increased from zero until the unwanted optical fringe signal is minimized. As M_1 and M_2 can be adjusted independently, the absorption signal can be maximized while the interfering signal is minimized. A substantial enhancement of absorption signal to fringe height can be obtained in this manner (Ref. 15, see also Fig. 4.7). However, problems arise if M_2 is similar to M_1, i.e., if the fringe spacing and absorption linewidth are comparable. In this case the addition of a jitter modulation significantly affects the detected harmonic line shape. The next section deals with the detected harmonic line shape as a function of two modulations.

3.4 Harmonic Line Shape for Two-tone Modulation

The signal at the detector, S(x), for two-frequency modulation over an isolated Lorentzian absorption line is

$$S(x) = \sum_{p,q=0}^{\infty} S_{pq}(x)\cos(p\omega_1 t)\cos(q\omega_2 t)$$

$$= \sum_{p,q=0}^{\infty} \varepsilon_p \cos(p\omega_1 t)\cos(q\omega_2 t)$$

$$\times \int_0^{2\pi} S_q(x + m_1\cos\theta)\cos p\theta \, \frac{d\theta}{2\pi} \qquad (22)$$

where

$$S_n(x) = \varepsilon_n \mathrm{Re}\ \frac{i^n\{[(1 - ix)^2 + m_2^2]^{1/2} - (1 - ix)\}^n}{m_2^n\,[(1 - ix)^2 + m_2^2]^{1/2}} \tag{14}$$

is the nth harmonic line shape for single-frequency modulation [47,45],

x is the distance from line centre, normalised by the line-width, $\Delta\nu$ (half-width, half-maximum)

and m_1 and m_2 are the dimensionless fundamental and jitter modulation amplitudes defined as

$$m_i = M_i/\Delta\nu \ , \ i = 1,2 \ . \tag{13}$$

A derivation of Eq. (22) is outlined in Appendix A.

We wish to consider two-tone second harmonic detection at $2\omega_1$ for a jitter modulation which is not harmonically related to ω_1. A phase sensitive detector referenced to $2\omega_1$ will pick out $S_{20}(x)$ from the sum in Eq. (22). $S_{p0}(x)$ is the pth harmonic line shape in the presence of a jitter modulation. Although Eq. (22) is an accurate representation of the detected harmonic signal, it does not readily provide a physical picture. If one assumes that $M_2 < M_1$, which is true for almost all interesting cases, then a binomial expansion of the denominator of Eq. (22) in powers of m_2/m_1 can be made. By retaining only the first order terms, the integration indicated in Eq. (22) may be performed analytically. Using this technique, a simple expression for $S_{p0}(x)$ is found.

$$S_{p0}(x) = \frac{1}{2}\left[S_p\left(x + \frac{m_2}{\sqrt{2}}\right) + S_p\left(x - \frac{m_2}{\sqrt{2}}\right)\right] \tag{23}$$

Equation (23) indicates that the two-tone harmonic line shape is the average of the appropriate single-frequency line shape shifted to the

left and right by $m_2/\sqrt{2}$. Thus the addition of an incoherent jitter broadens the harmonic line shape and reduces the magnitude of the signal. To check the accuracy of Eqs. (22) and (23) we performed a series of measurements on an isolated Lorentzian absorption line for various values of m_2. The results are presented in Fig. 3.5. The absorption was due to N_2O diluted in air to give a total pressure of 50 Torr. Second harmonic detection at $2\omega_1$ = 2 kHz was employed. m_1 was set to 1.67; this choice gives 95% of the maximum line centre signal (m_2 = 0) while minimising the modulation broadening of the detected harmonic line shape [47]. The jitter frequency was 370 Hz. The solid curve in Fig. 3.5 is the computer calculated second harmonic line centre signal, $S_{20}(x)|_{x=0}$, plotted as a function of m_2. The broken curve of Fig. 3.5 is a plot of the approximate expression, Eq. (23), evaluated at line centre as a function of m_2. As expected, the second harmonic line shape broadened, decreased in size, and split into two segments located symmetrically about line centre as m_2 was increased from zero. The signal at line centre decreased and eventually went negative for large values of m_2. Very good agreement between theory and experiment was obtained. No variable parameters were used in plotting the data points. All values were measured to an estimated precision of $\pm 2\%$. The experimentally determined line centre signal was normalised to the maximum line centre signal measured by varying m_1 with m_2 equal to zero. The theoretical points are normalised to the maximum (theoretical) second harmonic signal for m_2 equal to zero. m_1 and m_2 were determined by fitting the measured second harmonic line shape (single-frequency

Figure 3.5

Line centre second harmonic signal from an isolated Lorentzian line as a function of the incoherent jitter modulation m_2. The data points are normalised to the maximum second harmonic signal found by varying m_1 with $m_2 = 0$. The solid and broken lines are calculated curves based on the theory described by Eqs. (22) and (23). Experimental data points are indicated by triangles. Second harmonic line shapes for various values of m_2 are also shown.

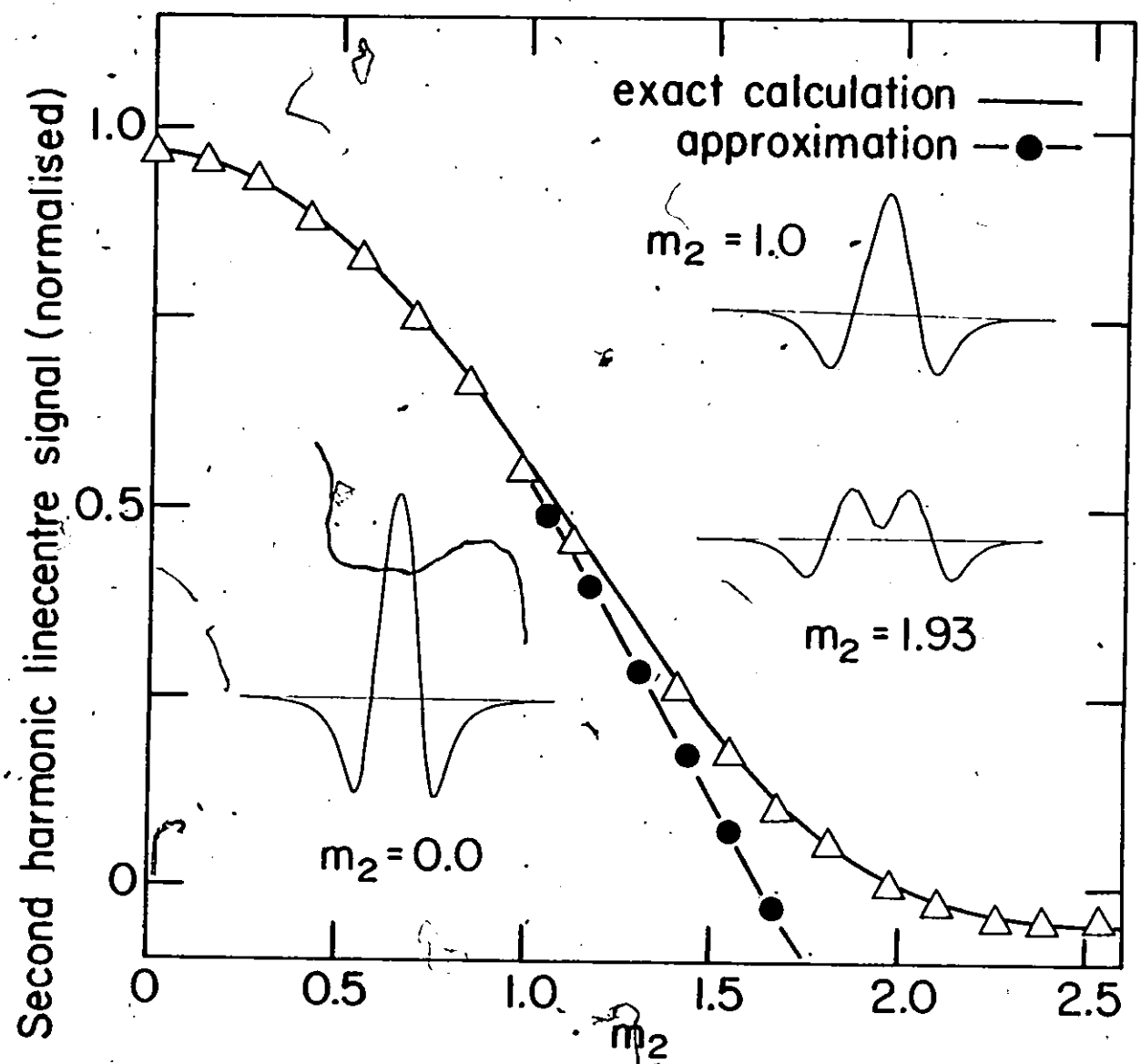
exact calculation
approximation
$m_2 = 1.0$
$m_2 = 1.93$
$m_2 = 0.0$
Second harmonic linecentre signal (normalised)
1.0
0.5
0
0
0.5
1.0
1.5
2.0
2.5
m_2

modulation) for many different depths of modulation to the theoretical line shape [47]. Note the good agreement between Eq. (23) and the experimental data for $m_2 < 0.75\ m_1$. It is clear from Figs. 3.3-3.5 that the theory described in Sections 3.3 and 3.4 provides a very accurate representation of the experimental behaviour.

A comparison of Fig. 3.4 and Fig. 3.5 indicates that the jitter modulation will be effective at increasing the ratio of absorption signal to fringe signal provided one can apply a sufficiently large amplitude of jitter modulation such that the first zero of $J_0(2\pi m_2')$ may be reached without significantly broadening the line shape. Quantitatively, the jitter modulation must equal 0.383 fringes while the fundamental modulation must be ~2.2 linewidths for optimum second harmonic detection of an absorption line. These conditions correspond to ensuring that the fringe free spectral range is $<\Delta\nu$. This condition is usually fulfilled experimentally, particularly for a 1 m base path length multipass cell and pressure broadened lines in the 5-10 μm region. However, in the case of widely spaced fringes, or very narrow absorption lines, the jitter technique described above may be inappropriate.

A careful examination of the theory suggests that it is possible to minimize fringes while <u>increasing</u> the line centre signal. If the jitter frequency ω_2 is picked such that $\omega_2 = 3\omega_1$, then there are several contributions to the second harmonic signal at $2\omega_1$. Second harmonic signals are obtained from sum and difference frequencies such as $\omega_2 - \omega_1$, $5\omega_1 - \omega_2$, $2\omega_2 - 4\omega_1$, etc., in addition to $\omega_1 + \omega_1$. A deriva-

tion indicating the importance of the sum and difference contributions is given in Appendix B. For $m_2 = m_1/2$ and $m_1 = 2.2$ linewidths, the second harmonic line centre signal is enhanced by 50% over the case $m_2 = 0$. The addition of a properly phased jitter modulation increases the line centre signal, as Fig. 3.6 demonstrates. On the other hand, if the two modulations are 180° out of phase, the line centre signal is decreased. The 50% increase in signal is obtained at the expense of a substantial increase in the complexity of the modulation electronics. However, one can use the coherent (i.e., $\omega_2 = 3\omega_1$) jitter modulation to enhance the absorption signal and minimize the fringes. The theoretical expressions are now rather long and cumbersome as one is attempting to modify signals at $2\omega_1$ which arise from several inter-related sources. Nevertheless, the effectiveness of coherent jitter in increasing the ratio of the absorption signal to fringe signal is easily demonstrated, as Fig. 3.7 shows. Appendix B examines the case of coherent jitter in more detail. While coherent jitter can increase the ratio of absorption signal to fringe signal, we feel that the additional complexity of coherent jitter may only be worthwhile when the fringe spacing and linewidths are comparable.

3.5 Discussion and Conclusion

We describe a general theory of two-tone harmonic detection. The theory of second harmonic detection is developed in detail for the case of Lorentzian absorption lines and sinusoidal optical fringes. However, it is a simple matter to extend the theory to deal with Doppler

Figure 3.6

Second harmonic signal from an isolated Lorentzian line. The middle trace was obtained for $m_2 = 0$, $m_1 = 2.2$ linewidths. For the upper trace, a coherent jitter at $\omega_2 = 3\omega_1$ was added, and both the phase and amplitude of the jitter modulation were adjusted to give a maximum signal. The observed enhancement is in excellent agreement with theory. For the lower trace, the relative phase of ω_2 and ω_1 was changed by 180°. Again, a good agreement between theory and experiment is observed.

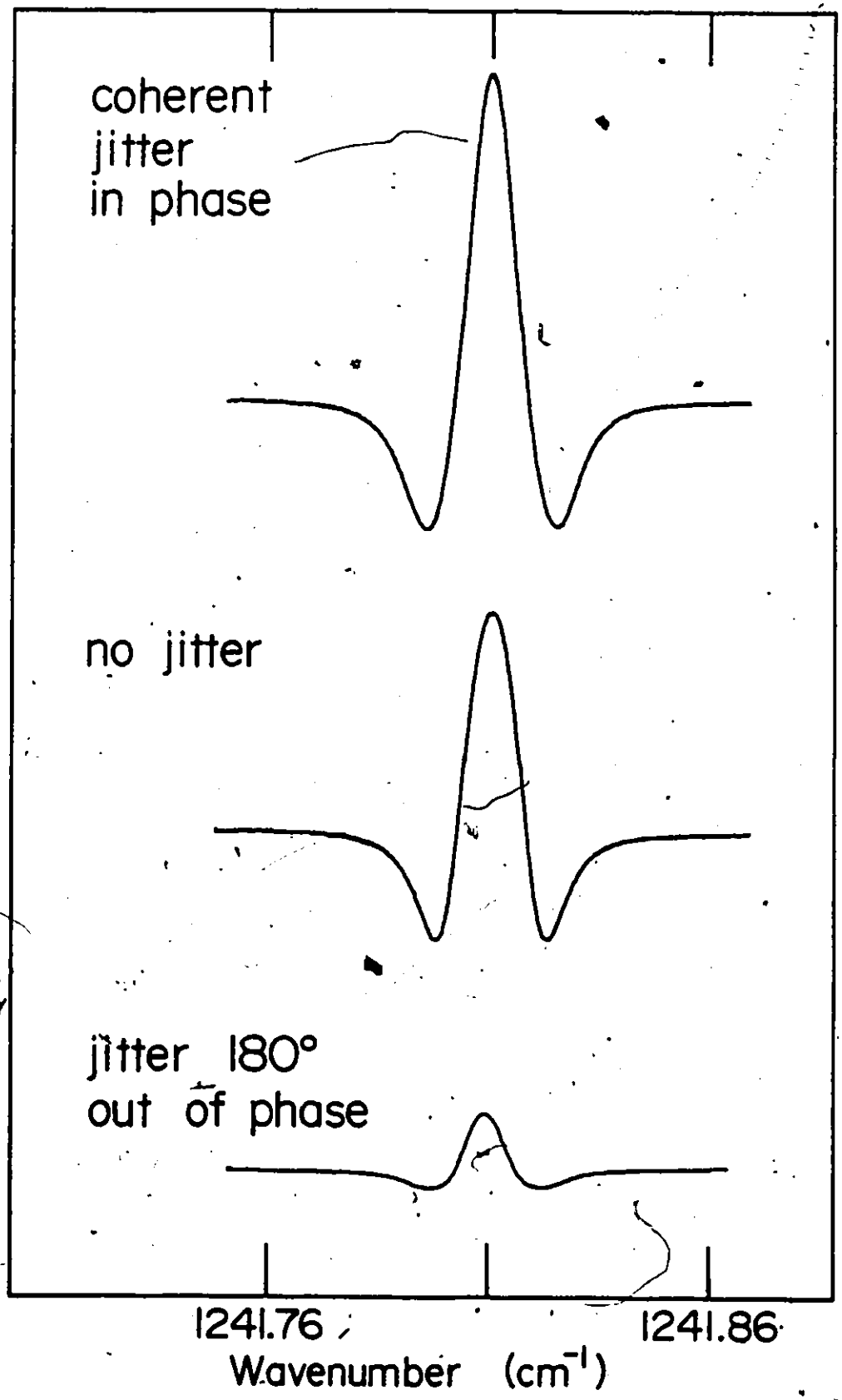
coherent
jitter
in phase
no jitter
jitter 180°
out of phase
1241.76
1241.86
Wavenumber (cm⁻¹)

Figure 3.7

Optimization of the ratio of second harmonic absorption signal to fringe signal using coherent jitter. All three traces are taken with both the gas cell and Ge etalon in the laser beam. The N_2O/N_2 mixture in the cell gives a weak absorption of ~1% near 1241.2 cm^{-1}, but this absorption can only be observed in the middle and lower traces after a jitter modulation of the correct amplitude has been applied. The coherent jitter modulation ($\omega_2 = 3\omega_1$, modulations in phase) reduces the fringe amplitude by ~40, while enhancing the absorption signal by 20%.

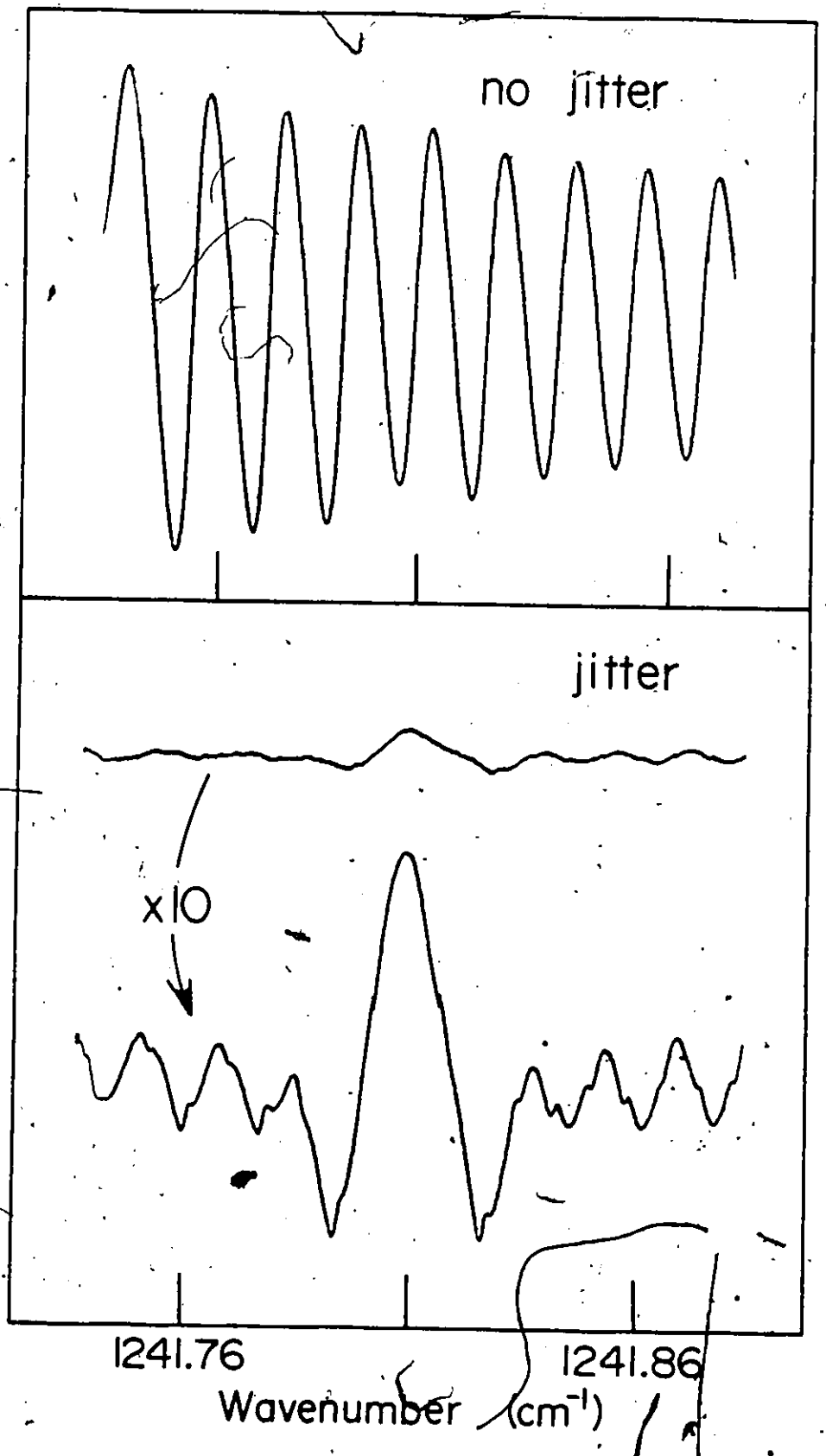
no jitter
jitter
x10
1241.76
1241.86
Wavenumber (cm⁻¹)

broadened line shapes, fourth harmonic detection, or detection at sum and difference frequencies. The theory is compared in detail with experimental results using a tunable diode laser as the source. Under a wide range of conditions excellent agreement is obtained between the theory and experiment. The results described in this chapter will find practical application in many tunable diode laser experiments where weak absorption lines have to be detected in the presence of optical interference fringes. We show that two-tone modulation can minimize the harmonic signal from optical fringes while producing an effect on the absorption signal which is easily calculated.

The application of harmonic techniques to the high-sensitivity detection of atmospheric pressure trace gases is considered in Chapter 4.

CHAPTER 4

ATMOSPHERIC PRESSURE MONITORING OF TRACE GASES USING TUNABLE DIODE LASERS

4.1 Introduction

Tunable diode laser spectrometers are often used for the monitoring of trace gases in the atmosphere. The spectrometers can be divided into two groups depending on the mode of operation; low-pressure point monitors and open-path or atmospheric pressure monitors [52]. The reported sensitivities of low-pressure point monitors are significantly better than the sensitivities reported for similar devices designed for operation at atmospheric pressure. Reid *et al*. [15] constructed a point monitor with a noise limited sensitivity equivalent to an absorption of 10^{-3}%. In contrast Ku *et al*. [16] reported a noise level equivalent to an absorption of 0.7% in the first demonstration of open-path monitoring using tunable diode lasers. The essential difference between the two monitoring schemes is the pressure of the gas sample to be analyzed. Both systems used tunable diode lasers and harmonic detection. The point monitors employ a commercial multipass cell and vacuum pump to achieve a long path length through a gas sample at reduced pressure, while the open-path monitors typically use a retroreflector up to several hundreds of metres distant from the source to define the measurement volume. The open-path monitors are inherently noninvasive, *in situ* measuring devices.

Detection of small absorptions at low pressures is simplified because the laser output power as a function of the lasing wavelength is linear over an interval corresponding to several linewidths. At atmospheric pressure where the linewidths are ~0.1 cm^{-1}, the laser output is a nonlinear function of lasing wavelength over the interval corresponding to several atmospheric pressure linewidths. This nonlinearity implies that for harmonic detection the background measured for the first several harmonics will not be zero. We have found that the minimum detectable absorption is of the order of the size of the background. As discussed in Sec. 2.4, the background is defined to be a harmonic signal due to modulating the intensity output of the laser.

In this chapter the results of an investigation of the sensitivity-limiting sources of an open-path monitor based on tunable diode lasers and harmonic techniques is presented. By applying the insights gained from the investigation we achieved a sensitivity limit which corresponds to detecting an optical absorption of 0.01% over path lengths up to 250 m. This sensitivity is a substantial improvement over previous work performed at atmospheric pressure.

A. Previous Results

In 1975 Ku *et al.* [16] reported the first measurements of trace gases with an open-path, tunable diode laser spectrometer. They reported a noise level equivalent to an absorption of 0.7%. The measurement path length was 600 m. Based on recommendations for the improved performance of a tunable diode laser, open-path monitor [52-54]

Chaney et al. [17] added wavelength stabilisation and mode selecting optics. The minimum sensitivity they achieved was actually worse than that reported four years previous by Ku et al. [16], but adequate for their purposes. Eng et al. [18] investigated the noise spectrum of several tunable diode lasers and characterised atmospheric turbulence over open laboratory paths. Relying only on the measurements of noise, they estimated their minimum sensitivity to be 0.1%. The results of Ku [16], Chaney [17], Eng [18], and co-workers were achieved using harmonic detection techniques. Max et al. [55] employed a method other than harmonic detection. They used tunable diode lasers in a pulsed mode of operation to perform differential absorption measurements. Sensitivity for this scheme was given as 100 ppb of SO_2 (~0.3% absorption) over a measurement path length of 120 m.

Open-path monitors employing lasers other than tunable diode lasers are not as sensitive as those which use tunable diode lasers. Differential absorption lidars based on fixed-frequency gas lasers have been described recently by Menyuk et al. [56] and Altmann et al. [57]. The minimum absorption detectable by differential absorption lidars is thought to be ~ 2% [57]. Continuum absorption by water and N_2 [56-58], and interference from neighbouring absorptions [42] are factors which presently limit the accuracy of fixed-frequency differential absorption lidars. Tunable diode laser, open-path monitors are less susceptible to continuum absorption and interferences than fixed-frequency laser monitors.

The sensitivity limit of 0.01% we report is not a fundamental

limit, but rather is due to optical fringes generated by scattered light. Redesigned optics would reduce the amount of scattered light and lead to an improvement in the achievable sensitivity.

B. Review of Material Covered in Chapter 4

The material of Chapter 4 can be conveniently divided into nine sections.

The apparatus used to record the measurements reported in Chapter 4 is described in Sec. 4.2. The apparatus differs from the apparatus described in the previous chapters only slightly. Optics to allow propagation over an open-path and some additional electronics to improve the signal-to-noise ratio are the changes. Section 4.3 contains a discussion on the background signal. We experimentally found that the minimum detectable absorption is of the order of the size of the background signal. Data to support this claim is presented in Sec. 4.3. Modulation schemes to minimize the background signal and hence increase the sensitivity are discussed in Sec. 4.4 and Sec. 4.5. We find that the simplest method to increase the sensitivity is to detect at the fourth, sixth, or eighth harmonic. Data demonstrating the sensitivity possible by detecting at the higher harmonics are presented in Sec. 4.6. We report a noise level equivalent to an absorption of ~ 0.01% in Sec. 4.6. The question of interferences from neighbouring absorption lines and techniques to minimize this type of interference are studied in Sec. 4.7.

Strong absorptions close to the absorption of interest can mask

or alter the signal from the absorption under study. One of the advantages of using tunable diode lasers is the ability to select the spectral region of operation. However, it may not be possible to always select a region removed from all strong, interferring absorptions. The magnitude of a region around the absorption of interest which must be free of absorptions for negligible interference is considered in Sec. 4.7. The size of the spectral region free of absorptions required for negligible interference is found to depend on the depth of modulation m. Harmonic signal can be sacrificed to avoid interference.

Up to this point, harmonic detection has been applied only to isolated absorption lines. Many molecules such as sulphur dioxide possess such a complex spectrum that at atmospheric pressure strong overlapping of lines occurs. The harmonic detection of band structure absorptions is the subject of Sec. 4.8.

Section 4.9 is a summary of the material covered in Chapter 4.

4.2 Apparatus

Figure 4.1 is a schematic diagram of the apparatus used for open-path monitoring. The optical arrangement is similar to that used by Ku *et al*. [16]. The distance between the launch mirror and the retroreflector can be varied from 1 to 600 m. Most of the signal processing is typical of that used for harmonic spectroscopy, thus we describe only the unusual features. The ratiometer is an anolog chip used to ratio the demodulated harmonic signal to the average received optical power. This process results in a power independent measurement

Figure 4.1

Schematic diagram of the apparatus used for long path open-air monitoring.

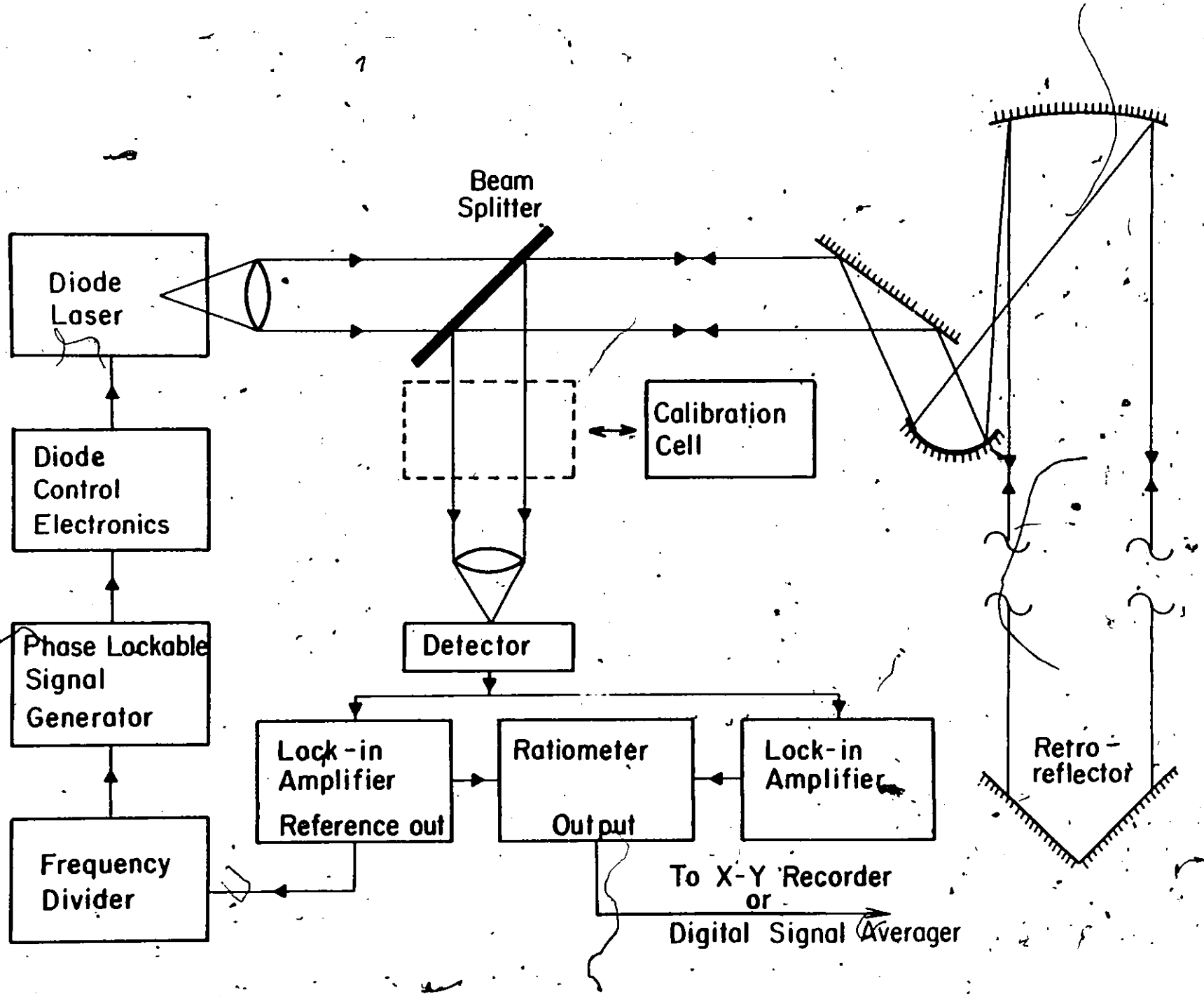
Beam Splitter
Diode Laser
Diode Control Electronics
Phase Lockable Signal Generator
Frequency Divider
Calibration Cell
Detector
Lock-in Amplifier
Reference out
Ratiometer
Output
Lock-in Amplifier
Retro-reflector
To X-Y Recorder
or
Digital Signal Averager

and provides a minor improvement in the signal-to-noise ratio [16,18]. The programmable frequency divider provides a digital pulse at the subharmonics of the internal oscillator of the phase-sensitive detector. With this device any harmonic from the first to the sixteenth of the diode modulating frequency can be examined.

Two disadvantages of the optical arrangement shown in Fig. 4.1 are that the laser beam is always subject to atmospheric turbulence [59], and it is impossible to remove the air sample from the beam path to determine the true zero level. Consequently, we made extensive use of a 5 m base path White cell to investigate systematically the effects of turbulence and alignment changes on the received signal. With the laser beam directed through the White cell it is a simple matter to determine the base line by evacuating the air sample or replacing it with pure nitrogen. In addition, the path length through the multipass cell can be changed easily in a well-controlled fashion. Comparisons of system performance through the White cell and through the open air proved invaluable in identifying the phenomena which limited sensitivity and in determining the reproducibility of the measurements. Further details of the apparatus and techniques of harmonic detection can be found in previous papers [47,48] and chapters.

4.3 The Background Signal

Since the background signal plays a significant role in determining the sensitivity of an open-path monitor based on tunable diode lasers and harmonic detection techniques, we take this opportunity

to clarify and emphasize the meaning of the term background. Harmonic detection is performed by sinusoidally modulating the optical frequency of the source and using a phase-sensitive detector to analyse the harmonic content of the transmitted beam. As pointed out in Chapters 2 and 3, absorption of the beam energy by isolated transitions produces harmonics of the modulating frequency.

The strength of the absorption is directly related to the magnitude of the harmonic signal caused by the absorption. However, under a wide range of operating conditions there are contributions to the harmonic signal from sources other than the absorption. To accurately determine the strength of the absorption one must be able to separate the contributions from the absorption and base line signal or background. Distinguishing between the absorption signal and the background signal is not always an easy task. The background signal arises as a result of the wavelength modulation required for harmonic detection. Modulating the optical frequency of a lead-salt laser produces simultaneous modulation of the output power. It is the appropriate harmonics of the intensity modulation which we term background signals. The laser intensity versus wavelength characteristic is approximately linear over a depth of wavelength modulation which corresponds to several low pressure linewidths. Hence the background is negligible for second harmonic detection of low pressure gases. If there is no absorbing gas present, there is no signal. This factor accounts for much of the success of second harmonic detection in monitoring low-pressure gases. In contrast, the second

harmonic background is large for atmospheric-pressure monitors due to appreciable diode nonlinearities over the greatly increased depth of wavelength modulation. Previous workers [16-18, 52-54] have assumed that the background is a reproducible feature of the diode laser and have taken the background as a base line for measurements. Reliable measurements require the base line to be accurately reproducible. We have found that this is definitely not the case.

We experimentally determined that the minimum measurable absorption is limited to the order of the background when the background signal is expressed as an equivalent absorption. This is a general result as the background is a sensitive function of alignment. The data presented in Fig. 4.2 illustrate this point. A minor alignment change results in a substantial background variation and, in some instances, a change of sign of the background. Two sources for this phenomenon have been identified. The power emitted by the diode varies across the active region, and optical feedback into the laser can substantially alter the background. These two effects result in a background which is a sensitive function of the exact portion of the active region imaged on the detector element by the optics.

A beam of light traversing the open air suffers deflections and wander due to turbulence [59]. Thus, for an open-path monitor the beam is randomly moved across the retroreflector resulting in a time-dependent alignment. Figure 4.2 clearly demonstrates that a time-dependent alignment translates into a degraded signal-to-noise ratio.

Figure 4.2

Effect of alignment changes on background signals. The upper traces show a typical fourth harmonic background and a fourth harmonic absorption signal scaled to correspond to an atmospheric line having an absorption of 1% at line centre. The lower traces demonstrate the reproducibility of the background for successive scans taken with and without a change in alignment.

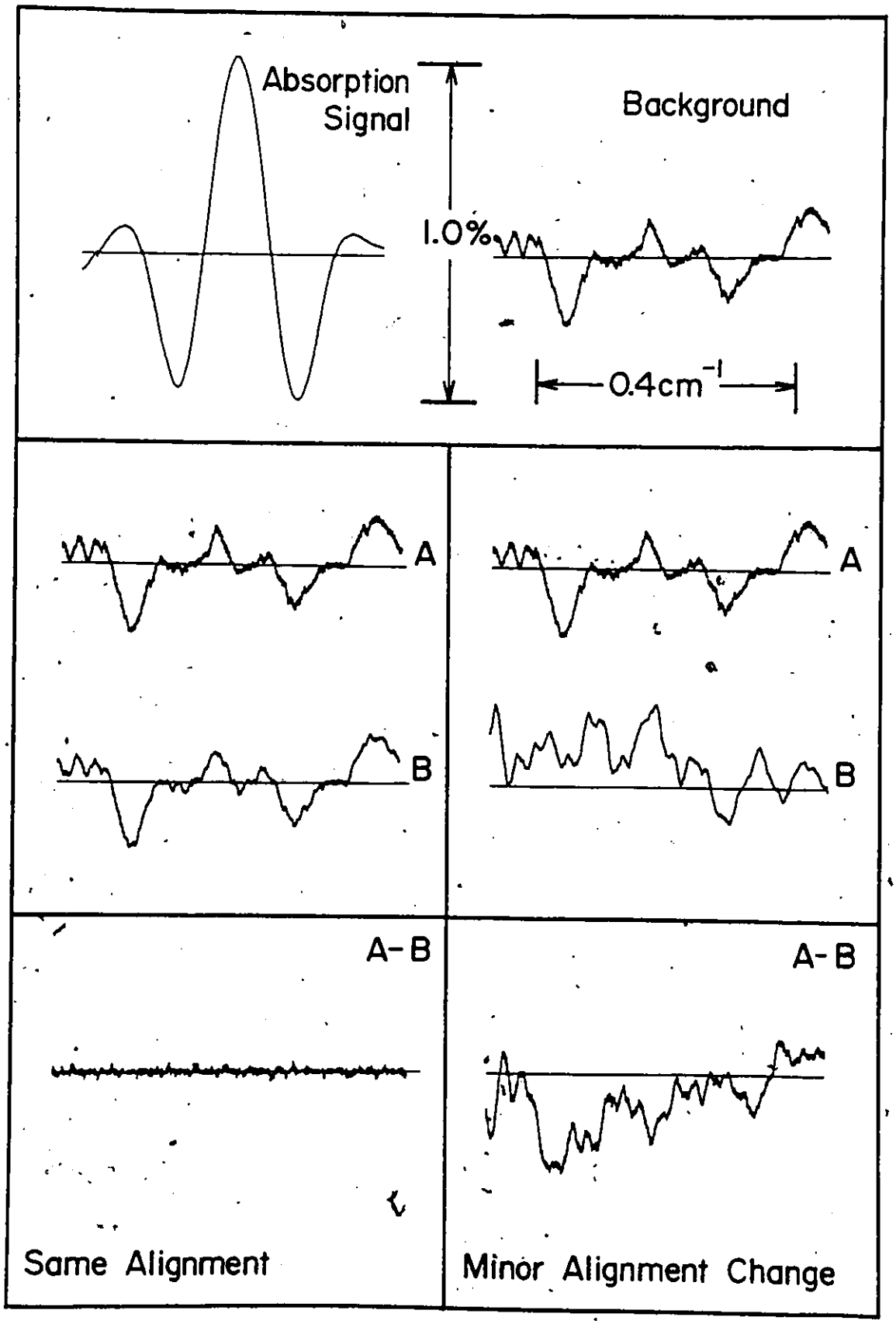
Absorption Signal
Background
1.0%
0.4cm⁻¹
A
B
A
B
A-B
A-B
Same Alignment
Minor Alignment Change

We attribute the limiting noise not directly to intensity fluctuations caused by turbulence but to turbulence causing a vignetting which results in a time-varying background. Consequently we have adopted the philosophy that it is appropriate to seek a modulation scheme which minimizes the background signal.

4.4 Modulation Schemes

Several different techniques of modulating the laser optical frequency were examined in the hope of reducing the background. The standard procedure for modulating the optical frequency is to maintain the laser heat sink at a constant temperature and to vary the injection current. The wide-spread use of this method is based on the ease with which it can be applied. However, the same optical frequency modulation can be obtained by keeping the injection current constant and varying the heat sink temperature. For an atmospheric pressure line, a temperature change of $\sim\pm 0.1$ K is sufficient to cause optical frequency modulation of the magnitude required for an optimum harmonic signal. Attempts to modulate the heat sink temperature by modifying the feedback loop of the temperature stabilization unit were unsuccessful, as were attempts made by expoxying a small, heating element to the laser package. The large thermal mass of the copper heat sink limited the response time to several seconds. Efforts with a CO_2 laser were more rewarding and informative.

Approximately 40 mW of CO_2 laser radiation, chopped at 600 Hz, was focussed on the diode laser. Second harmonic detection, at twice

the chopper frequency, was employed. When the background obtained from (CO_2) thermal modulation was compared to the background obtained from injection current modulation at similar frequencies and depths of modulation, the background from thermal modulation was found to be a factor of two to three times smaller. At modulation frequencies of 150 Hz, both types of modulation produced backgrounds of similar size, yet smaller than the backgrounds observed for 600 Hz modulation frequencies.

The reason for the near equality of the background signals at low modulation frequencies can be explained with the help of the data of Fig. 4.3. Figure 4.3 shows the variation of the depth of optical frequency modulation as a function of the modulation frequency. To obtain the data for Fig. 4.3 the injection current was modulated with a sinusoid of constant amplitude 10 mA rms and the tuning rate determined by counting the number of fringes swept over when a Ge etalon was placed in the beam. We found that for a specified depth of wavelength modulation the magnitude of the background signal decreased as the modulation frequency decreased. The data of Fig. 4.3 indicates that this result is reasonable. The output power of a diode laser is an increasing function of the injection current [60]. To maintain a constant depth of wavelength modulation as the modulation frequency is increased, it is necessary to increase the injection current modulation. Increased injection current modulation increases the modulation of the output power and hence the background.

As a result of the extensive investigation of thermal modulation, of which CO_2 laser modulation is the most successful, the conclusion to

Figure 4.3

Tuning characteristics of a specific diode laser as a function of the modulation frequency. The injection current of the laser was modulated with a sinusoid of constant amplitude 10 mA rms. Modulation at frequencies of 150 Hz or less is most efficient in producing the wavelength excursions necessary for harmonic spectroscopy. The half response point is diode and temperature specific.

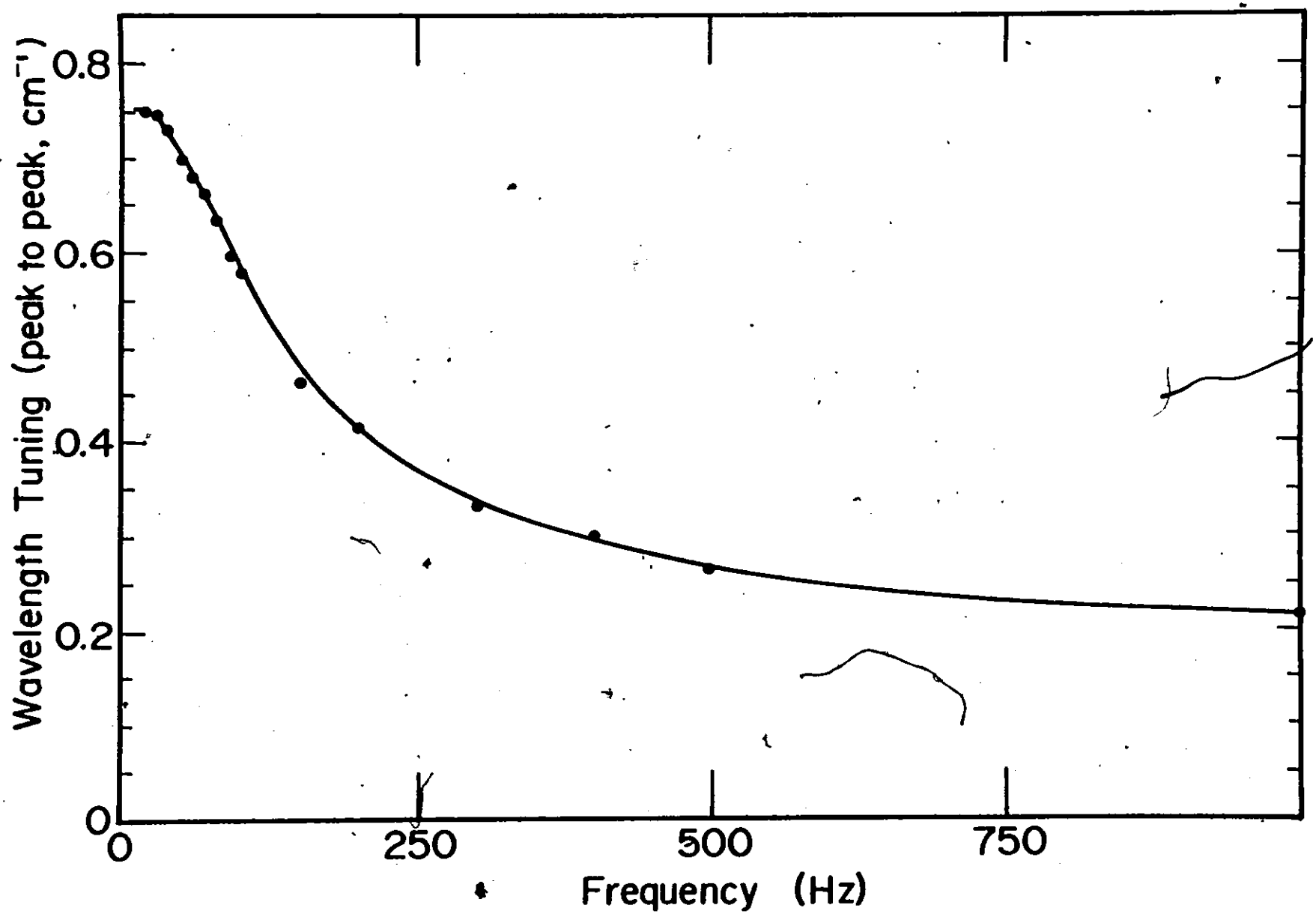
Wavelength Tuning (peak to peak, cm⁻¹)
0.8
0.6
0.4
0.2
0
0
250
500
750
Frequency (Hz)

be drawn is as follows. Provided that the frequency of modulation is kept $\leq$ 150 Hz there is no clear advantage in adopting the more complex schemes, and one may as well use injection current modulation.

4.5 Optimization of Sensitivity

A. Choice of Harmonic

The simplest method of increasing sensitivity is to reduce the magnitude of the background signal relative to the signal produced by an atmospheric absorption line. We found that the most effective means of achieving this is to detect at the fourth, sixth or eighth harmonic rather than the second or first.[a] Experimentally we observe that the magnitude of the background decreases much faster than the magnitude of the absorption signal as one changes to higher harmonic detection. The second harmonic response for a Lorentzian line profile has been calculated by Arndt [45], and compared to experiment by Reid and Labrie [47]. We extended this analysis to the higher harmonic signals. For the optimum depth of modulation the signal at line centre decreases in the ratio 1:0.68:0.36:0.24:0.18 as one switches from direct detection to second, fourth, sixth and finally eighth harmonic detection. In identical conditions the background decreases much more

---

[a] The background signal can be reduced by decreasing the magnitude of optical frequency modulation. However this approach is not successful in reducing the magnitude of the background signal relative to the signal produced by an atmospheric absorption line. Experimentally we find that the absorption signal decreases faster than the background signal as the depth of optical frequency modulation is reduced.

rapidly from 1% at second harmonic to 0.1% at the fourth harmonic to < 0.01% for the sixth and eighth harmonic. The sixth and eighth harmonic background signals were dominated by interference fringes. For several diodes, sixth harmonic detection appeared optimum, although the choice will be diode specific.

To further investigate the decrease in the background as one switches to higher harmonic detection a Hewlett Packard model 3580A spectrum analyzer was used to measure the spectral content of the laser intensity modulation. The injection current of the laser was sinusoidally modulated at 450 Hz. The amplitude of the current modulation was sufficient to provide optimum optical frequency modulation for fourth harmonic detection of an atmospheric pressure line. Figure 4.4 is a typical output from the spectrum analyzer. Note the ~ 20 dB decrease in the background signal as the harmonic number is increased. The signal level at the fifth and greater harmonics is indistinguishable from the noise of the measurement equipment. The sidebands about the fundamental and second harmonic are due to intensity noise on the laser beam. These noise sources will be discussed in more detail in Chapter 6. The lower trace of Fig. 4.4 indicates the distortions on the laser injection current. The harmonics on the current supply are much smaller than those created in the laser output. Figure 4.4 demonstrates that the background signal is reduced by detecting at the higher harmonics.

The background signal can also be reduced by modulating the wavelength at two frequencies and detecting at sum and difference

Figure 4.4

Magnitude of the background signal as a function of harmonic. The upper trace is the frequency spectrum of the laser output. The lower trace is the frequency spectrum of the injection current. For both traces the injection current modulation was a sinusoid of amplitude sufficient to enable optimum fourth harmonic detection of an atmospheric pressure line. The intensity modulation was ~20% of the total laser power output. Measurement bandwidth was 3 Hz.

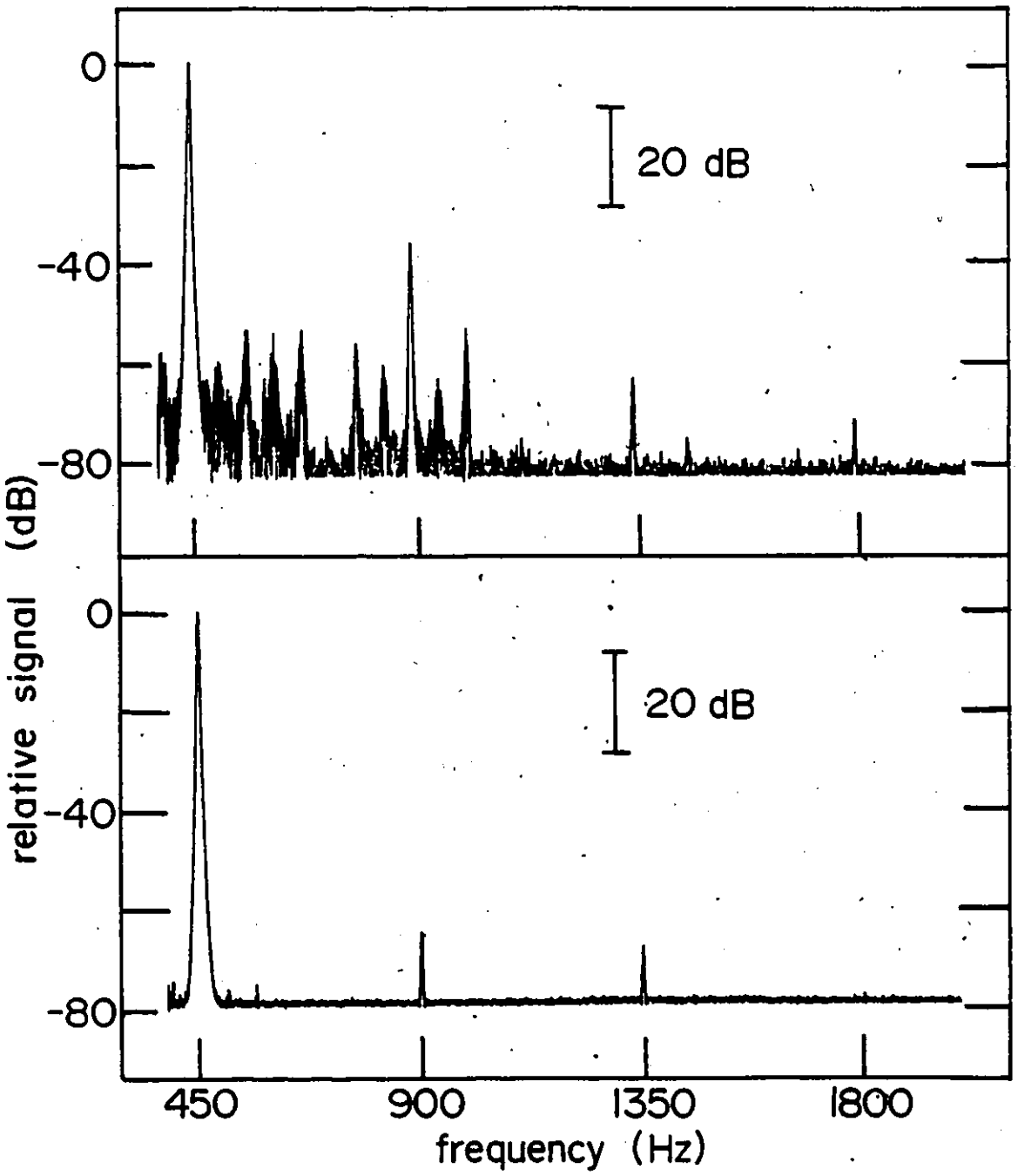
0
-40
-80
20 dB
0
-40
-80
20 dB
relative signal (dB)
450
900
1350
1800
frequency (Hz)

frequencies. Paoli and Svacek [61] pointed out that it is not necessary to detect at the harmonics of a given frequency to obtain derivative signals. The appropriate derivative signal may be obtained by modulating with more than one frequency and detecting at sum and difference frequencies. Although the background is reduced for sum and difference detection, particularly when one of the frequencies is < 150 Hz, the added complexity is a nuisance. We find it more efficient to detect at a higher harmonic of the fundamental rather than at sum and difference frequencies.

Considerations of noise power levels make detection at a frequency of 1 kHz or greater necessary [18,59,62] while considerations of background dictate modulation frequencies of ~ 150 Hz and fourth or sixth harmonic detection. Fortunately the above requirements are compatible. For example, the detection frequency could be set at 1 kHz and sixth harmonic detection employed. The modulation frequency in this example would then be 167 Hz.

B. Feedback Problems

Harward and Hoell [63] demonstrated that feeding back a minute fraction of the laser energy into the diode laser cavity can significantly affect the laser output. Our results confirm this observation and demonstrate the importance of reducing feedback to obtain maximum sensitivity. The retroreflector and beam splitter configurations shown in Fig. 4.1 are particularly susceptible to feedback problems. The effects of feedback on laser linewidth are

dramatically demonstrated in Fig. 4.5. The diode used in this case operates near 1900 cm^{-1} and tunes in a single mode through the $R_{1/2}(6.5)$ doublet of NO. The NO is contained at low pressure in a short cell, and for trace A of Fig. 4.5 the laser beam traverses a short path length in the laboratory with negligible feedback. Trace B is taken a few moments later with the laser beam directed to a retroreflector 600 m distant. We estimate that < 0.3% of the laser power is coupled back into the cavity under these conditions and yet the diode laser linewidth has increased substantially. A more subtle effect of feedback can be seen on examining the harmonic background signals. Even at the sixth harmonic the presence of feedback can increase the background signal by an order of magnitude. As little as 3×10^{-4} of the laser power is found to cause significant effects when fed back into the laser cavity. We have used several techniques to reduce feedback. One method is to insert attenuators into the laser beam near the initial collimating lens. Any power fed back must make two passes through the attenuators. We generally use thin sheets of plastic to attenuate the laser beam by factors of 10-100. A second method is to use an aperture in the laser beam. This technique is particularly effective when the retroreflector is closer than 100 m as the launch and return beams need no longer be exactly collinear. However, to protect against feedback one must drastically reduce the detected power, making measurements detector noise limited. An obvious solution is to use an optical arrangement that does not require coaxial transmit and receive beams.

Figure 4.5

Effect of feedback on laser line width. Trace A is taken in the absence of feedback. For Trace B < 0.3% of the laser power is directed back into the laser cavity from a retroreflector 600 m distant. In each case the laser tunes over the same NO doublet. The absorbing gas was contained in a low pressure reference cell.

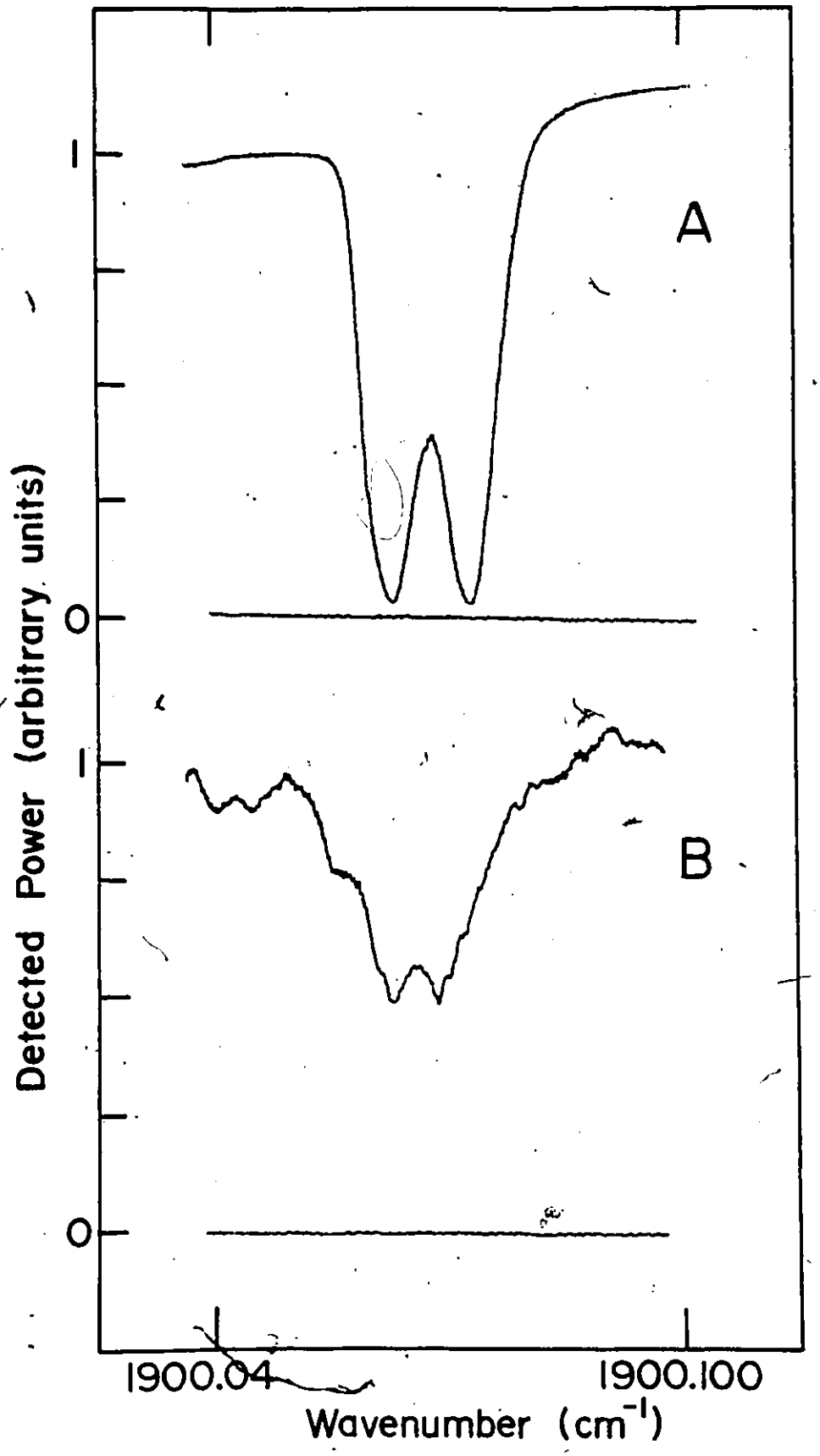
1
0
1
0
A
B
Detected Power (arbitrary units)
1900.04
1900.100
Wavenumber (cm^{-1})

C. Signal Normalisation

For the small optical depths considered in this work the magnitude of the harmonic signal is linearly proportional to the number of absorbing molecules present in the laser beam and to the power falling on the detector. In the presence of turbulence or whenever different path lengths are used this detected power can vary significantly. We therefore divide the demodulated harmonic signal by the average detected power to eliminate the effect of these power fluctuations. The simplest method of determining the power level is to insert a mechanical chopper in the laser beam and to use a second lock-in amplifier. However, the use of a mechanical chopper increases the noise level in the harmonic channel by an order of magnitude. We therefore remove the chopper and use the demodulated first harmonic background signal as an indication of the power reaching the detector. Provided an aperture is present to select a uniform portion of the beam, the first harmonic background signal is linearly proportional to the power. An analog ratio circuit is used to divide the demodulated harmonic signal by the average power. The ratioed signal is almost independent of fluctuations in the received power; a decrease of a factor of 5 in received power resulted in < 5% change in the ratioed signal. This is an extremely useful feature as the system is now immune to power changes caused by turbulence, misalignment, rain, or even shorting out the optical path by placing a second retroreflector close to the launch optics for calibration purposes.

The techniques described in this section have been applied to

several different lasers operating in different spectral regions and optical configurations. We have measured absorptions over path lengths ranging from 1 m to 1.2 km through the atmosphere and for path lengths of up to 240 m through a White cell. All detection was performed at atmospheric pressure. Some typical results are given in Sec. 4.6.

4.6 Results

All the results described in this section were obtained with a tunable diode laser operating in a single mode near 1145 cm^{-1}. Atmospheric absorption lines of N_2O were chosen for detection as they are weak enough to demonstrate the sensitivity of the system. Figure 4.6 shows typical calibration, background, and measurement traces taken over a 60 m round-trip open-air path. Although the line has a line centre absorption of only 0.08%, it can be clearly distinguished in the middle trace. For these traces two factors limited the sensitivity. The laser beam had been attenuated until detector noise was equivalent to an optical absorption of 0.005% while the background signal was found to vary by an amount equivalent to a 0.01% absorption. We therefore feel we can measure weak absorption lines with a sensitivity of $\pm$ 0.01%.

The factors which limit sensitivity over 60 m do not depend on turbulence. Hence sensitivity should remain approximately constant as the path length is increased. Figure 4.7 shows detection of an absorption line in the atmosphere over a 240 m round trip. In this case the noise level is equivalent to an absorption of 0.01 $\simeq$ 0.02%.

In addition to the work carried out with a retroreflector in the

Figure 4.6

Measurement of an atmospheric absorption line at 1142.17 cm^{-1} due to an N_2O line and a weaker overlapping H_2O line. The upper trace shows a sixth harmonic signal observed at 800 Hz by placing an atmospheric pressure calibration cell in the beam. The middle trace shows the same region observed over a round-trip open air path of 60 m. For the lower trace a mirror was placed immediately in front of the telescope in order to observe the background. Each trace took 4 min to complete.

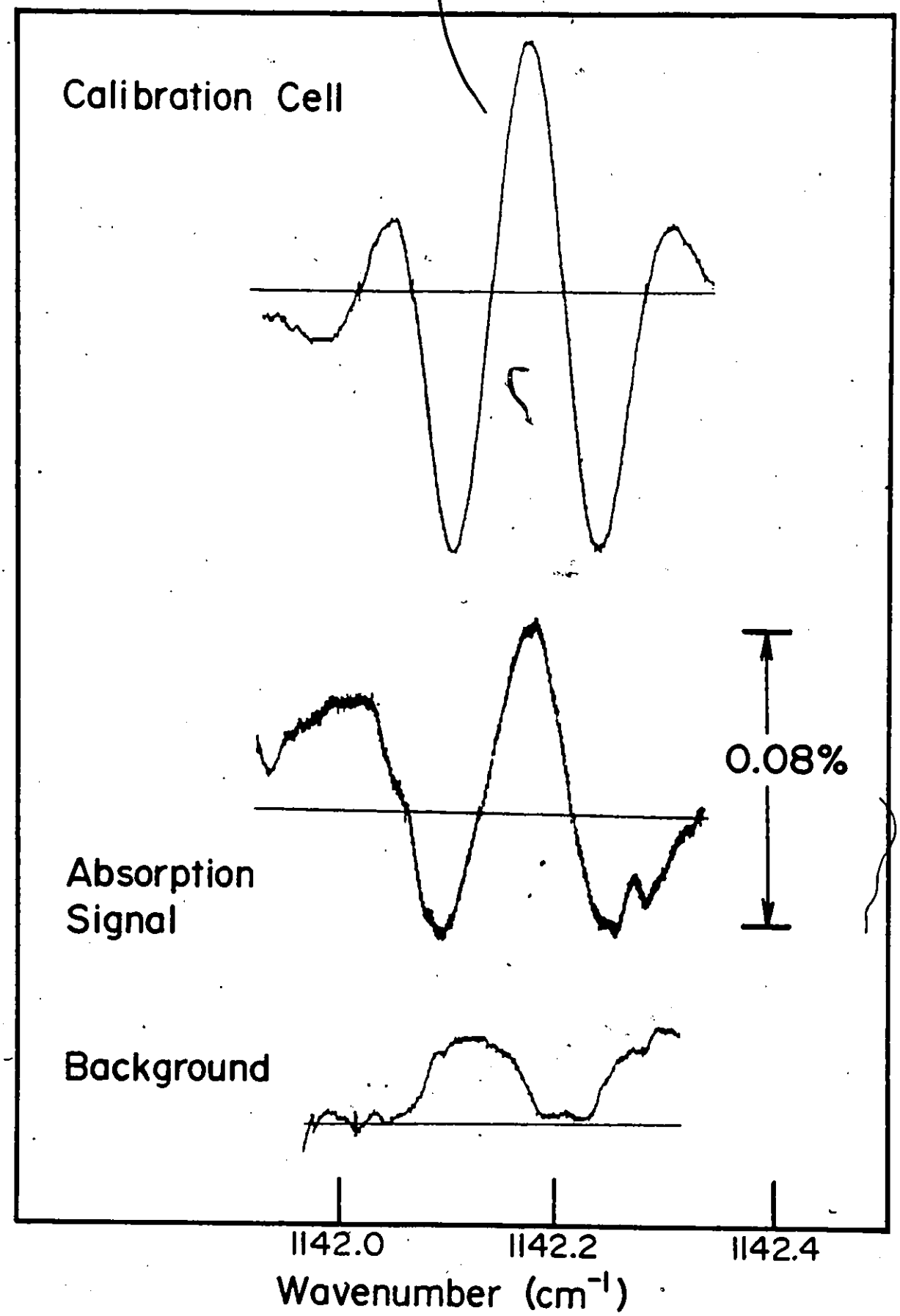
Calibration Cell
0.08%
Absorption Signal
Background
1142.0
1142.2
1142.4
Wavenumber (cm^{-1})

Figure 4.7

Detection of an atmospheric line over a 240-m round trip. Sixth harmonic detection at 800 Hz was used. The distortion to the right is caused by a mode hop. Scan time was 4 min.

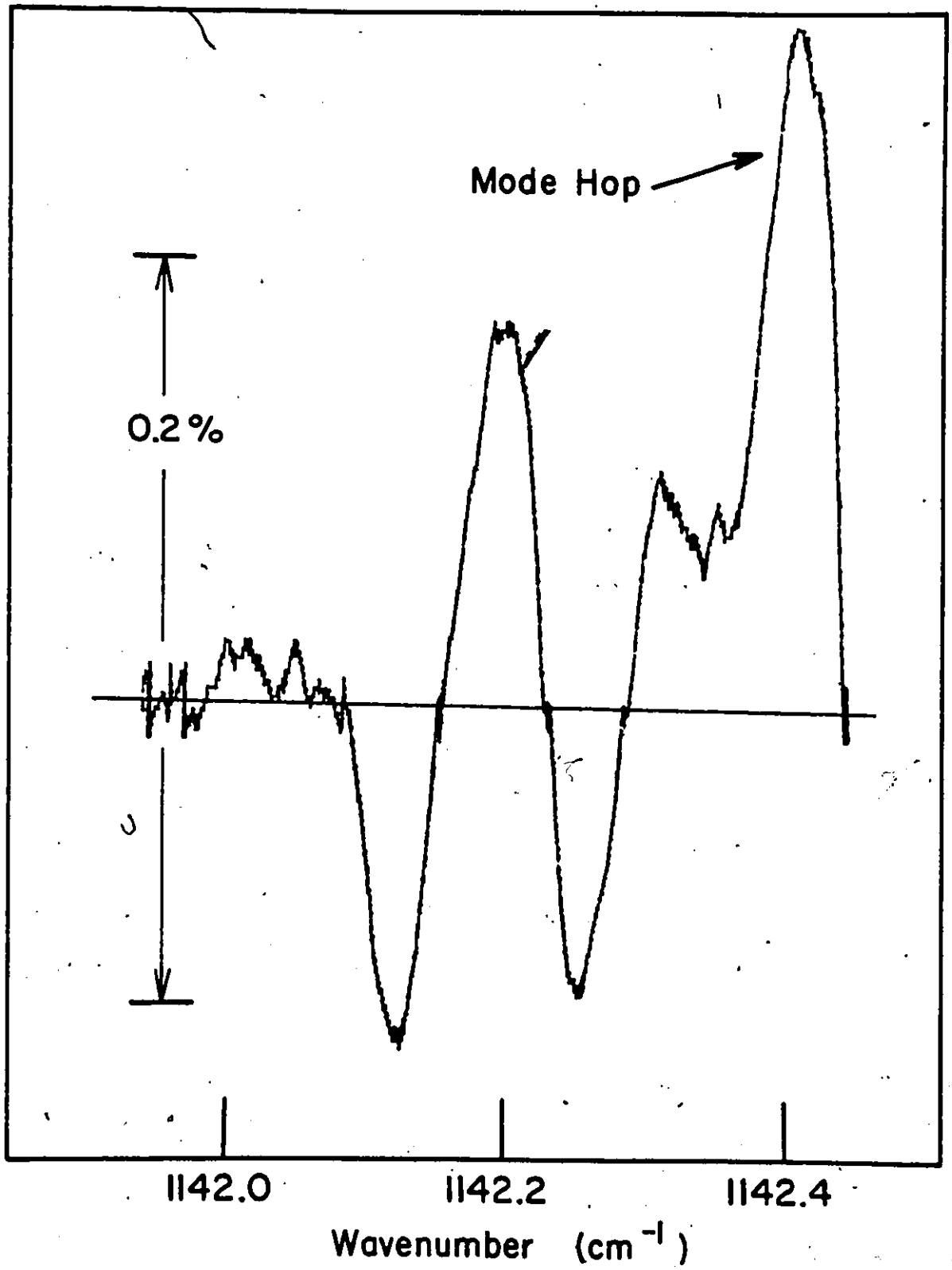
Mode Hop
0.2 %
1142.0
1142.2
1142.4
Wavenumber (cm^{-1})

open air we also examined sensitivity using a 5 m multipass cell filled with air at atmospheric pressure. The multipass cell allows the path length to be quickly varied between 40 and 240 m. Figure 4.8 shows the results of such an experiment carried out with the laser wavelength fixed at the line centre of an N_2O line. The observed incremental absorption of 0.25% is in reasonable agreement with the value of 0.29% calculated from the AFGL [64] data and an assumed atmospheric N_2O concentration of 300 ppb [65]. To determine the reproducibility of this technique the multipass cell was filled with pure N_2 and the path length changed repeatedly from 40 to 240 m. A slight shift of base line was observed with the changing alignment, and this shift limits the accuracy of these measurements to 0.01%. The inset trace of Fig. 4.8 illustrates the reason for this shifting base line. The use of sixth harmonic detection reduced the background signal to below ~0.01%. At this level of sensitivity we begin to observe optical fringes or chanelling spectra equivalent to a Fabry-Perot etalon of ~4 cm spacing. As the optical alignment is changed these fringes shift and hence cause an apparent base line shift at a fixed wavelength.

We have developed the present techniques to the stage where optical fringes of the type shown in Fig. 4.8 limit our sensitivity. Alignment changes, including the effects of turbulence, cause these fringes to alter and hence make base line levels indeterminate at the 0.01 to 0.02% level. We have attained this same level of sensitivity over path lengths ranging from 1 to 240 m in the open air and also over a folded 200 m path length in a multipass cell. Thus we can detect

Figure 4.8

Results obtained in a multipass cell. For the lower trace the laser wavelength is set to line centre of an N_2O line at 1145.331 cm^{-1}. As the path length is changed from 40 m to 240 m the sixth harmonic signal increases, corresponding to an incremental absorption of 0.25%. The inset is a scan of the demodulated sixth harmonic signal as a function of wavelength taken for a path length of 240 m in pure N_2. Optical fringes are clearly visible in this trace.

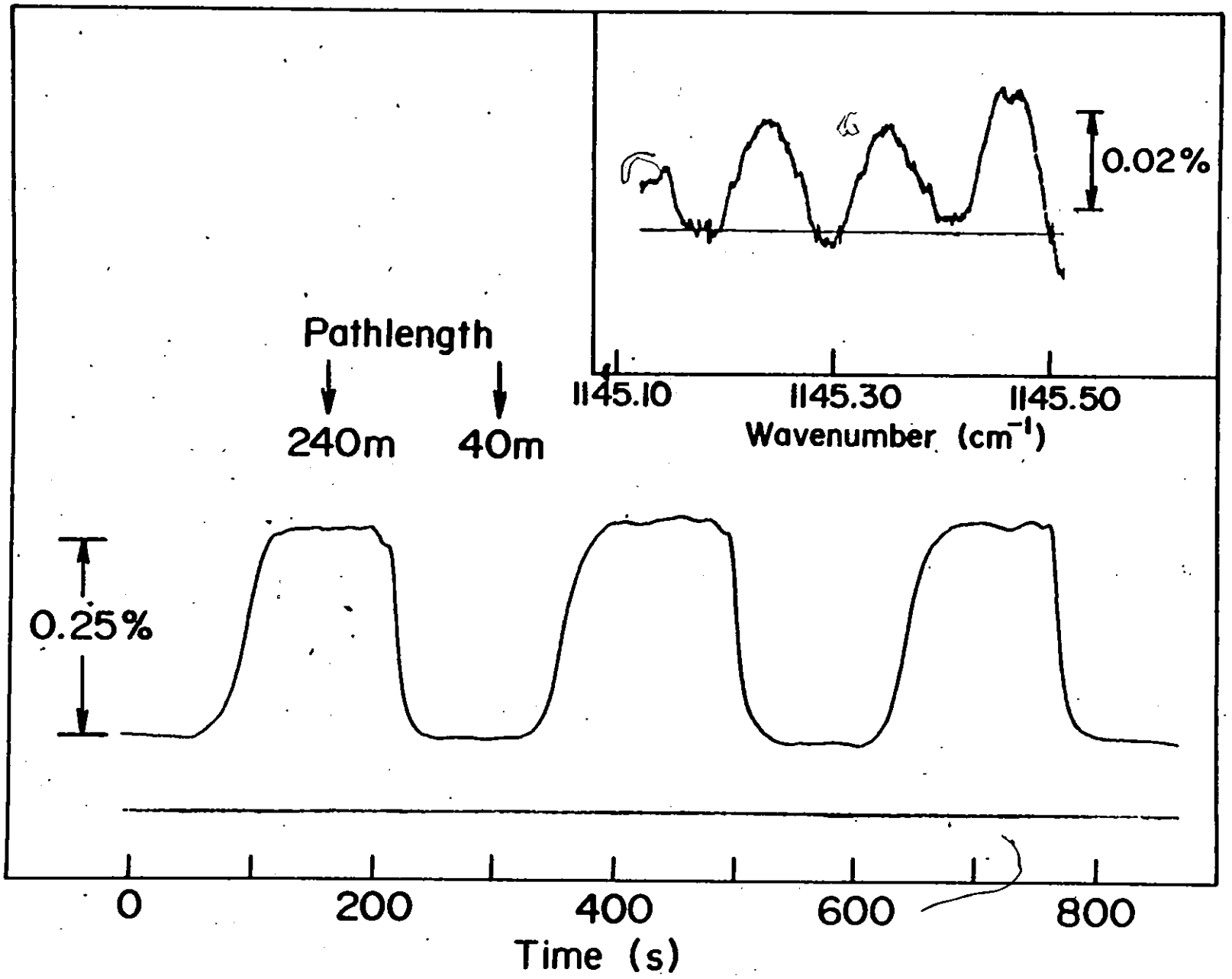
0.02%
1145.10
1145.30
1145.50
Wavenumber (cm⁻¹)
Pathlength
240m
40m
0.25%
0
200
400
600
800
Time (s)

76b

isolated absorption lines in the atmosphere with a sensitivity of $\sim 10^{-6}$ m^{-1} for a measurement time of a few seconds.

4.7 Interferences

One of the problems associated with any atmospheric monitoring system is the lack of control over the composition of the sample to be analysed. All the constituents of the atmosphere, by definition, are present and these constituents may produce absorptions near the absorption of interest. One of the advantages of a tunable diode laser system is the ability to monitor on lines which have minimum interference. For systems using harmonic detection, one has the additional option of reducing the depth of optical frequency modulation m to minimize the effects of the nearby absorption. The reduction in interference possible by reducing the depth of modulation is illustrated in Fig. 4.9. Trace a of Fig. 4.9 is a direct detection scan at low pressure. The fundamental absorption, labelled A, and the weaker line B are 0.1983 cm^{-1} apart. For the purposes of demonstration, the gas pressure for scans b and c was 300 Torr. At this pressure, lines A and B are separated by 6.48 $\Delta\nu$, where $\Delta\nu$ was taken from Ref. [64] and scaled to a pressure of 300 Torr. When the depth of modulation m is large, the lines A and B are not resolved. Line A masks or interferes with B. For small m, the lines are clearly resolved. The asymmetry of the fundamental line is due to the unlabelled absorption 0.0344 cm^{-1} to the right of A. The results are in good agreement with the theoretical predictions presented in Fig. 2.8. Sixth harmonic detection was used

Figure 4.9

Demonstration of the reduction of interferences possible by decreasing the depth of modulation.

(a) Low-pressure scan over the region of interest indicating the separation of the interfering line A and line B, absorption of interest.

(b) m = 4.5. The interfering line masks line B.

(c) m = 2.1. Both lines are resolved. The scale for trace b is 2.5 x less sensitive than for trace c. Agreement with the data of Fig. 2.8 is excellent. Sixth harmonic detection was used.

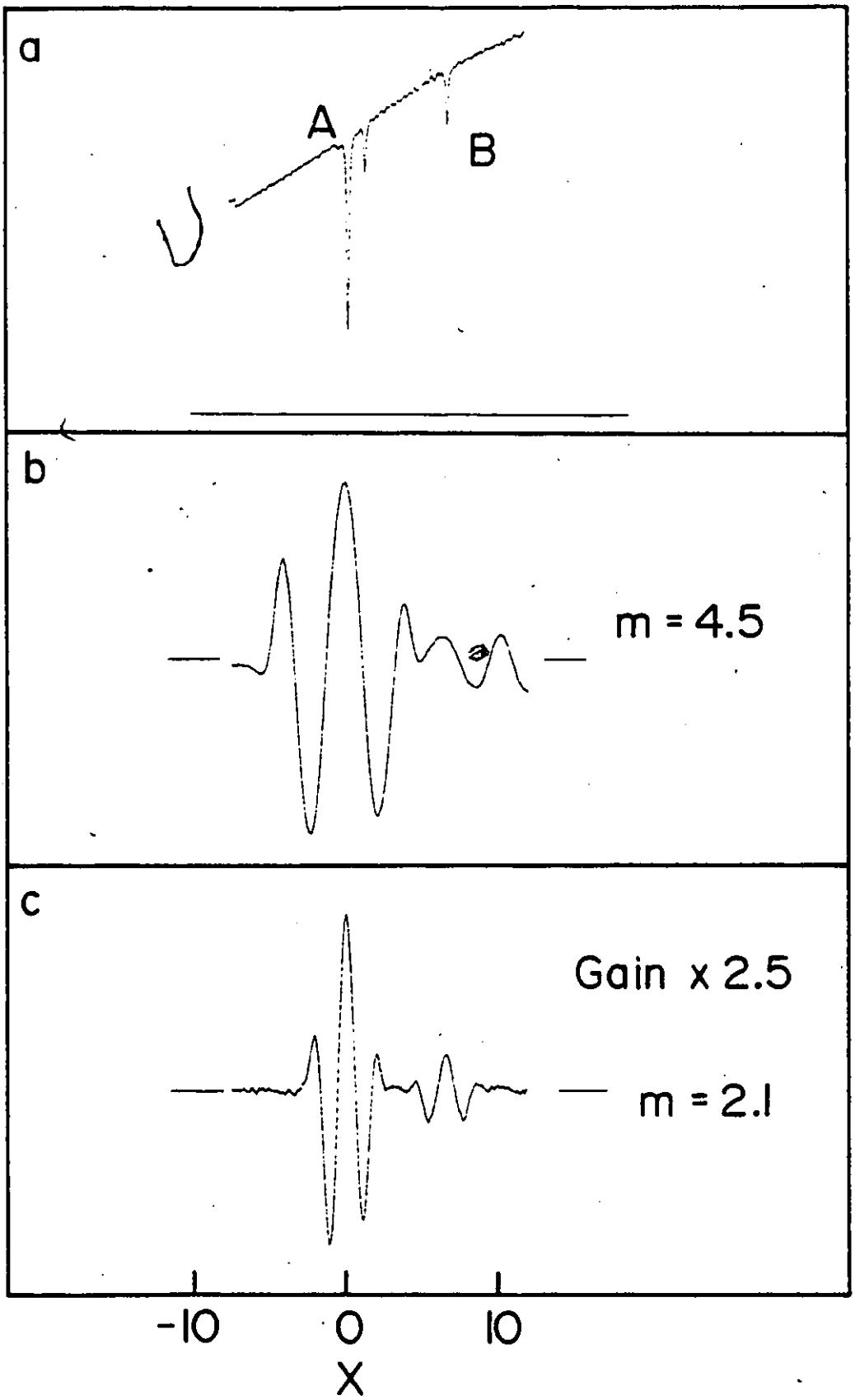
a
A
B
b
m = 4.5
c
Gain x 2.5
m = 2.1
-10
0
10
X

for scans b and c.

Another source of interference are the mode hops characteristic to the lead-salt diode lasers. When using harmonic detection a strong mode hop looks similar to a 10% absorption line. The interference and distortion from mode hops adjacent to lines of interest can be reduced by decreasing the depth of modulation. Clearly, the price paid for avoiding interferences from mode hops and foreign gases is a decreased signal level. Between scans b and c of Fig. 4.9 there is a 2.5x scale change.

The data displayed in Fig. 2.8 may be used to estimate the amount of interference a nearby absorption will contribute. From Fig. 2.8, the interfering line will contribute $\leq$ 1% of its line centre value to the neighboring line provided it is ~ $4\Delta\nu$ away. Lines separated by < $4\Delta\nu$ will suffer more interference.

In concluding this discussion on interferences we mention that, with a tunable diode laser monitoring system, one can always measure the strength of the interfering line and then subtract off the interference. We also mention that interferences have not posed a major problem in any of our investigations to date. We have always been able to pick regions where there is little interference and have been able to minimise any residual interference by a proper choice of the depth of modulation. The immunity to interference which we observed is in contrast to other atmospheric pressure monitoring systems where interfering species, particularly water, pose severe problems [56-58].

4.8 Harmonic Detection of Band Structure Absorptions

To this point we have only considered the detection of isolated absorptions. Many molecules, of which SO_2 and NO_2 are examples, posses complex spectra. This section demonstrates that it is possible to detect complex spectra with sensitivities comparable to the results already presented.

Atmospheric SO_2 is of interest for the role it plays in air pollution and acid rain. Detection of SO_2 is difficult because of the combination of small ambient concentration, relatively weak line strength, and complex absorption spectra. SO_2 is not a linear molecule. The absorption lines appear to be randomly spaced and closely packed -- so closely packed that at atmospheric pressure the lines coalesce to form a strong absorption continuum. Nevertheless, spectral regions for which there are significant changes in absorption over ~0.1 cm^{-1} spacing exist. Direct detection scans over one such region are shown in Fig. 4.10. The average transmission for the atmospheric pressure scan was ~35%. The low transmission at atmospheric pressure indicates the degree of overlapping of lines and the strength of the absorption continuum relative to the changes in absorption. Harmonic detection of SO_2 is possible by utilizing the changes in absorption. One of the changes in absorption and the low-pressure lines which coalesce to form the absorption change are illustrated in Fig. 4.10. In general, the harmonic line shape will not be symmetric about the peak absorption. We experimentally determined that harmonic detection of the SO_2 absorption profile is as sensitive as detection of an isolated line. Although many

Figure 4.10

Absorption of SO_2 at low pressure (~30 Torr) and atmospheric pressure.

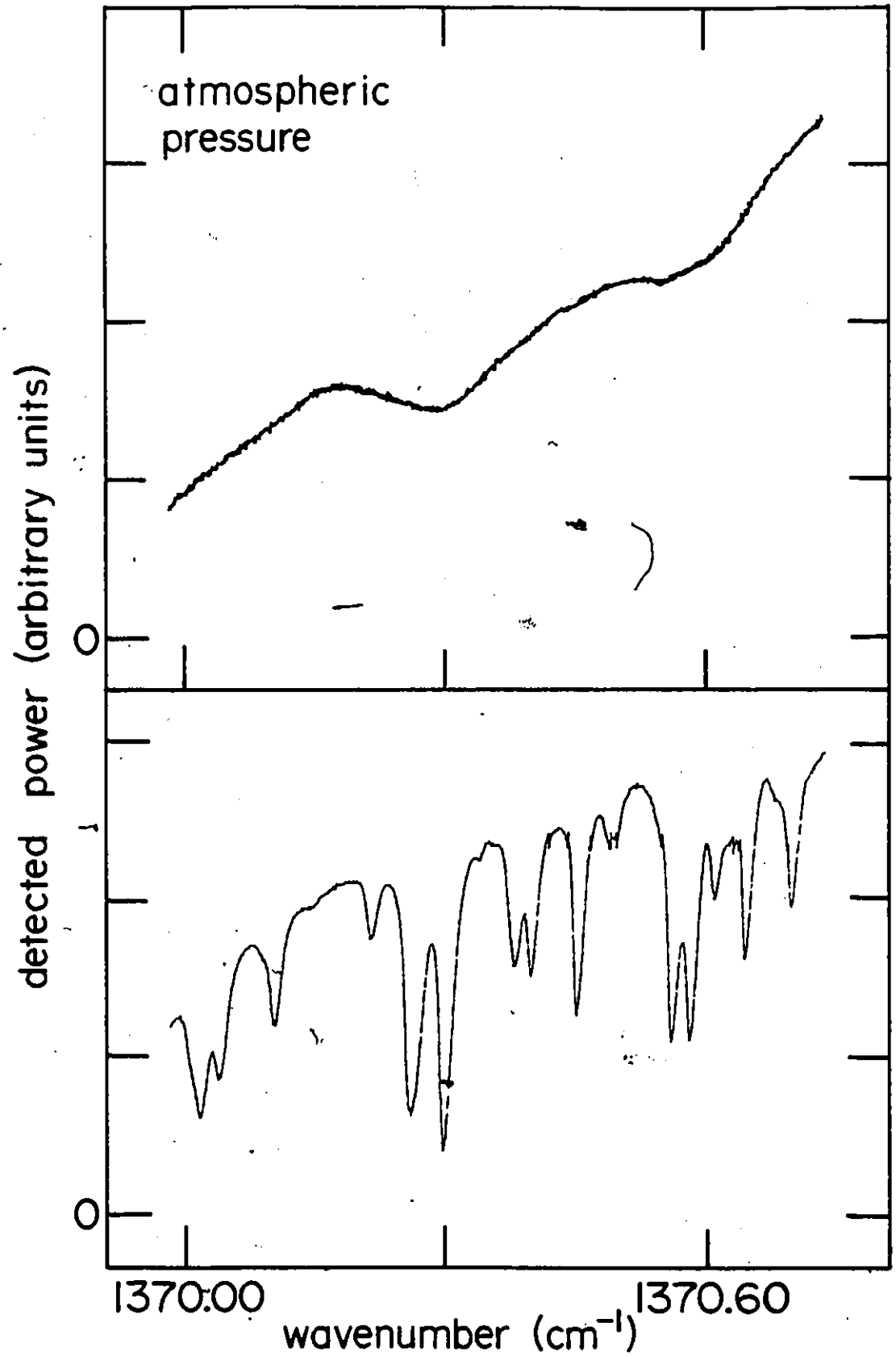
atmospheric
pressure
0
detected power (arbitrary units)
0
1370.00
1370.60
wavenumber (cm⁻¹)

lines overlap to form the continuum, in several regions these lines overlap in such a manner that harmonic detection of the resultant structure is as sensitive as detection of an isolated line.

To identify potential regions where harmonic detection could be successfully applied we calculated the absorption coefficient for SO_2 at atmospheric pressure. The line positions for SO_2 [66] were linearly interpolated and quantized at 0.01 cm^{-1} intervals. The quantized data were convolved with a Lorentzian absorption profile of the appropriate width and the resulting absorption coefficient[a] tabulated at 0.05 cm^{-1} intervals. The transmission calculated from this data agreed with the data of Fig. 4.10 to within $\pm 5\%$. Theoretical data and experiment were normalized at one wavelength. In addition to the absorption data, first, second, and fourth harmonic signals were tabulated. Figure 4.11 shows an experimentally measured fourth harmonic signal and the calculated fourth harmonic signal. Reasonable agreement between theory and experiment exists. Therefore the computer data are useful to predict spectral regions where maximum sensitivity may be obtained.

Table 4.1 lists regions where the fourth harmonic signal was calculated to be large and lists the calculated absorption coefficient and fourth harmonic signal. To place the numbers of Table 4.1 in perspective, the absorption coefficient and fourth harmonic signal for an isolated, atmospheric pressure broadened transition are given below. The strongest absorption in the ν_3 band of SO_2 consists of a doublet of

---

[a]See the note at the bottom of Table 4.1.

Figure 4.11

Experimental and calculated fourth harmonic signal for detection of a band structure absorption. The calculated harmonic signal was normalised to the experiment at one wavelength.

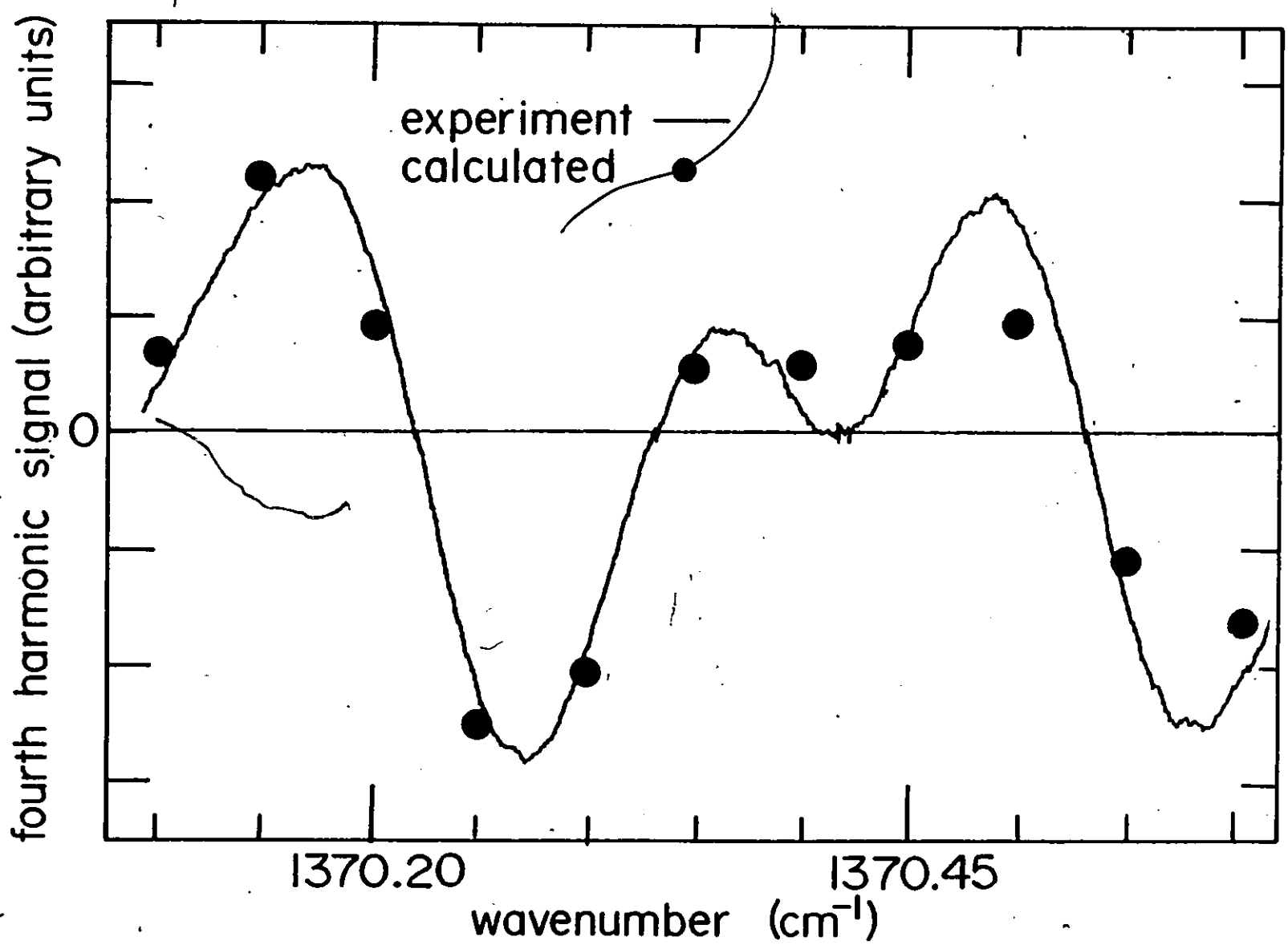
experiment
calculated
fourth harmonic signal (arbitrary units)
0
1370.20
1370.45
wavenumber (cm^{-1})

Fig 4

Table 4.1

Calculated Atmospheric-Pressure Absorption Parameters for the ν_3 Band of SO_2

Position (cm^{-1})	Absorption Coefficient ($x10^{-20}$ cm^{-2}/molecule)[a] DIRECT DETECTION	FOURTH HARMONIC DETECTION
1338.50	41.95	-3.02
1344.40	63.55	-3.08
.45	62.12	-3.21
1346.80	67.40	3.33
1347.00	87.25	-3.34
.10	71.09	3.18
.60	69.82	-3.15
1348.30	90.33	-3.93
.35	90.62	-4.15
1353.25	53.88	-3.12
.95	68.65	-5.39
1354.00	65.64	-3.30
.10	48.60	3.01
1356.70	60.74	-3.18
1361.25	108.8	[illegible].28
.35	104.4	3.14
1369.40	69.08	-3.30
.80	69.18	-3.98
.90	66.61	3.26
1370.15	75.45	4.11[b]
.25	88.62	-4.35[b]
.30	91.17	-3.61[b]
1372.85	103.0	-3.89
.95	98.24	3.33
1373.05	90.55	-3.32

Table 4.1 (continued)

Position (cm^{-1})	Absorption Coefficient ($x10^{-20}$ cm^{-2}/molecule)[a] DIRECT DETECTION	FOURTH HARMONIC DETECTION
1375.00	85.68	4.05
.10	104.7	-4.33
.60	71.58	3.13
.70	81.99	-3.63
1377.25	85.02	-5.63
.35	82.00	3.87
.70	83.57	3.11
.80	80.52	-3.09
.85	77.37	-3.48
1378.85	82.84	-3.21

[a]We use the term absorption coefficient somewhat loosely. To convert the given number to an extinction coefficient, it is necessary to multiply by the number of absorbing molecules/cm^3. Only the parameters for the fourth harmonic signal greater than 3 are listed.

[b]This region is graphed in Fig. 4.11 and Fig. 4.10.

combined strength 2×10^{-19} cm^{-4} and occurs at 1370.29 cm^{-1} [66]. The fourth harmonic signal expected from this isolated line (calculated using the computer code used to compile the data for Table 4.1) is 3.70×10^{-20} cm^{-4}. As can be observed in Table 4.1, there are several regions where the harmonic signal from the band structure absorption is expected to be larger than the harmonic signal from an (hypothetical) isolated line of maximum strength.

The data presented in Figs. 4.10 and 4.11, and Table 4.1 clearly demonstrate that high-sensitivity detection by harmonic techniques is not limited to the detection of isolated absorption lines. Harmonic techniques may be used whenever a molecular band has significant changes in absorption over a ~0.1 cm^{-1} frequency range.

4.9 Summary

A detailed investigation of high-sensitivity detection of atmospheric pressure absorptions is reported in this chapter. The limiting noise sources are identified and detection schemes which possess a certain amount of immunity to the noise are described and applied to the detection of trace gases. As a result, a significant increase in the sensitivity of open-path monitors employing tunable diode lasers and harmonic detection is reported. The question of interferences from adjacent absorptions and the harmonic detection of band structure absorptions is also studied in this chapter. It is revealed that monitors based on tunable diode laser technology suffer only minimally from interferences and that high-sensitivity detection of molecules

which possess complex absorption spectra is possible provided a significant change in absorption occurs over a ~0.1 cm^{-1} spectral region.

The limiting noise sources are found to be due to a background signal which varies with alignment and the deleterious effects of optical feedback on the laser output. The contribution of the background signal to the limiting noise can be made negligible by detecting at the higher harmonics and modulating at as low a frequency as possible. Feedback can be reduced in the coaxial optical arrangement used for open-path monitors with the use of attenuators and apertures. By applying the noise reducing techniques outlined above we achieved a noise level equivalent to an optical absorption of 0.01% for path lengths up to 250 m long. This result represents a significant increase in sensitivity over that previously attained. The factors which presently limit the sensitivity of the absorption measurements are well understood. One problem involves feedback to the diode laser from the retroreflector which defines the measurement path. A noncoaxial transmit-receive arrangement will eliminate the need for feedback-reducing attenuators and hence allow integration times to be shortened. The remaining problem is one of optical fringes, which we suspect are caused by spurious reflections in the cold head containing the diode laser and in the detector. Efforts to eliminate the optical interference fringes should further improve the system sensitivity.

Open-path monitoring of trace gases in the atmosphere has many practical applications. <u>In situ</u> detection of pollutants over long path

lengths and the monitoring of stack emissions are two obvious examples. The open-path monitoring system described in Chapter 4 may also be used to measure the ambient levels of reactive gases such as NH_3 which are difficult to detect with other techniques. The versatility and speed of response of a tunable diode laser spectrometer should make it useful for field measurements of trace gases and possibly for the determination of dry deposition rates of a variety of gases. Table 4.2 lists several gases of atmospheric interest, with the detection levels which correspond to our present sensitivity of $\sim 10^{-6}$ m^{-1}.

This section concludes the investigation on open-path monitors. The next chapter is devoted to the study of rapid sweep techniques for the fast accumulation of absorption data over a ~ 0.4 cm^{-1} spectral region.

Table 4.2

Minimum Detectable Concentration for Several Molecules of Atmospheric Interest. Concentrations are Quoted for Detection at Atmospheric Pressure and a Sensitivity of 10^{-6} m^{-1}.

Molecule	Spectral Region (cm^{-1})	Comments	Concentration (ppb)
N_2O	1145	Isolated line	20
	2240	Isolated line	0.1[a]
CH_4	1304	Isolated line	2
CO	2111	Isolated line	0.25
CO_2	2336	Isolated line	0.03[a]
NH_3	1103	Five overlapping lines	0.5
	1074	Isolated line	0.75
HNO_3	1334	Band structure	0.35[a]
NO	1890	Doublets	0.5
NO_2	1610	Band structure	0.5[a]
SO_2	1360	Band structure	3
	1140	Band structure	12

[a] In these spectral regions a sensitivity of 10^{-6} m^{-1} may not be attainable due to severe attenuation of the laser beam by the atmosphere.

CHAPTER 5

HIGH-SENSITIVITY DETECTION USING SWEEP INTEGRATION

The previous chapters have been mainly concerned with the application of harmonic methods to the high-sensitivity detection of trace gases. The principal subject of this chapter is data acquisition by sweep integration using presubtraction. Use of the sweep integration technique allows direct determination of line shapes and linewidths from the recorded data, and enables one to carry out rapid searches of ~0.4 cm^{-1} spectral intervals. The sweep integration method is described in Sections 5.1 - 5.4.

A successful effort to improve upon the minimum sensitivity of harmonic detection of low-pressure gases using concepts discussed in Chapter 4 is reported in Section 5.5. Section 5.6 contains a short discussion of the material of Chapter 5 and Section 5.7 summarizes the chapter.

5.1 Introduction

In recent years tunable diode lasers have been used extensively to monitor trace gases. The most sensitive technique employs harmonic detection, which works well in pollution monitoring applications where the feature of interest is solely the strength of the line centre absorption over a given path length [15-18,20,21,43,48,54]. However, identifying the shape of the absorption features is complicated due to

the mathematical transform which relates the actual line shape to the line shape observed in harmonic detection [45-47]. This identification problem is particularly acute for doublets, triplets, and other closely spaced lines. When one is interested in fundamental quantities such as line position, linewidth, and line shape the confusion introduced by harmonic techniques via the transform may not be desirable.

Jennings [19] described a method of direct detection which displays the optical transmission through a sample directly as a function of wave number. In addition the wave number linearity and stability of the technique, which he denoted as sweep integration, is much improved over previous work [68]. Sun et al. [69] reported similar results. We extended the method of Jennings [19] to enable the detection of absorptions as small as 10^{-3}% over path lengths of up to 200 m. This is a substantial improvement in sensitivity and compares favourably with the minimum detectable absorptions reported for second harmonic detection [15]. We have also investigated the application of this modified technique to the detection of gases at atmospheric pressure. We find the minimum detectable differential absorption at atmospheric pressure to be 10^{-3}% for path lengths of a few metres.

In the following sections we describe the apparatus, discuss the techniques employed, and present some experimental results.

5.2 Method

A schematic diagram of the apparatus is shown in Fig. 5.1. The output of the lead salt laser is collimated by an f/1 lens and directed

Figure 5.1

Schematic diagram of the apparatus and signal processing electronics used for the sweep integration technique.

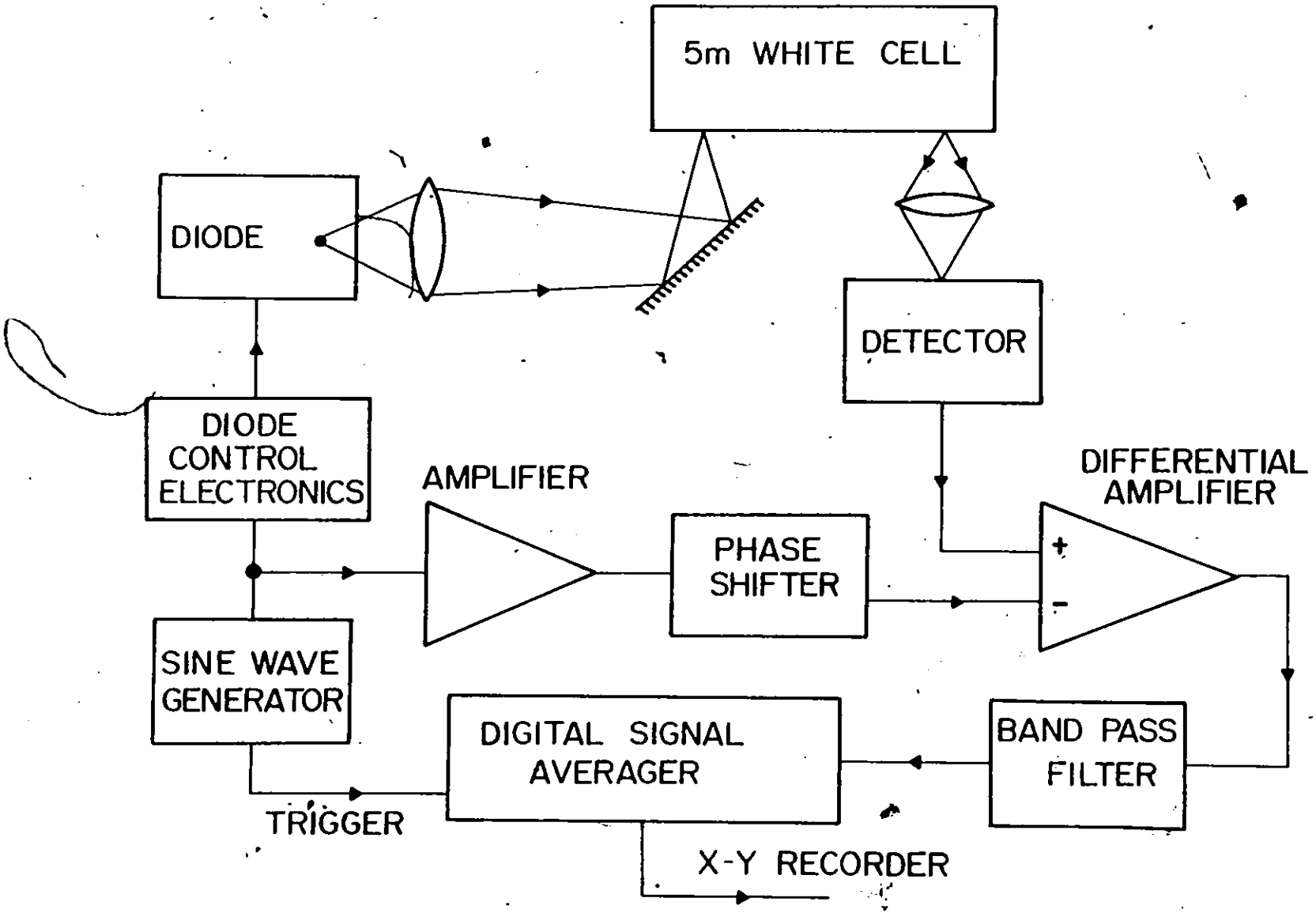
5m WHITE CELL
DIODE
DETECTOR
DIODE CONTROL ELECTRONICS
AMPLIFIER
PHASE SHIFTER
DIFFERENTIAL AMPLIFIER
+
-
SINE WAVE GENERATOR
DIGITAL SIGNAL AVERAGER
BAND PASS FILTER
TRIGGER
X-Y RECORDER

by mirrors either through a 5 m base path White cell or directly to a HgCdTe detector. The temperature of the laser heat sink and the steady state injection current are adjusted to give single mode operation in the spectral region of interest. Further details of the apparatus are given in previous publications [15,48] and chapters; the only major change is the method of signal processing.

Data acquisition is by the sweep integration technique [19]. The diode control electronics are set to repeatedly sweep the laser wavelength through a spectral region of ~0.4 cm^{-1} by applying a 200 Hz modulation to the injection current. The optical transmission recorded on each sweep is digitized and stored in the 1024 memory locations of the signal averager [70]. The signal averager is triggered by the laser sweep modulation so that successive sweeps can be averaged. The transmission measured during each sweep is averaged with the previously recorded scans until the noise is reduced to an acceptable level. This is in contrast to conventional techniques [15,48], where the wavelength is slowly swept once through the spectral region of interest while a long time constant is used to reduce the noise. Our sweep frequency is substantially higher than that used by Jennings [19]. We use as high a frequency as possible (limited by the 5 μs/data point acquisition speed of the signal averager) in conjunction with a high-pass filter at the input to the signal averager to attenuate the low-frequency noise of the laser [71]. The high pass filter is designed to give maximum attenuation of the low frequency noise while causing a minimum distortion to the detected line shapes. At these high sweep frequencies

we find that sine wave modulation is just as effective as the more conventional sawtooth [19] in producing a linear wavelength sweep and is much more suited to the signal processing described below.

The chief obstacle to obtaining high sensitivity with the sweep integration technique is the substantial change in laser output power produced by a 0.4 cm^{-1} tuning of the diode laser. Wavelength tuning of this amplitude results in an intensity modulation at the same frequency as the sweep modulation, with a magnitude which is typically equivalent to ~20% absorption. As we are interested in detecting absorptions of 10^{-3}% in the presence of this large intensity modulation, we use an analog circuit to null the intensity modulation before quantizing the signal. An amplifier, phase-shifter, and differential amplifier are used in the configuration depicted in Fig. 5.1. The results obtained by carrying out this presubtraction are indicated in Fig. 5.2. The upper trace shows the detector output as the diode laser injection current is sinusoidally modulated at a frequency of 200 Hz. The waveform of the detector output closely follows the sinusoidal current modulation as no absorbing gases are present in the optical path. The middle trace shows the signal recorded by the digital signal averager after an optimally amplified and phase-shifted 200 Hz signal has been subtracted. The remaining signal is reduced in amplitude by two orders of magnitude and is now composed predominantly of the second harmonic of the sweep frequency. A second analog circuit (not shown in Fig. 5.1) performs presubtraction of the second harmonic, yielding the residual signal shown in the lower trace of Fig. 5.2.

Figure 5.2

Demonstration of improvement in sensitivity by performing presubtraction. Trace a shows the intensity modulation caused by wavelength tuning, while Traces b and c indicate the remaining intensity modulation after the first harmonic and the first and second harmonic have been subtracted. For demonstration purposes several periods of the modulating waveform are shown. Normally the digital signal averager is set to trigger at point D and end the sweep at point E. Points D and E are separated by 0.17 cm^{-1} in this example.

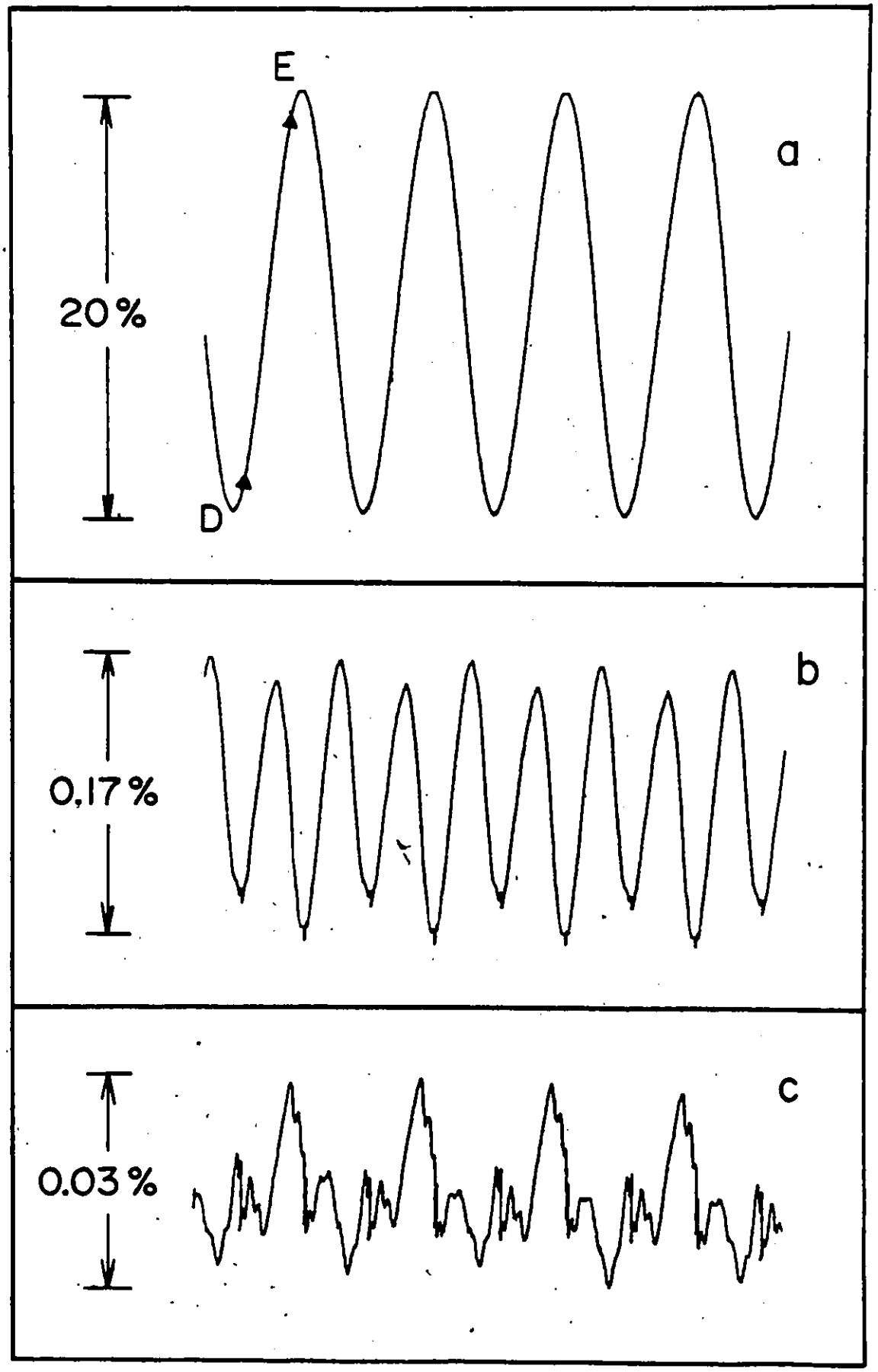
E
D
20%
a
0,17%
b
0.03%
c

One advantage of the presubtraction technique illustrated in Fig. 5.2 is that it substantially reduces the dynamic range required of the input channel of the signal averager. In the absence of presubtraction any absorption lines will be displayed on a sloping background with an amplitude of ~20%. Presubtraction reduces the background amplitude to ~0.03%, thus allowing the full scale input sensitivity to be increased by a factor of almost 1000. Presubtraction reduces the number of input bits or averaging time required to achieve a given resolution. The input channels of the signal averager use 9-bit analog-to-digital converters [70], and, therefore, have 512 quantization levels. Hence, when measuring a weak absorption line using presubtraction, the bit quantization noise is (0.03/512)% = 6×10^{-5}% for a single sweep. In the absence of presubtraction 19-bit analog-to-digital converters would be required for the same resolution.[a]

The presubtraction technique described above enables absorption features in a 0.2 to 0.4 cm^{-1} region to be displayed on a background which is flat to ~0.03%. However, if one wishes to detect very weak absorptions, a further increase in sensitivity may be attained by one of two methods. For very high-sensitivity work we utilize the reproducible nature of the background and subtract measurements made with the

---

[a] The bit quantization noise, or resolution, can also be improved by averaging. If N is the number of traces averaged over, the bit quantization noise should reduce as $\sqrt{N}$. For a 9-bit input channel and an intensity modulation of 20%, 4.4×10^5 summations would be required to attain a resolution of 6×10^{-5}%.

absorber present from measurements made with no absorber in the beam. This reduces background variations to < 0.01%, and allows detection of absorption lines with as little as 0.001% line centre absorption. The degree of success of the background subtraction depends on the stability of the optical alignment. The same portion of the beam must be detected for measurements performed with the absorber present and with the absorber absent. For data accumulation systems which are interfaced to a digital computer the background may be removed without the need for a measurement of the 100% transmission level. The remaining background, which consist predominantly of the first and second harmonic (compare Fig. 6.2), can be minimized by a mathematical manipulation of the data. Further signal processing in this manner would eliminate the need for a highly stable alignment and decrease the time spent recording data by not requiring a measurement of the 100% transmission level.

Results are presented in Sections 5.3 and 5.4.

5.3 Detection of Gases at Low Pressure

The tunable diode laser used to obtain the data shown in Fig. 5.2 lases in the spectral region between 1200 and 1400 cm^{-1}. Rather than demonstrate sensitivity by monitoring a trace gas such as SO_2 [48], we chose to extend previous work on hydrogen quadrupole [72] and oxygen quadrupole [73] transitions by searching for quadrupole transitions in CO_2. Our goal was to observe quadrupole transitions in the $[00^00 \rightarrow (10^00)_I]$ or $[00^00 \rightarrow (10^00)_{II}]$ bands, both of which are electric dipole forbidden. Single mode operation of the diode laser could be obtained

in the 1285.5 cm^{-1} region, which includes the Q-branch of the $[00^{o}0 \rightarrow (10^{o}0)_{II}]$ band [74]. Data acquisition by sweep integration is ideal in this case. We expect the Q-branch lines to be spaced by ~0.025 cm^{-1} which would make interpretation of second harmonic data difficult. To carry out the experiment we aligned the laser beam for a 200 m path length through the White cell, which was filled with CO_2 (Matheson, nominal 99.8% pure) at a pressure of 20 Torr. A total of 32,000 sweeps was recorded using the presubtraction technique, then a further 32,000 sweeps were taken with the White cell evacuated and subtracted from the stored spectrum. Figure 5.3 shows a portion of the result as read out of the signal averager memory onto an X-Y recorder. Note that the absorptions appear as such; there is a direct relationship between the recorded absorption profile and the actual absorption profile. Using AFGL data [64,66] and reference gas cells we were able to identify most of the observed lines as impurities in the CO_2. Note that an N_2O doublet is well-resolved even though the line centre absorption coefficients are only 2×10^{-6} m^{-1} and the individual lines are separated by ~185 MHz. We estimate that the CO_2 sample contains 38 ppb N_2O and 3 ppm CH_4. A Ge etalon was placed in the laser beam to determine the wave number scale for Fig. 5.3. Although a sine wave is used to modulate the injection current, we observe that the tuning rate of the laser is approximately linear in the region removed from the turning points of the modulation.

Based on several scans of the type shown in Fig. 5.3, we estimate that the noise level is equivalent to a line center absorption of ~5 x

Figure 5.3

Absorption spectrum taken through 200 m of CO_2 at 20 Torr. The displayed trace took a total of 6 minutes to record and shows the difference between two scans taken with and without CO_2 in the White cell. Most of the observed lines are identified as being caused by impurities. The anticipated positions of the CO_2 quadrupole transitions are shown along the abscissa.

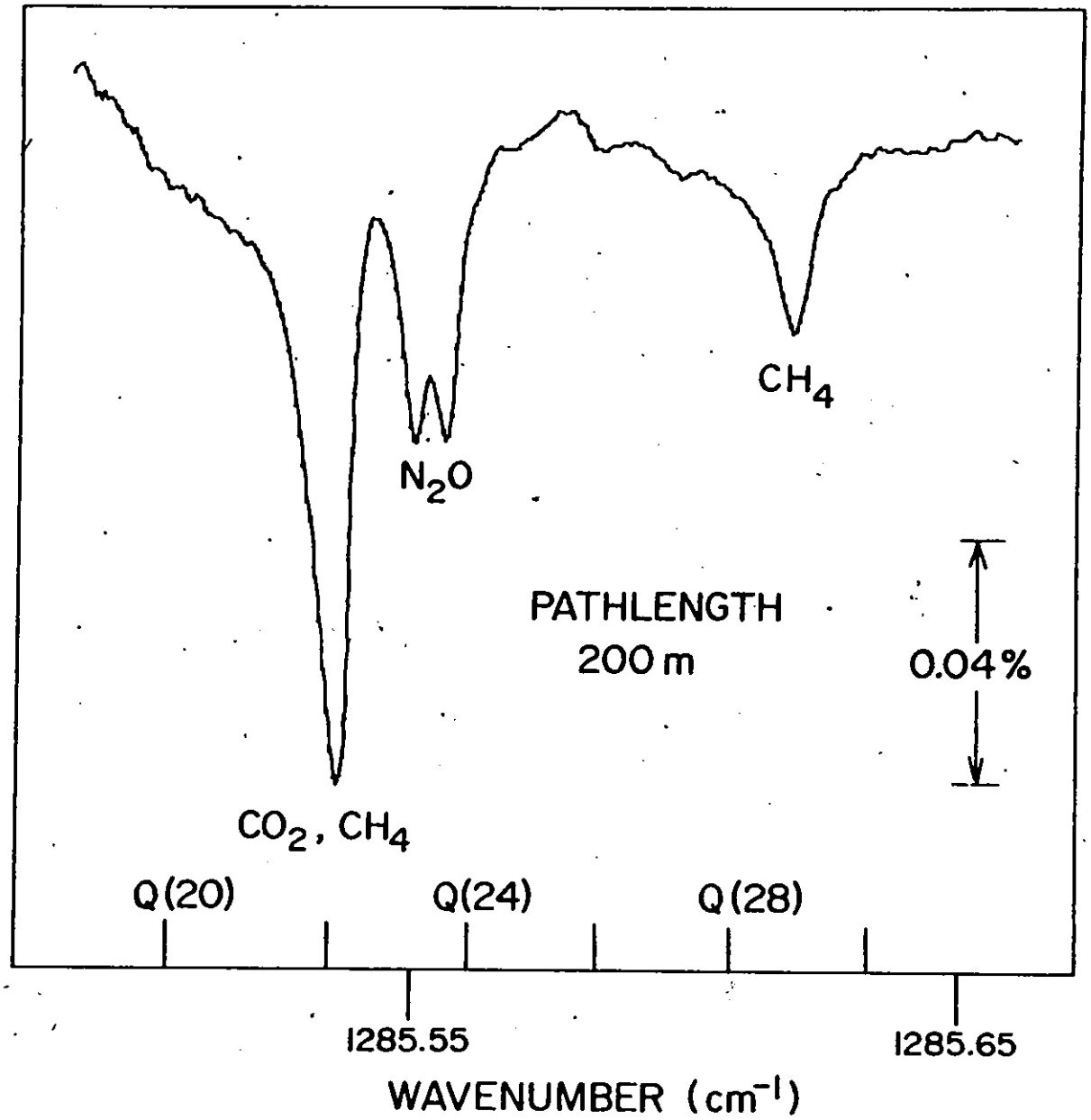
CH_4
N_2O
PATHLENGTH
200 m
0.04%
CO_2, CH_4
Q(20)
Q(24)
Q(28)
1285.55
1285.65
WAVENUMBER (cm^{-1})

10^{-8} m^{-1}. Even with this sensitivity we were unable to observe the Q-branch transitions in CO_2. Thus we can place an upper limit of 10^{-7} m^{-1} on the line centre absorption coefficient of these transitions. If one assumes that the linewidth is similar to that of the electric dipole infrared lines in CO_2, the intensity of the individual Q-branch transitions must be $< 1.3 \times 10^{-29}$ cm^{-1}/molecule. Note that our present sensitivity limit of 5×10^{-8} m^{-1} is approximately the same as the best achieved with second harmonic detection, i.e., 3×10^{-8} m^{-1} [48]. However, in the time it took to measure a single line centre absorption with harmonic techniques the sweep integration method recorded absorption data over a 0.3 cm^{-1} region.

5.4 Detection of Gases at Atmospheric Pressure

The sweep integration method described in the previous sections can be used to detect optical absorptions of 10^{-3}% over a sweep range of ~0.4 cm^{-1}. Hence the technique should be ideal for observing atmospheric pressure absorption lines which have linewidths of ~0.1 cm^{-1}. We have carried out some preliminary work at atmospheric pressure, and have indeed detected atmospheric pressure lines with a sensitivity of 10^{-3}%.

Figure 5.4 illustrates results taken at low pressure and at atmospheric pressure. The diode laser was tuned to sweep over ~0.4 cm centered at 1241.9 cm^{-1}. This region covers two CH_4 lines and one N_2O line, all of which can be observed in air given sufficient sensitivity. For the upper trace of Fig. 5.4, the laser beam was directed through the

Figure 5.4

Traces indicating sensitivity at atmospheric pressure. The upper scan is the recorded absorption due to air in a low pressure calibration cell, while the lower trace is the observed differential absorption at atmospheric pressure when a minute amount of methane was injected along a one metre path length. Scan time was 50 seconds.

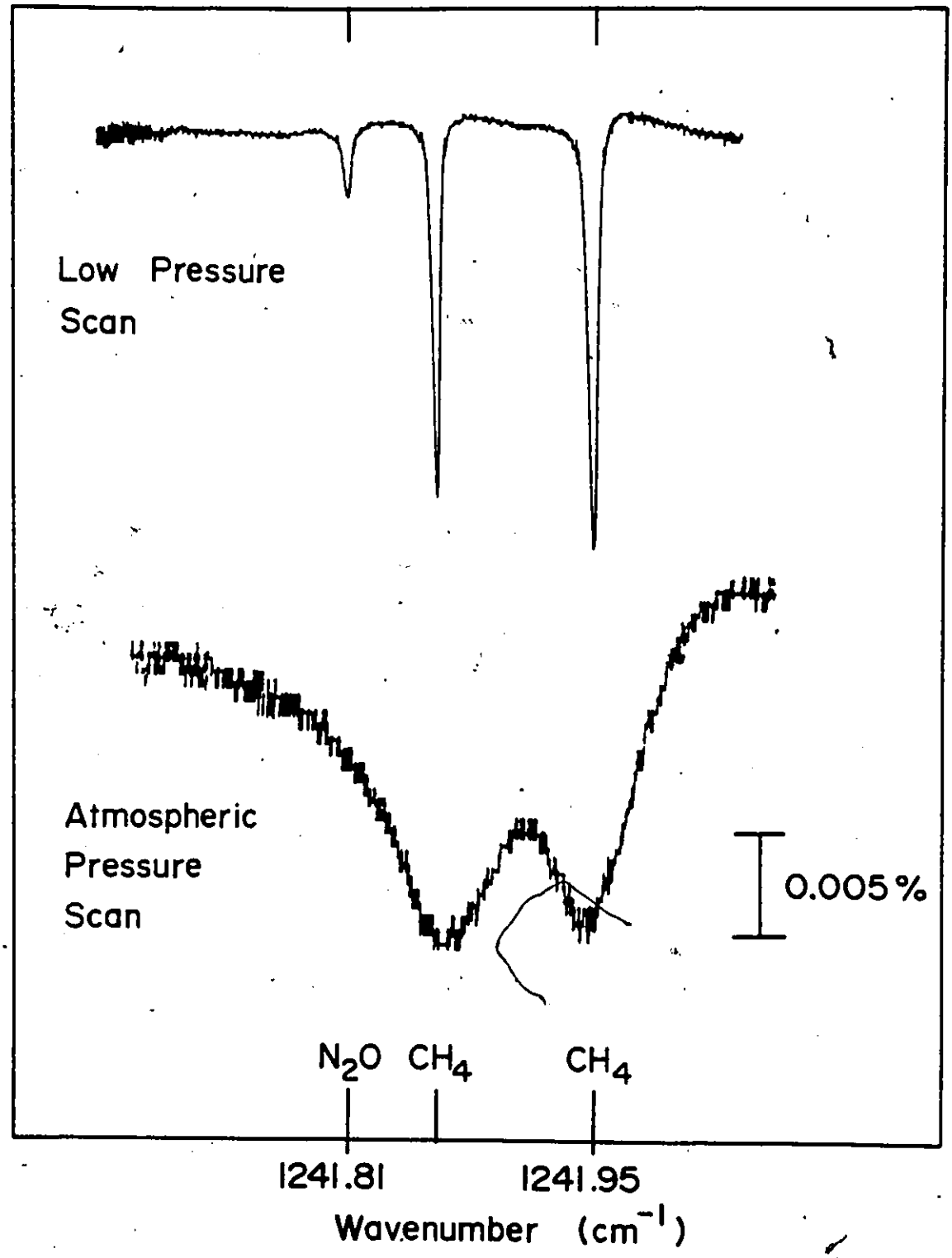
Low Pressure
Scan
Atmospheric
Pressure
Scan
0.005%
N_2O
CH_4
CH_4
1241.81
1241.95
Wavenumber (cm^{-1})

White cell, and 5100 scans were taken with 30 Torr air in the cell. The cell was then evacuated, and a further 5100 scans were recorded and subtracted to give the relatively flat background seen in the upper trace. Superimposed on this background are the three narrow absorption lines caused by N_2O and CH_4 which are naturally present in air. For the lower trace, the laser beam simply traverses a 1 m path in the open air before being focussed on the detector. Initially we injected a minute quantity of methane into this air path and recorded 5100 scans. After a few minutes, the additional methane had dispersed, and we could record a further 5100 scans of normal air. When the two measurements were subtracted, the lower trace of Fig. 5.4 remained, i.e., the differential absorption caused by the injected methane. In this fashion, we can detect atmospheric pressure lines with a sensitivity of 10^{-3}%.

Unfortunately this may not be a very general technique for atmospheric pressure work. To achieve a sensitivity of 10^{-3}% it is essential that the background observed after subtraction be flat over the entire range of the scan. At low pressure the presence of a gently sloping background does not prevent observation of narrow absorption lines. However, when broad atmospheric lines are to be detected, it is difficult to distinguish between background slopes and the lines themselves. In a previous chapter, we showed that the background will only be reproducible when the optical alignment remains identical from scan to scan. Hence, when measurements are made over long path lengths (particularly if turbulence is present) the background changes with time, and the differential measurement described above becomes less

sensitive. Nevertheless, the technique may find application whenever gas concentration changes quickly with time (i.e., in dry deposition measurements) or in the measurement of linewidths at atmospheric pressure in the laboratory.

5.5 Low-Pressure Harmonic Detection

Much research has been carried out in the past on the detection of low-pressure absorption lines using harmonic techniques. To a large extent optimum sensitivity has already been obtained with this technique [48]. However, the systematic study of the noise sources of an open-path monitor which we performed and described in Chapter 4 puts us in a good position to evaluate low-pressure detection. In this section we briefly discuss the results of an investigation of high-sensitivity, low-pressure harmonic detection. Application of the knowledge we gained from the study of open-path monitoring has permitted us to be moderately successful in improving on the best low-pressure sensitivities achieved in the past. We have achieved noise levels equivalent to an absorption coefficient of 3×10^{-8} m^{-1} for a 10 s integration period, as compared to the 100 s time constant required for the best result (3×10^{-8} m^{-1}) reported to date [48].

The principal reason for the improvement in sensitivity is the reduction of optical feedback to the diode laser. It had not been realised in the past that feedback plays a significant role in determining the noise level nor had it been recognized that White cells reflect appreciable amounts of energy back into the source. Feedback is

detrimental to the operation of tunable diode lasers, as can be observed in Fig. 5.5. The data of Fig. 5.5 were displayed by recording the output of the detector with a digital signal averager. The signal averager was operated in a transient record mode so that the signals were not averaged but simply recorded as a function of time. The sinusoidal form of the traces is due to the characteristic intensity modulation which accompanies the sinusoidal injection current modulation. For the traces of Fig. 5.5 a path length of 200 m through an evacuated White cell and a depth of wavelength modulation m appropriate for the harmonic detection of low-pressure absorptions were employed. The upper trace of Fig. 5.5 was recorded with no reduction of the feedback. In the presence of feedback, the frequency of the laser does not sweep in a sinusoidal form. Feedback tends to make the laser frequency lock to one value and then jump to another. The jaggedness of the upper trace is associated with the random frequency and intensity jumps associated with feedback. The magnitude of the jumps can be reduced by decreasing the amount of feedback, as illustrated in the next two traces of Fig. 5.5. For these traces attenuators were placed between the diode and White cell to decrease the feedback by ~10 and ~100 times. The bottom trace of Fig. 5.5 is the noise-free sine wave used to modulate the laser. The dramatic increase in the signal-to-noise ratio possible upon reducing feedback is apparent. For all four traces the signal was electrically amplified so that upon recording, all the traces were approximately the same size. The peak-to-peak height of the intensity modulation was ~4% of the total laser power.

Figure 5.5

Improvement in the signal-to-noise ratio as feedback is reduced. The traces show the instantaneous detector output as a function of time for:

(a) upper trace - no attenuation of feedback.

(b) upper middle trace - ~10 x attenuation of feedback.

(c) lower middle trace - ~100 x attenuation of feedback.

(d) lower trace - sine wave applied to recorder input.

The data were recorded for beam propagation over a path length of 200 m through an evacuated White cell.

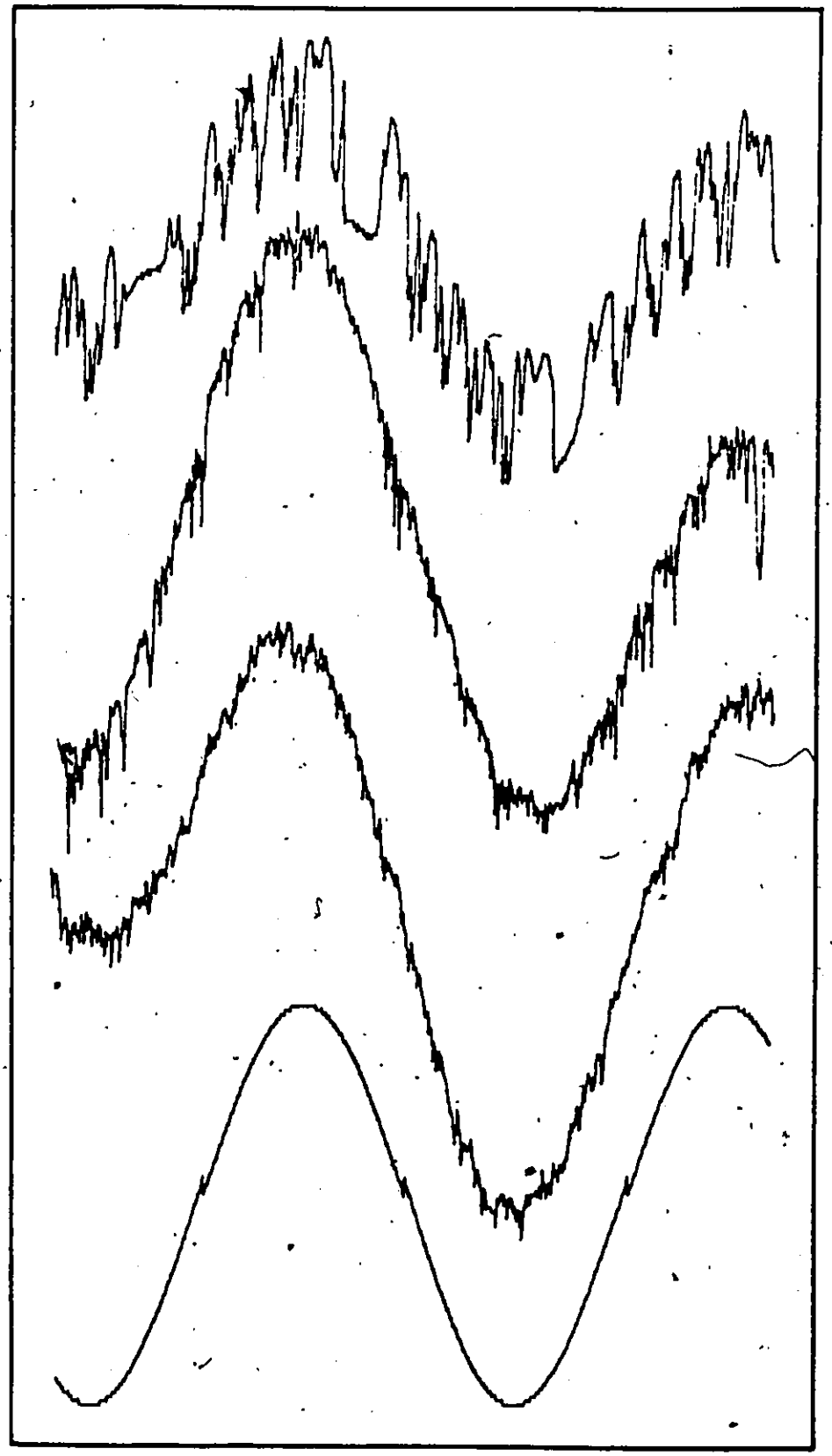

time

A high-sensitivity trace of a weakly absorbing N_2O line at 1241.7487 cm^{-1} is shown in Fig. 5.6. The measurement was performed using fourth harmonic detection and an effective time constant of 12.8 s.[a] A measurement path length of 200 m through laboratory air at a pressure of ~15 Torr was used. The measured absorption of 3.4×10^{-3}% is 5% larger than the value expected [64] for an assumed concentration of 300 ppb N_2O [65] in the lab air. The magnitude of a signal equivalent to $3. \times 10^{-8}$ m^{-1} is indicated in the figure. The small, regular oscillations on the trace are due to optical interference fringes caused by stray reflections within the White cell. In this case the existence of fringes does not significantly limit the sensitivity. The magnitude of the fringes is a sensitive function of the optical alignment. Two-tone modulation techniques, as discussed in Chapter 3, may be employed to further reduce the recorded fringe signal. The fringes are shown as the lower trace of Fig. 5.6. For demonstration purposes the White cell was evacuated and the alignment adjusted to enhance the fringes by 2 ~ 3 times. Although the fringes themselves do not limit sensitivity, they are indicative of a more serious problem. The scattering of light which gives rise to the fringes also causes feedback, an effect which we have shown in this section and in Chapter 4 to be very detrimental to high-sensitivity detection. Before recording the data for Fig. 5.6 an attenuator was placed between the diode and

---

[a] A lock-in amplifier referenced to the fourth harmonic and a time constant of 100 ms was used to recover the signal. The output noise was further reduced by averaging 128 sweeps over the line in a digital signal averager [70].

Figure 5.6

High-sensitivity trace for low-pressure detection. The upper trace is the fourth harmonic signal due to modulating over a low-pressure N_2O line. The bottom traces are magnified fringes (2 ~ 3 x) observable after the gas has been pumped out. The path length was 200 m and the time constant 12.8 seconds. A ~10 x attenuator was used to reduce feedback by ~100 x.

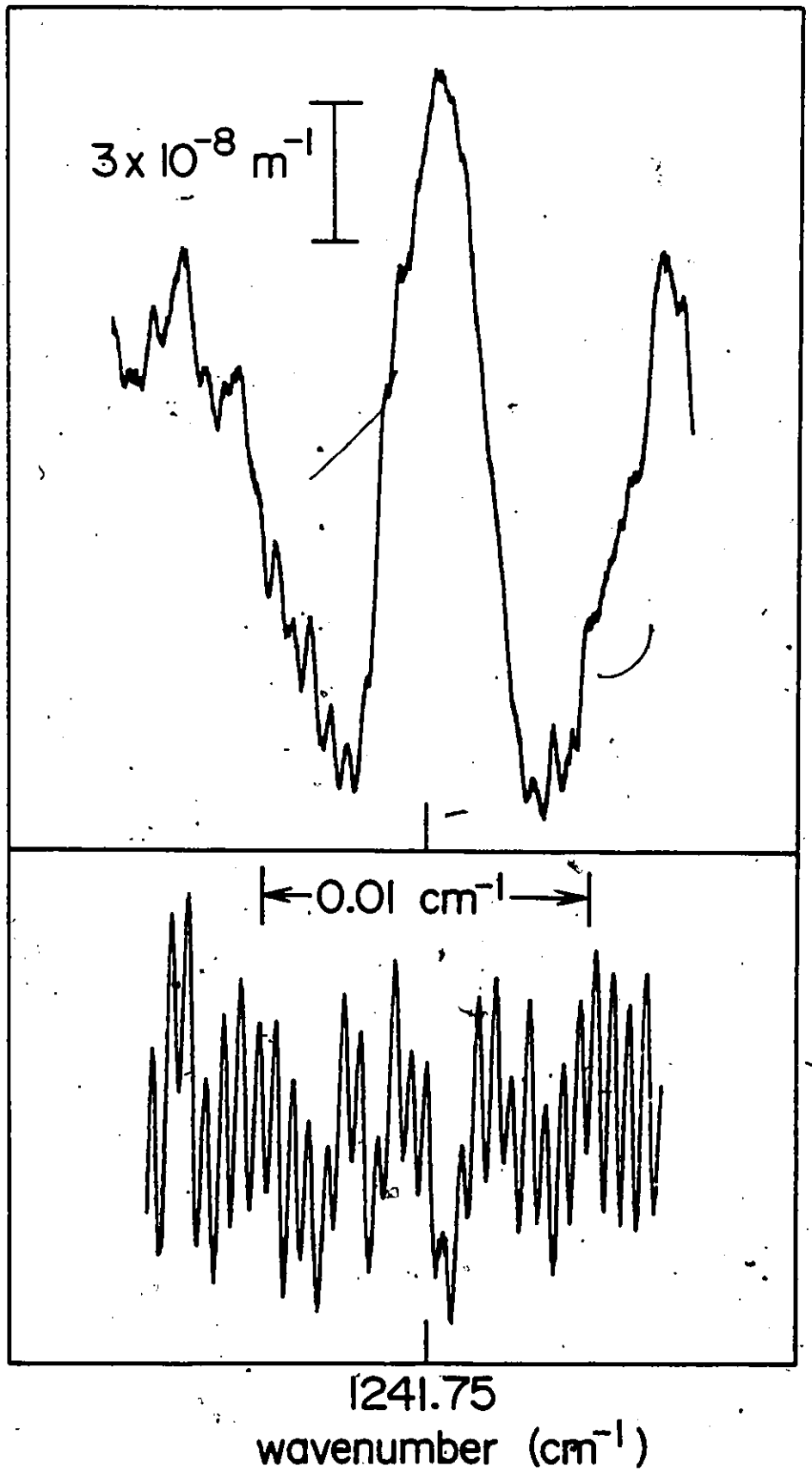
3 x 10^-8 m^-1
0.01 cm^-1
1241.75
wavenumber (cm^-1)

White cell to decrease feedback 100 times. This additional precaution allowed us to achieve the same sensitivity as Reid et al. [48] but in one-tenth the integration time. Fourth harmonic detection was used for the high-sensitivity, low-pressure work although we experimentally found that second harmonic detection was as sensitive. Studies of the noise sources of open-path monitors indicated that the background contributed significantly to the noise. We wished to [illegible]sure that the background contributed minimally to the limiting noise in the present series of experiments.

Our investigation of high-sensitivity, low-pressure detection of absorptions using harmonic techniques indicates that the effects of optical feedback are the factors which presently limit sensitivity. Methods to eliminate feedback, such as employing high quality optics to minimize the scattering of light and the use of polarizing optics to provide isolation, will undoubtedly allow higher sensitivities to be achieved.

5.6 Discussion and Conclusions

We have developed a new technique for obtaining very high sensitivity spectra with tunable diode lasers. The success of this work relies on the presubtraction of the first and second harmonic intensity modulations from the detector output before the spectrum is digitized. This presubtraction allows much more efficient use of a signal averager and h[illegible]bled us to detect absorptions as small as 10^{-3}% over path leng[illegible]00 m for low-pressure gases. At atmospheric pressure, we

can detect differential absorptions of 10^{-3}% over path lengths of a few metres. At present one limitation on sensitivity is caused by idiosyncrasies of the signal averager which prevent use of the full sensitivity in subtraction modes. The result is the quantization noise seen in the lower trace of Fig. 5.4. A dedicated data acquisition system may substantially improve sensitivity, and will definitely reduce the time required to obtain the spectra.

A second limitation on sensitivity is the detrimental effect of optical feedback on the performance of the tunable diode lasers. Efforts to avoid feedback by using good quality optics and polarizing optics should be rewarded with increased sensitivity. Our sweep integration technique retains the improved frequency stability described by Jennings [19] and Sun et al., [69] and gives the absorption data in a form which is easy to interpret. In many experiments involving high-sensitivity detection with tunable diode lasers sweep integration may be preferable to the second harmonic techniques described in previous work [15,48] and chapters.

5.7 Summary

We present in this chapter a new technique of recording high-sensitivity absorption data over a ~0.4 cm^{-1} spectral region. This technique will find application in studies of line shape, linewidth, and searches of relatively large spectral regions for weak lines. We also present an investigation of low-pressure, harmonic detection of trace gases. We find that an increase in sensitivity is possible by

decreasing optical feedback caused by the optics.

In Chapter 6 the influences of the properties of the laser radiation itself on the achievable sensitivity are considered. In particular we consider how the linewidth of the laser and fluctuations of the detected power (which we term beam noise) are correlated with the operating cycle of the closed-cycle cooler. In general, the beam noise is found to be an important factor which limits the sensitivity while the laser linewidth is found to have a negligible effect on the achievable sensitivity.

CHAPTER 6

FREQUENCY AND INTENSITY CHARACTERISTICS OF LEAD-SALT DIODE LASERS

Absorptions measured using tunable diode laser spectrometers are seldom limited by detector noise. We have always found the primary limit on sensitivity to be the properties of the lasers themselves. Hence in this chapter we describe a systematic investigation of both the frequency and intensity stability of these lasers, and explain how this stability affects the sensitivity of a laser absorption spectrometer. We find that the operation of the closed-cycle coolers required to maintain the necessary cryogenic environment for operation of the lasers significantly affects the frequency and intensity characteristics of the lasers.

Shimoda [75] considered the limits of sensitivity of laser spectrometers. He found the theoretical limit for infrared resonance absorption measurements to be 4×10^{-6}% absorption.[a] This value is computed by equating the minimum detectable change in power to the signal power which produces a response equal to the rms noise of the detector. Shimoda's analysis assumes that the laser and the associated

---

[a] The minimum detectable absorption was calculated for a 1 Hz electrical bandwidth, a detector area of 1 mm^2, and a D* of 2.3×10^{11} mm $\sqrt{Hz}$ W^{-1}. The D* value and detector element area were taken from the manufacturer's specifications for the detector used in the work reported in this thesis. An incident power of 100 μW was assumed.

optical components contribute negligible noise. The experimental minimum detectable absorption, measured with lead-salt tunable diode lasers, of ~5 x 10^{-4}% for a 100 s time constant [48] clearly indicates that the properties of the lasers, rather than detector noise, limits the attainable sensitivity. Thus to attain maximum sensitivity it is important to understand and minimize the noise contributions from the laser. To this end we investigated the stability of the laser source under the action of closed-cycle coolers. We developed a simple technique of measuring the linewidth of a tunable diode laser. The finite linewidth, in addition to being of interest for high-resolution measurements, is a potential noise source. In the presence of frequency-dependent transmissions, fluctuations of the optical frequency result in a noise signal at the detector. Linewidth measurements are presented in Sec. 6.1 and Sec. 6.2 of this chapter. Fluctuations in the detected power due to the influence of the cooler are discussed in Sec. 6.3.

6.1 Introduction

Lead salt, tunable diode lasers (TDLs) have been used extensively for conventional high-resolution spectroscopy. In many of these applications, the finite linewidth of the TDL can be neglected in comparison with the much broader linewidths of the spectral features under observation. However, in some recent experiments the finite TDL linewidth has posed a problem. This is particularly true in experiments involving absorption linewidth measurements [72,76], nonlinear effects

[77-79], and heterodyne techniques [80].

Early heterodyne experiments on TDLs mounted in liquid helium dewars reported linewidths as narrow as 54 kHz full-width half-maximum (FWHM) [81], but more recent results obtained using commercial TDLs mounted in closed-cycle refrigerators quote linewidths in the range of 10 to 40 MHz FWHM [77,78,80,82]. Some of this excess linewidth is undoubtedly caused by pressure and temperature fluctuations associated with the environment of the closed-cycle coolers, but experiments to improve the vibration isolation of the TDL do not always result in a significant narrowing of the linewidth [82,83]. The linewidths of the TDLs were studied by two techniques. The heterodyne measurements were performed by John Reid [24] at the Jet Propulsion Laboratory, California Institute of Technology, Pasedena, California. The heterodyne measurements are presented here because they provide a standard by which it is possible to judge the merits and shortcomings of the second linewidth measurement method.

Four diode lasers which operate in the 9 μm region were heterodyned against a 9.4 μm CO_2 laser. For these TDLs the effect of a new, commercially available vibration isolation system [34] was evaluated by comparing the linewidths with the closed-cycle cooler on and off. These TDLs had a minimum linewidth in the range 1 to 20 MHz, but this linewidth was often more than doubled by the action of the refrigeration system. In addition, the observed linewidth was found to depend strongly on operating temperature and injection current.

For many experiments using TDLs it is advantageous to operate with

as narrow a linewidth as possible, but it is not possible to a priori know the operating conditions which lead to minimum linewidth. Heterodyning the TDL with a CO_2 laser is a relatively complex procedure requiring specialised equipment. Also, the heterodyne technique of measuring linewidths cannot be applied in the spectral regions where CO_2 (or CO) lasers do not operate. Consequently we have devised a simple technique using a Fabry-Perot etalon which allows one to make a quantitative estimate of the TDL linewidth. This technique can be applied to any TDL and allows the modes which exhibit narrow linewidths to be quickly and easily identified.

The heterodyne measurements are discussed in Sec. 6.2A while the etalon technique is reported in Sec. 6.2B.

6.2 Experimental Apparatus and Results

A schematic diagram of the experimental arrangement used in the experiments is shown in Fig. 6.1. The CO_2 laser construction is based on the Freed design, and is expected to give a negligible contribution to the measured linewidths [84]. The photomixer is an SAT photovoltaic HgCdTe detector, and is coupled to an Avantek UTO 500 series rf amplifier and a Hewlett-Packard Model 8553B/8552B rf Spectrum Analyzer. Under favourable conditions, we were able to observe beat notes out to 800 MHz. Many successive sweeps of the spectrum analyzer could be summed and stored in a digital signal averager [70]. The optical arrangement enabled us to simultaneously observe the TDL beat note and the TDL mode behaviour.

Figure 6.1

Schematic diagram of the experimental apparatus used for the linewidth measurements.

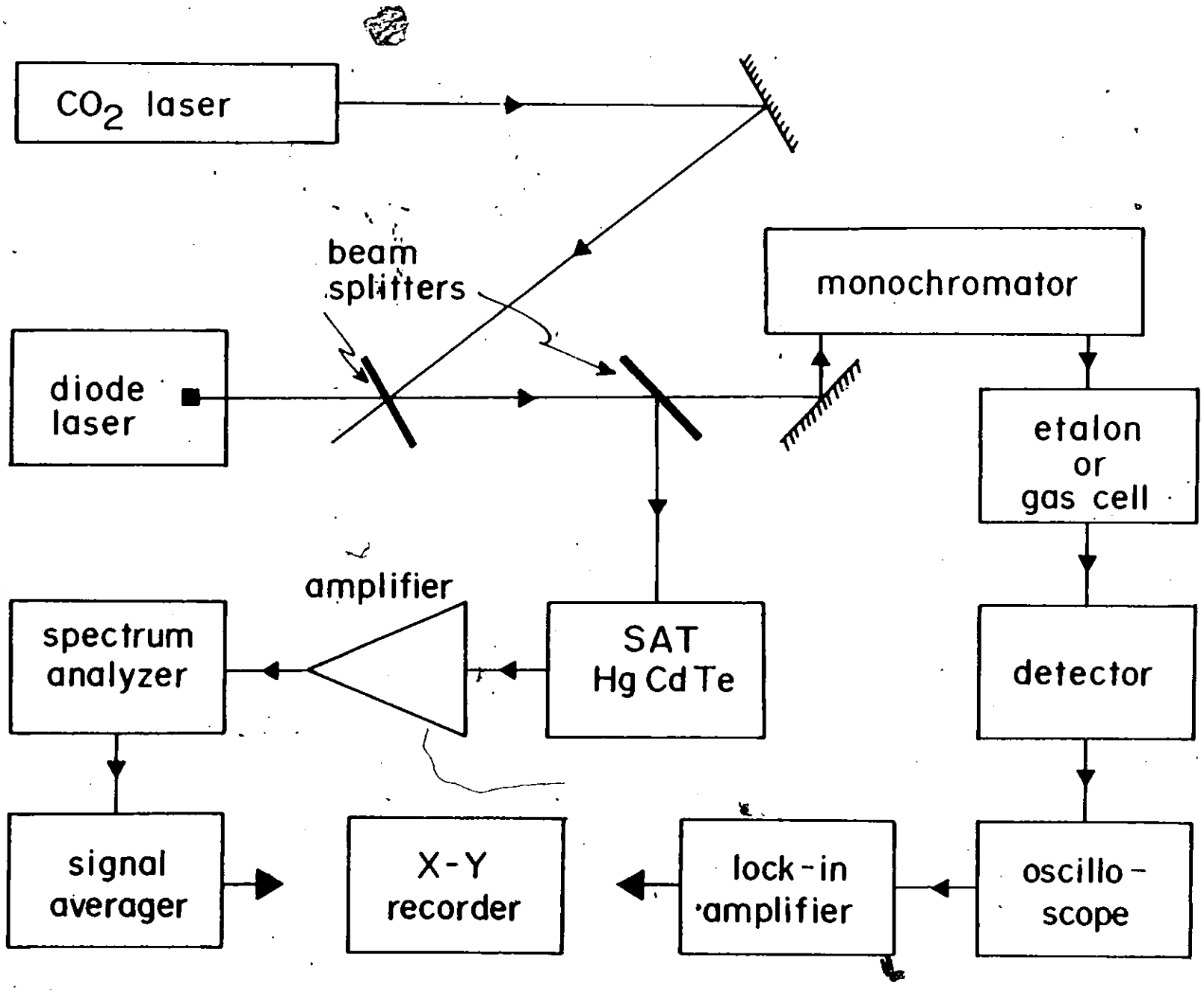
CO_2 laser
beam splitters
monochromator
diode laser
etalon or gas cell
amplifier
spectrum analyzer
SAT Hg Cd Te
detector
signal averager
X-Y recorder
lock-in amplifier
oscillo-scope

A. Heterodyne measurements

A total of five TDLs operating in the 9 μm region were obtained from Laser Analytics Inc. [34] and mounted in two successive batches in a cold head with a tripod isolation mount. Beat notes were observed with four of these TDLs; the fifth TDL gave very little optical output. Figure 6.2 shows a typical beat note as observed on the spectrum analyzer, and the average of 50 scans as recorded with the signal averager. For this particular diode and operating conditions the linewidth FWHM was ~25 MHz. The linewidths of all four diodes were examined as a function of temperature, injection current, and wavelength. In many cases, several beat notes could be observed as the injection current was varied at a fixed temperature. This corresponded to successive modes tuning past the fixed CO_2 laser line. Often the successive beat notes would show widely different linewidths. There did not appear to be any sure way of predicting linewidths from the mode pattern, but narrower linewidths tended to be observed when one mode was dominant and there was no evidence of mode competition. Operation of the TDL near threshold or in a single mode did not ensure a narrow linewidth.

The minimum observed linewidth was obtained with a TDL which gave a peak multimode output power of only 100 μW. With the cooler switched off a beat note of 0.6 MHz FWHM could be observed for several seconds until the slow drift of the junction temperature resulted in the TDL output tuning away from coincidence with the CO_2 laser line. However, with the cooler operating, the effect of vibrations were very evident --

Figure 6.2

Typical beat note between a TDL and the P(28) 9.4 μm CO_2 laser line. The oscilloscope photograph shows 10 scans superimposed with a total exposure time of 0.1 s. The spectrum analyzer was set for a linear display. The lower trace shows an average of 50 scans as summed by the signal averager.

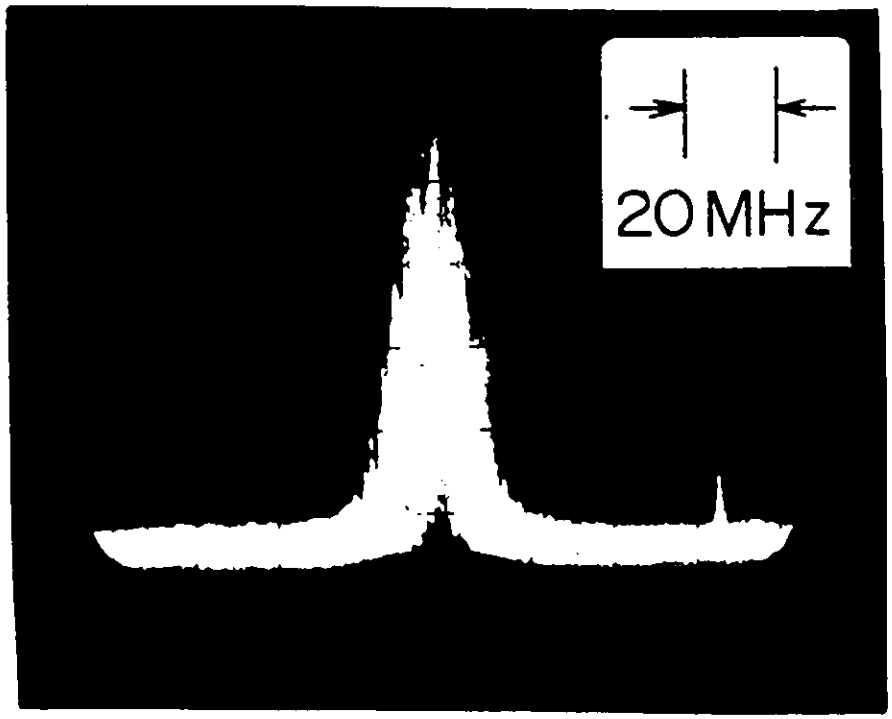
20 MHz

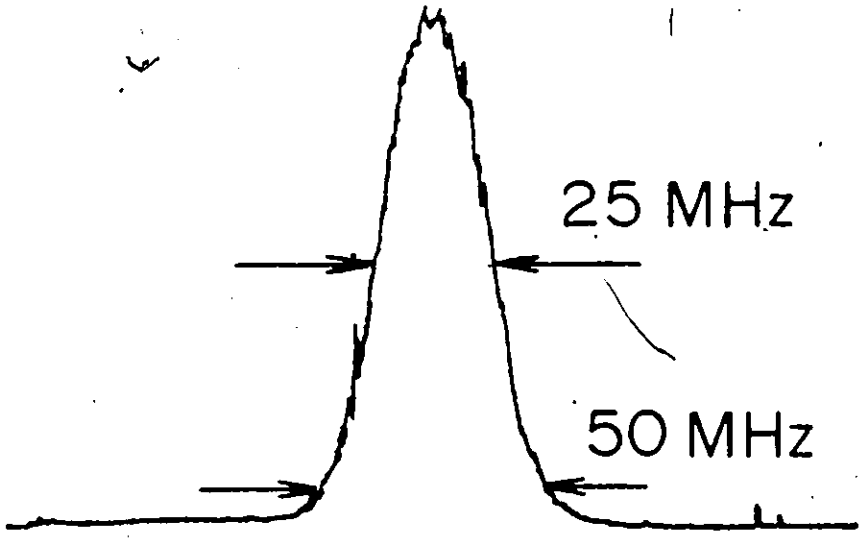
25 MHz
50 MHz

the TDL linewidth increased dramatically every time the piston cycled. Under these conditions, the average linewidth increased to 3.3 MHz FWHM. None of the remaining TDLs operated with linewidths < 10 MHz FWHM, even under optimum conditions. Two of the TDLs were quite powerful, with multimode output powers in the range 2-4 mW. The minimum linewidth observed with either TDL was similar to that shown in Fig. 6.2. The results shown in Fig. 6.2 were obtained with the cooler on and the TDL wavelength coincident with the P(28) 9.4 μm CO_2 laser line. No significant change in linewidth occurred after switching the cooler off. However, when the same TDL was tuned into coincidence with the P(18) 9.4 μm CO_2 laser line, the observed linewidth decreased from 60 MHz to 30 MHz FWHM upon switching the cooler off. In general, the vibrations associated with the operation of the cooler increase the laser linewidth despite the much improved amplitude stability of the TDLs in the new tripod mount.

A fourth TDL with low output power was tested to determine if the TDL linewidth was correlated with power. Typical linewidths were > 20 MHz, even in the absence of vibrations. Careful tests were carried out on the current supply to the TDLs to ensure that it was not responsible for the observed linewidths. The specified ripple on the current supply corresponds to a maximum of 2 MHz FWHM jitter,[a] and the fact that a 0.6

---

[a] This maximum optical frequency jitter was calculated by experimentally determining the maximum tuning rate of the diodes, and using this tuning rate to convert the manufacturer's specification for the current supply ripple into optical frequency jitter.

MHz linewidth was observed on occasion suggests that the stability of the current supply is very good. Tests were also carried out to ensure that feedback to the TDL was not affecting the linewidth [63]. Clearly, some mechanism inherent to the TDLs and independent of pressure, temperature and current fluctuations is producing the finite TDL linewidth. The magnitude of this inherent linewidth varies dramatically from TDL to TDL, and over the tuning range of the individual TDLs; modes which gave linewidths of several hundred MHz were not uncommon. This behaviour probably explains the wide range of TDL linewidths reported in the literature, from < 5 MHz [83] to ~100 MHz [76].

B. Etalon Measurements

Clearly, it would be very useful if one could diagnose the narrow linewidth regions and estimate the TDL linewidth without having to resort to the complexity of the heterodyne technique. We find that a measurement of the linewidth can be obtained by placing an etalon in the laser beam and observing the behaviour of the transmitted beam as the TDL tunes through the etalon fringes. Figure 6.3 illustrates the technique. A 7.62 cm uncoated Ge etalon was placed in the laser beam and carefully aligned to give maximum contrast fringes. Similar results can be obtained by placing the etalon before or after the monochromator, but if the etalon is placed before the monochromator, care must be taken to ensure that there is no feedback to the TDL. The trace on the left side of Fig. 6.3 shows the etalon fringes as recorded with conventional direct detection, i.e., a lock-in amplifier referenced to the chopper

Figure 6.3

Behaviour of the TDL signal with an etalon in the laser beam. The left-hand trace shows the etalon fringes observed as the TDL is tuned in wavelength. The photographs indicate the short-term amplitude stability at the detector when the TDL is tuned to positions A, B and C on the fringes. Exposure time is 0.5 s, and the chopper frequency is 126 Hz. The linewidth of the TDL is as shown in Fig. 6.2.

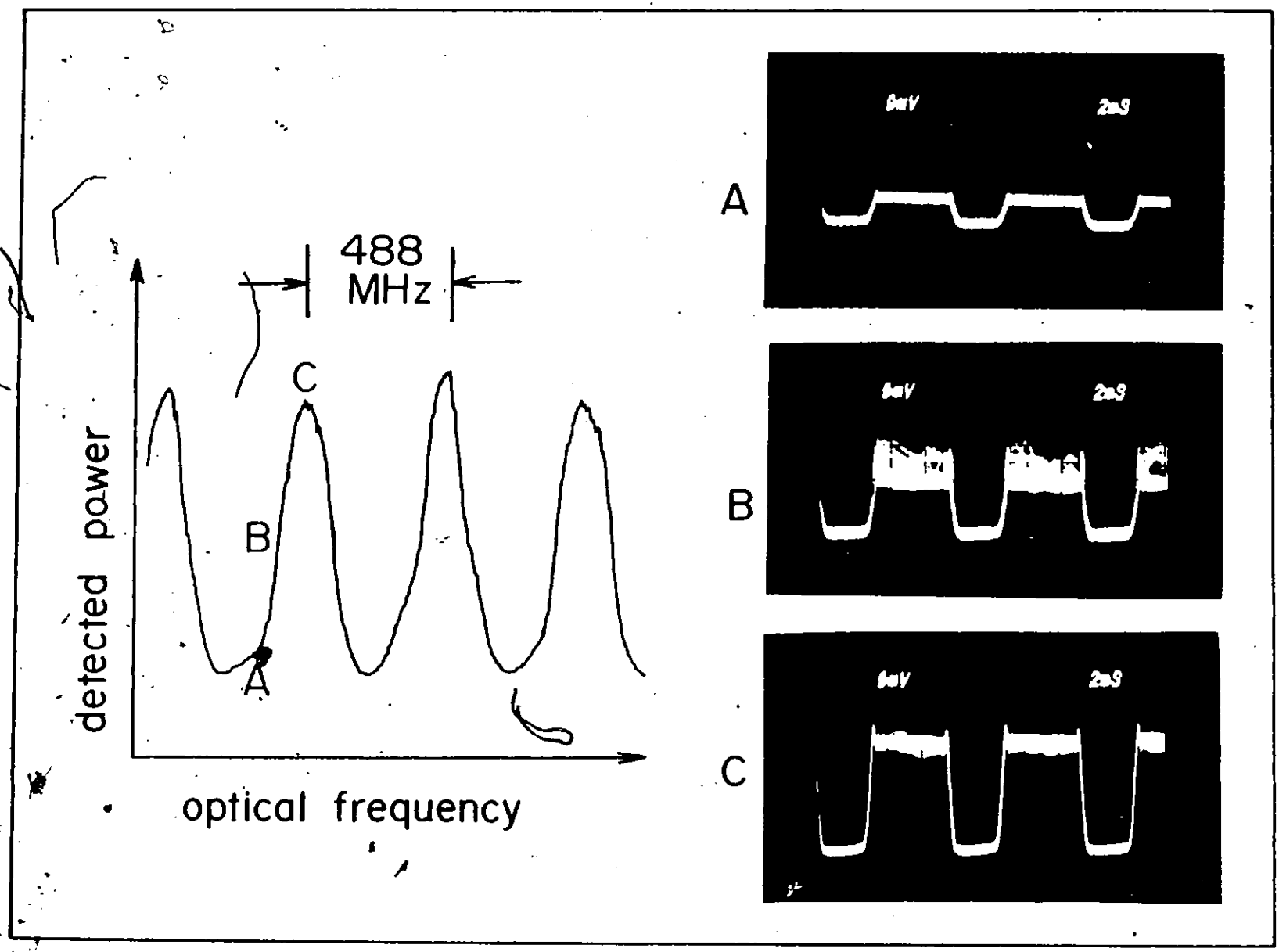
488
MHz
C
B
A
detected power
optical frequency
A
B
C

frequency. The observed ratio of maximum to minimum intensity is ~4.2:1, reasonably close to the value of 4.5:1 one would predict for a perfectly aligned etalon with a reflectivity of 36%, scanned by a laser of negligible linewidth. Note that on the steeply rising (and falling) portion of the fringes, a frequency change of only 10 MHz corresponds to an intensity change of ~6% of the peak intensity. One can use the steeply sloping portion of the fringe to convert TDL frequency fluctuations into more easily detected intensity fluctuations. This is indicated in the photographs on the right of Fig. 6.3. The output of the detector is shown as the TDL is tuned to the top, bottom and middle of a fringe. Note the increased amplitude noise at position B. This amplitude noise is equivalent to a total frequency excursion of approximately ± 25 MHz about the central position. As expected, this corresponds to the approximate peak-to-peak linewidth as measured by the heterodyne technique - see Fig. 6.2. Similar experiments were carried out for two other TDL modes of varying linewidth. We observed a good quantitative correspondence between the linewidth as measured by the heterodyne technique and the magnitude of the amplitude noise at position B on the fringes. Thus the etalon technique can be used to make a quick estimate of the TDL linewidth and does not require the TDL wavelength to be tuned into coincidence with a fixed laser line, or a narrow absorption line [83]. We estimate that the technique can be applied to TDLs with linewidths in the range < 1 to 100 MHz FWHM. Beyond 100 MHz, the etalon fringes begin to disappear, but this occurrence is sufficient to identify the mode as unsuitable for

high-resolution spectroscopy. To investigate the lower limit of the technique, and to obtain accurate quantitative results, we switched to an 8 μm TDL which previous measurements had suggested operated with a narrow linewidth in a single mode.

The 8 μm TDL was mounted in an older cold head with a two-point vibration isolation system. The TDL operated in a single mode with an output power of ~0.5 mW. This enabled us to eliminate the monochromator and thus achieve a very high signal-to-noise ratio. The etalon was placed in the laser beam and the TDL tuned to the position of maximum slope (i.e., position B of Fig. 6.3). Increased amplitude noise could be observed on the laser beam, but because of the narrow TDL linewidth the noise was limited to ± 10% of the peak power. Figure 6.4 shows photographs of this amplitude noise taken with the chopper removed. In the upper photograph the cooler is running. Note the large increase in noise, i.e., linewidth, every 0.15 s as the cold head piston cycles. There is also a substantial 120 Hz noise component present. The 120 Hz noise is caused by vibrations due to the compressor motor coupling to the cold head through the helium lines. The middle photograph shows an enlarged scan of the amplitude noise taken with the cooler off. The TDL now has a much narrower linewidth in the absence of mechanical and temperature fluctuations. The peak-to-peak frequency excursions are only ~4 MHz. For the lower photograph the cooler was on and the etalon removed. Note the absence of any significant amplitude noise.

To place the measurement technique illustrated in Figs. 6.3 and 6.4 on a firm, quantitative basis we used an rms voltmeter to measure the

Figure 6.4

TDL amplitude noise observed on tuning to the steeply sloping portion of an etalon fringe. The upper photograph is taken with the cooler on, while the middle photograph is taken with a factor of 4 increase in sensitivity, and the cooler off. The known slope of the etalon fringe enables one to convert amplitude noise to frequency excursion, as indicated. The lower photograph was taken with the etalon removed, and illustrates the low level of residual system noise.

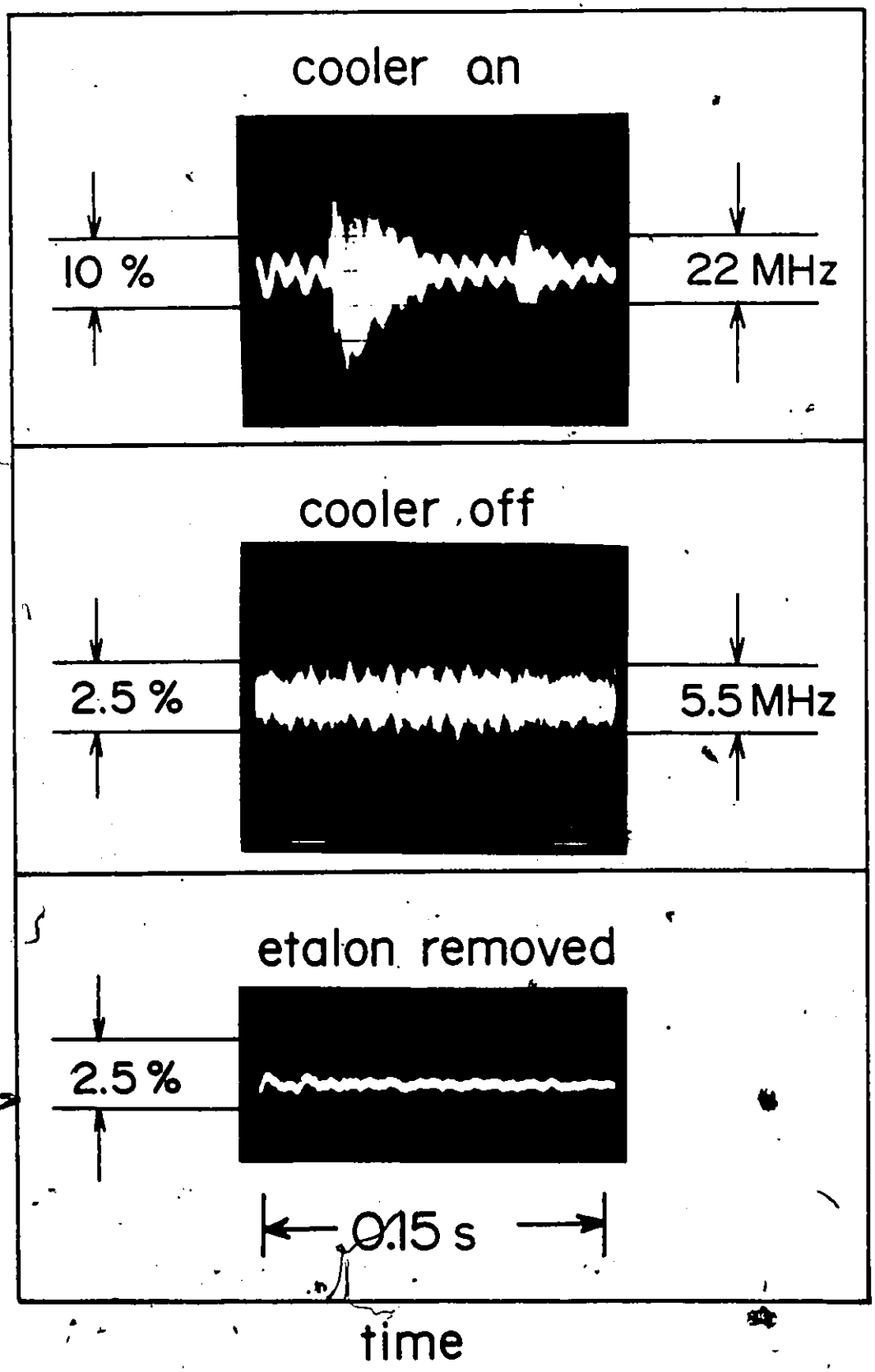
cooler on
10 %
22 MHz
cooler off
2.5 %
5.5 MHz
etalon removed
2.5 %
0.15 s
time

amplitude noise. The lock-in-amplifier (PAR Model 126) was switched to rms mode, and the signal channel filters set to maximum width (0.2 Hz to 210 kHz).[a] We then measured the rms noise as the TDL tuned through the etalon fringes. Figure 6.5 shows typical results. The upper trace is a conventional direct detection scan of the etalon fringes taken with a chopper in the beam. For the middle trace the chopper was removed and the lock-in amplifier switched to the rms mode. Maximum noise is observed at the positions of maximum slope of the etalon fringes. The lower trace shows the substantial narrowing of linewidth obtained by switching off the cooler. It now only remains to calibrate these traces to obtain a direct measure of the laser linewidth.

1. Calibration Techniques

If the TDL is tuned to position B on the fringes, and the TDL frequency ν makes small excursions about its mean value ν', then the power P falling on the detector can be written as

$$P = P' + A'(\nu - \nu') \tag{24}$$

where P' is the power level appropriate to ν', and A' is a measure of the fringe slope (assumed linear). As the detector is ac coupled, the rms voltmeter will only measure the fluctuations associated with the second term in Eq. (24), i.e., the rms signal is given by

---

[a] Narrowing the signal channel to 1 kHz - 100 kHz produces a negligible effect on the measured signal as the noise is approximately uniform in the region up to 50 kHz. The frequency spectrum of the amplitude noise can be observed in Fig. 6.8.

Figure 6.5

Illustration of etalon technique of linewidth measurement. In the upper trace the TDL is scanned over several etalon fringes using a chopper and conventional direct detection. For the lower traces the chopper is removed and the amplitude noise shown in Fig. 6.4 is measured with an rms voltmeter. (With the cooler switched off, the TDL tuning rate is slightly different from that in the upper two traces).

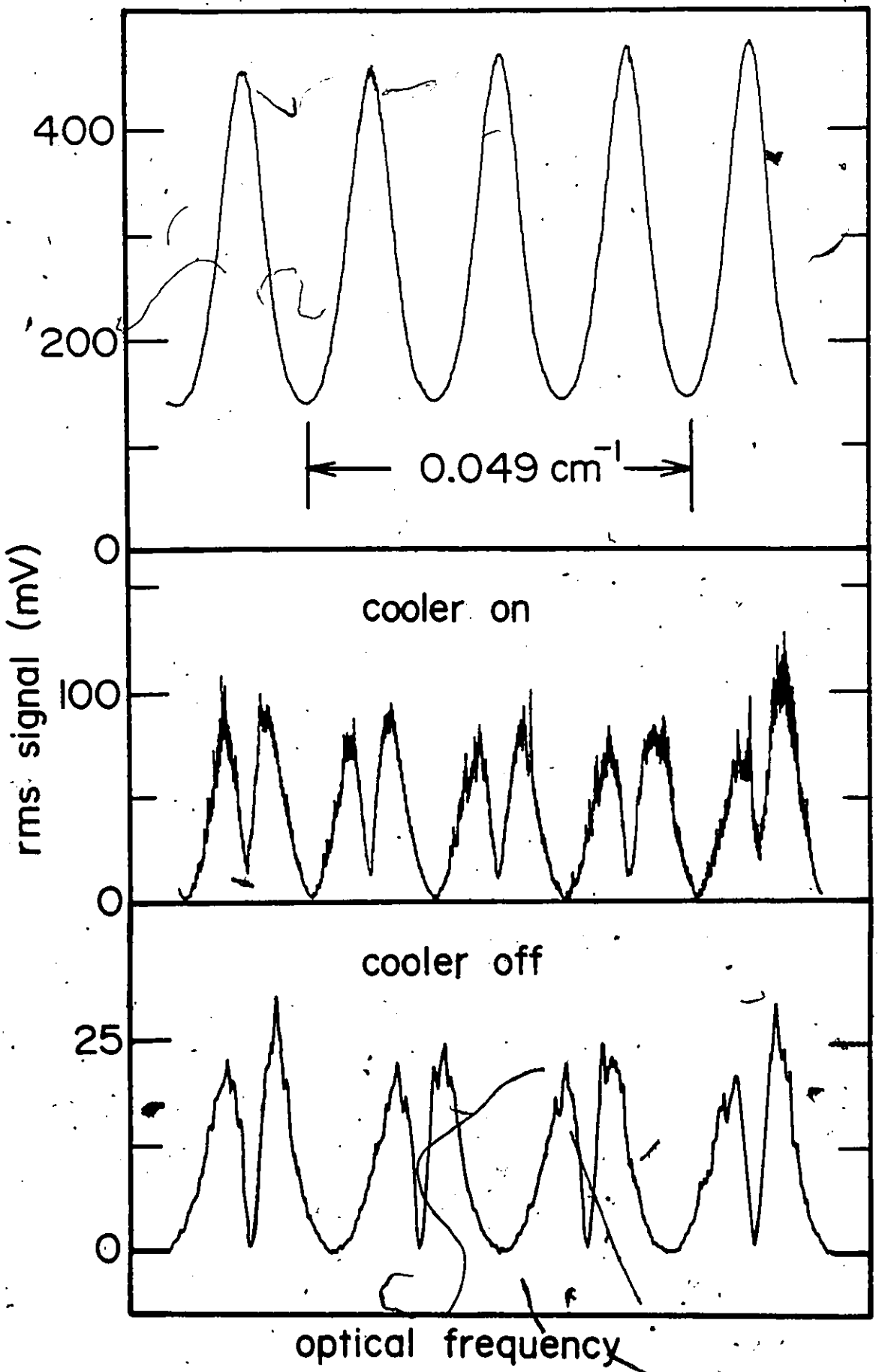
400
200
0
0.049 cm^{-1}
cooler on
100
0
cooler off
25
0
rms signal (mV)
optical frequency

$$\langle P^2\rangle^{1/2} = A'\langle (\nu - \nu_o)^2 \rangle^{1/2}$$
$$= A'\sigma \qquad (25)$$

where σ is the rms deviation of the TDL frequency. To eliminate the dependence of (25) on laser power, detector sensitivity etc., we normalise both sides to the peak power P_m measured at the top of a fringe,[a] i.e.,

$$\langle P^2\rangle^{1/2}/P_m = A\,\sigma \qquad (26)$$

Thus to measure σ, we need only determine A.

This constant has been measured by two independent techniques. One method is to measure the slope of the fringes shown in the upper trace of Fig. 6.5 and allow for the difference in response of the system with and without the chopper in place.[a] In this fashion A was determined to be 0.68%/rms MHz. For the second method we added a known frequency jitter to the TDL and recorded the rms signal as the laser tuned through the fringes. A 500 Hz sine wave was used to modulate the TDL current, and the amplitude of the corresponding optical frequency modulation was determined as described in Chapter 3. One can plot the normalised rms response as a function of σ to obtain A. A plot of this type is shown in Fig. 6.6. The values of σ were kept small to ensure measurements were made in the linear region of the fringe slope. The results of Fig. 6.6 confirm the linearity of the technique. The calibration constant was determined from the slope as 0.64%/rms MHz, in good agreement with

---

[a] The chopper used in these experiments had a duty cycle of 0.5. Hence a correction factor of 2 must be used in normalising the rms noise signals.

Figure 6.6

Plot of normalised rms amplitude noise as a function of the rms magnitude of the applied sinusoidal wavelength modulation. The insert shows a typical scan over the fringes taken with an optical frequency modulation of 8.6 rms MHz.

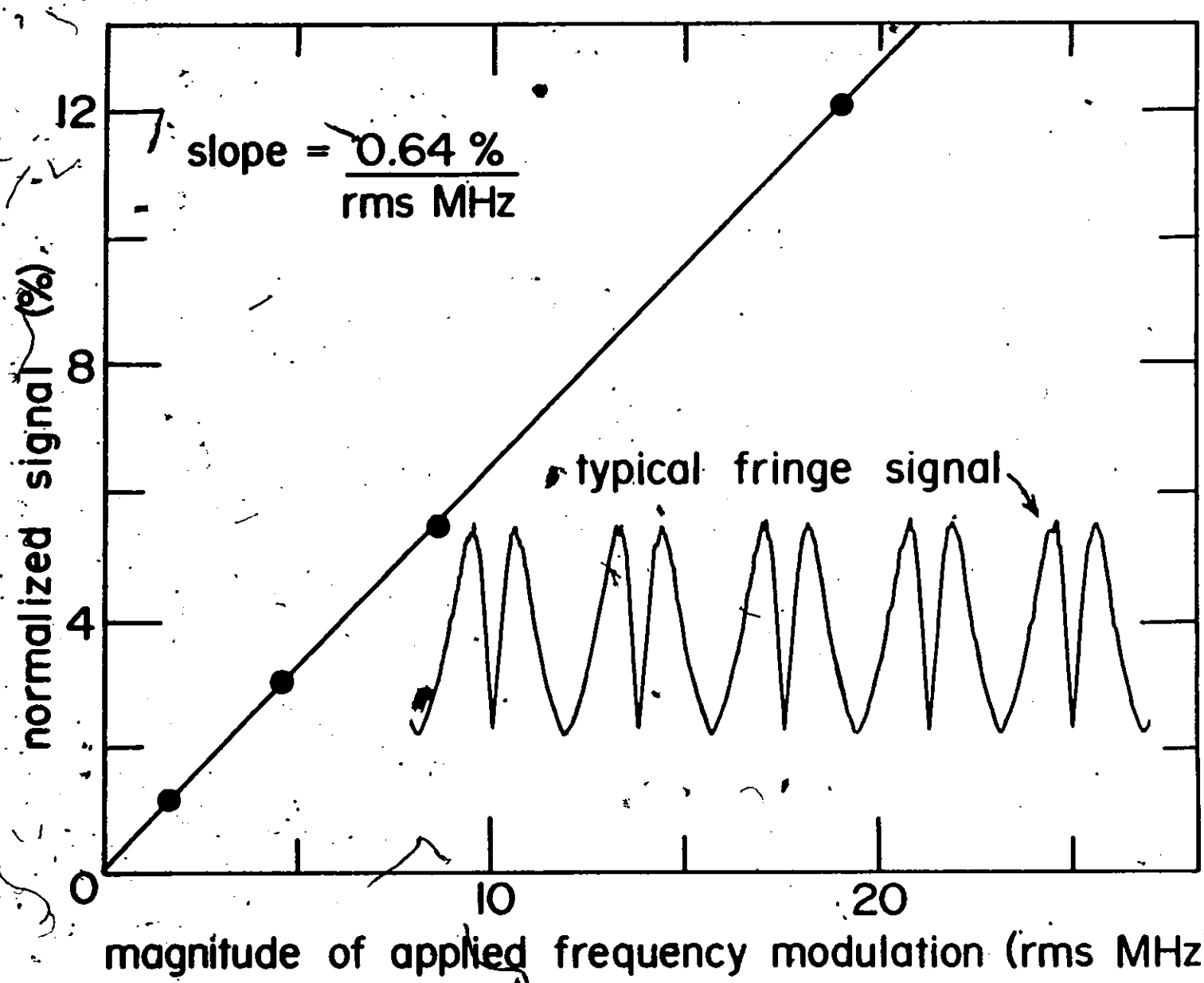
slope = 0.64 % / rms MHz
typical fringe signal
normalized signal (%)
0
4
8
12
10
20
magnitude of applied frequency modulation (rms MHz)

the earlier measurement. The data of Fig. 6.5 can now be converted into rms linewidths. With the cooler on, the rms TDL linewidth is 2.9 rms MHz, while with the cooler off σ = 0.83 rms MHz. To convert these values into a FWHM one requires the line shape function. This is particularly ill-defined with the compressor on, as the linewidth is clearly time-dependent. However, if one assumes a Gaussian line shape, the equivalent linewidths are 6.8 MHz and 1.9 MHz FWHM, respectively. (In many experimental situations, the rms frequency deviation σ may be more relevant than the FWHM linewidth). A second TDL operating at 1140 cm^{-1} was also examined using this technique. The measured linewidths were σ = 1.3 rms MHz (compressor off) and σ = 4.4 rms MHz (cooler on). The technique appears to be very general, and can be used for linewidths substantially narrower than 1 MHz, provided a satisfactory signal-to-noise ratio exists.

C. Linewidth Measurements using Narrow Absorption Lines

The etalon technique of linewidth measurement uses the steep transmission slope to convert frequency fluctuations into amplitude fluctuations. While the use of an etalon is very convenient, an alternative is to use a narrow absorption line. The replacement of the etalon by a low-pressure gas cell has some advantages; there is no longer any feedback from the front surface of the etalon and problems associated with alignment dependent finesse are avoided. For Doppler broadened lines the constant A can be calculated directly from the known Gaussian line shape. Figure 6.7 shows typical results obtained by

Figure 6.7

Linewidth measurements using a narrow absorption line. The upper trace shows a conventional direct detection scan taken with a low pressure N_2O cell in the laser beam. The two lower scans measure rms noise with the cooler on and off.

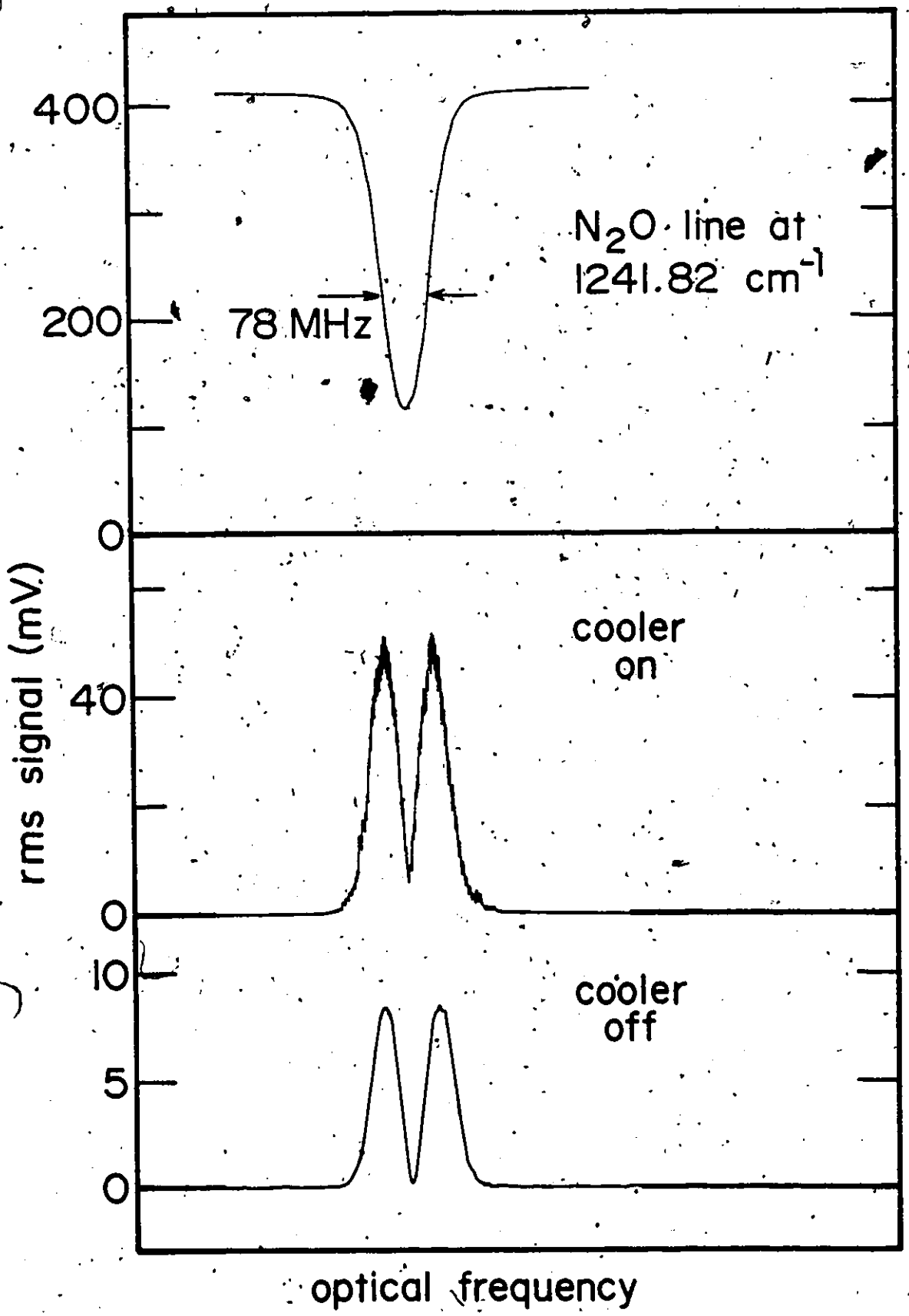
400
200
0
78 MHz
N_2O line at
1241.82 cm^{-1}
rms signal (mV)
40
0
cooler
on
10
5
0
cooler
off
optical frequency

scanning over an N_2O absorption line. Once again, the maximum rms signal is observed at the position of maximum slope on the absorption line and the improvement on switching off the cooler is clearly demonstrated. By using Doppler broadened lines, one can easily measure linewidths of < 1 MHz FWHM, while TDLs with linewidths > 100 MHz could also be investigated using suitable higher pressure gas cells. For most applications the technique illustrated in Fig. 6.7 is much more accurate than relying on deconvolution of a measured linewidth to determine the TDL instrument function [85]. For example, a TDL with a 5 MHz Gaussian linewidth FWHM tuning across a 50 MHz FWHM Doppler line will give a measured linewidth of 50.25 MHz, i.e., only a 0.5% increase due to the finite TDL linewidth.

The etalon method for determining the laser linewidth requires a transmission slope to convert frequency fluctuations into more easily measured intensity fluctuations. Thus whenever a frequency dependent transmission exists, random frequency fluctuations associated with the finite linewidth of the laser increase the noise level in the signal channel. The increased noise level is easily observed by tuning the laser to the side of an absorption line. An oscilloscope which is connected to the detector will display a trace reminiscent of white noise when the laser is tuned to the side of an absorption. The frequency content of the noise may be determined by processing the detector output with a spectrum analyzer. Figure 6.8 shows the increase in noise and the spectral characteristics of the detected signal for the laser tuned on and off the side of a low-pressure absorption line (N_2O,

Figure 6.8

Line width noise as a function of frequency. The upper trace is the linewidth noise for the laser tuned to a steeply sloping transmission. The resonance at 27 kHz is probably due to vibrations of the electrical contacts on the diode [18,71]. The lower trace is the noise for the laser tuned off the transmission slope. Except for the small region < 1 kHz, the lower trace is identical to one recorded with the laser off. The data was recorded with a Hewlett Packard model 3580A spectrum analyzer, a 100 Hz bandwidth, and the same laser as used for the measurements presented in Figs. 6.4 - 6.7.

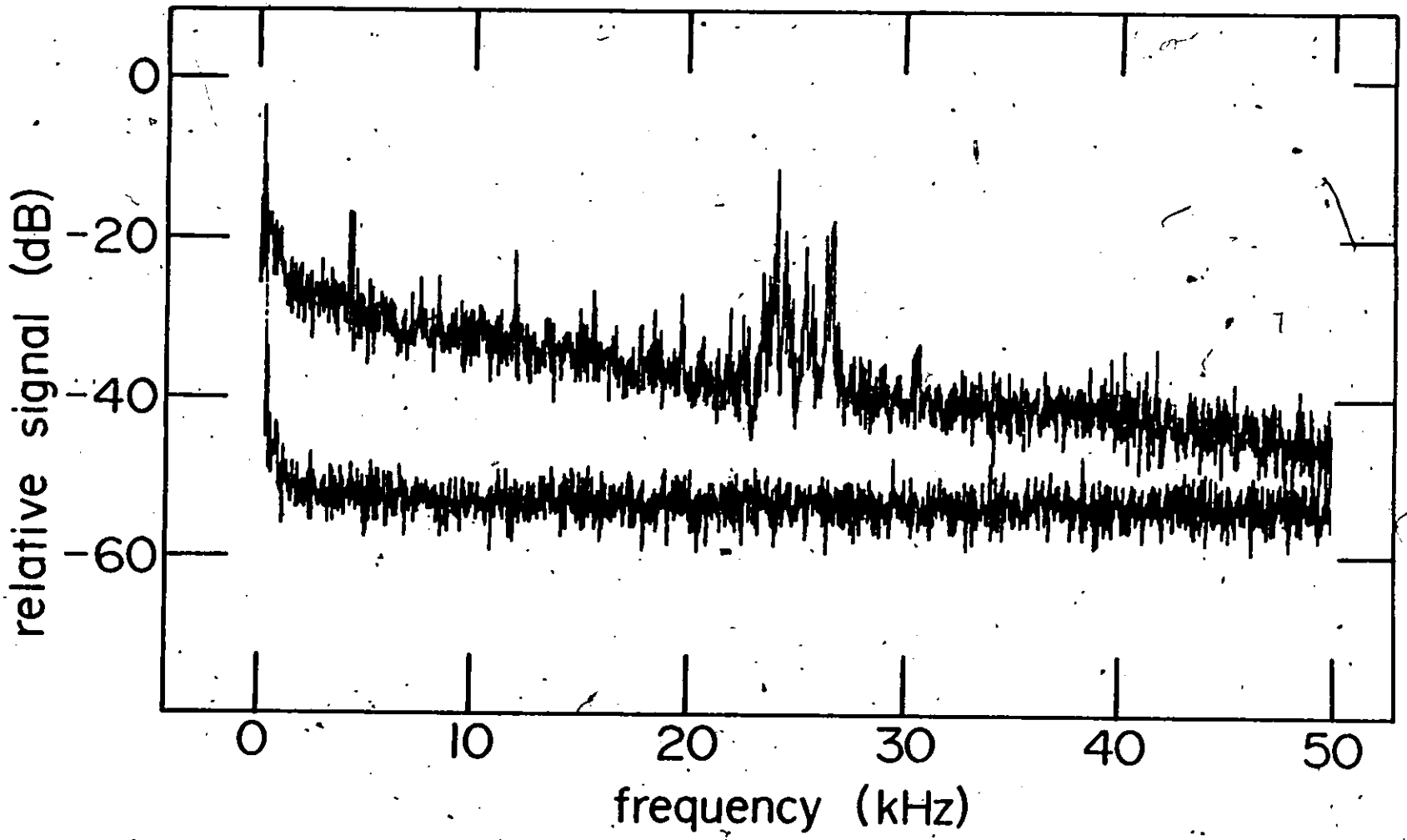

13/10

at ~1 Torr). The upper trace of Fig. 6.8 is the linewidth noise for the laser tuned to the side of the steeply sloping transmission. The lower trace of Fig. 6.8 is the recorded noise for the laser tuned away from any transmission slope. Since there is no transmission slope to convert wavelength fluctuations into intensity noise for the lower trace, this trace simply indicates the beam noise as a function of frequency. The difference of the two traces is the noise caused by the convolution of the finite linewidth of the laser and the transmission slope. Figure 6.8 clearly demonstrates that frequency-dependent transmissions generate a substantial quantity of noise. Thus for maximum sensitivity it is necessary to avoid optical fringes. However, provided the optical fringes have been minimized the frequency noise of the laser should not limit the sensitivity. A much more serious limitation on the sensitivity is the presence of beam noise.

We define beam noise to be random fluctuations in the detected power due to instabilities in the laser output power and aperturing of the propagating beam.

Beam noise is considered in Sec. 6.3.

6.3 Beam Noise

The operation of the closed-cycle cooler not only significantly affects the linewidth of the laser but ~~also~~ causes considerable beam noise. In this section we consider beam noise and, in particular, look at the effect of the operation of the closed-cycle cooler on the beam noise. Eng *et al*. [18,71] studied the low-frequency noise

characteristics of lead-salt diode lasers. Our results confirm their conclusion that vibrations associated with the cooler contribute significantly to the low-frequency beam noise. We find that in addition to the 3.3 Hz noise reported by Eng et al. [18,71] there is a strong component at 120 Hz. The influences which produce beam noise at specific frequencies also produce linewidth noise at the same frequencies. This fact may be confirmed by comparing Fig. 6.4 with Figs. 6.9-6.11.

Figure 6.9 is a typical plot of beam noise as a function of frequency. To acquire the data for Fig. 6.9 the laser beam was collimated, allowed to propagate over a 1 m path on the optical table, and then focussed on the detector. The detector output was connected directly to a spectrum analyzer (Hewlett Packard model 3580A). The laser was mounted in the cold head using the conventional two-point vibration isolation system developed by Laser Analytics Inc. [34]. The dominant beam noise source is 120 Hz vibrations associated with the operation of the compressor of the refrigeration system. This point is further demonstrated in Fig. 6.10 where the noise is plotted on a linear scale. The effect of the 120 Hz noise is to produce an almost perfect sinusoidal ripple of ~1% of the total laser power. The action of the cold head piston produces a signal at 3.3 Hz, and electrical pick-up and vibrations account for the peak in the noise spectrum at 60 Hz. The broad background extending from 0 to 500 Hz is due to mechanical vibrations of the support structure of the laser and fluctuations of the radiation diode current component [71]. Since the noise is impressed on

Figure 6.9

Beam noise as a function of frequency. The upper trace is for frequencies in the range 0 to 500 Hz. The lower trace is 450 to 950 Hz. The measurement bandwidth was 1 Hz.

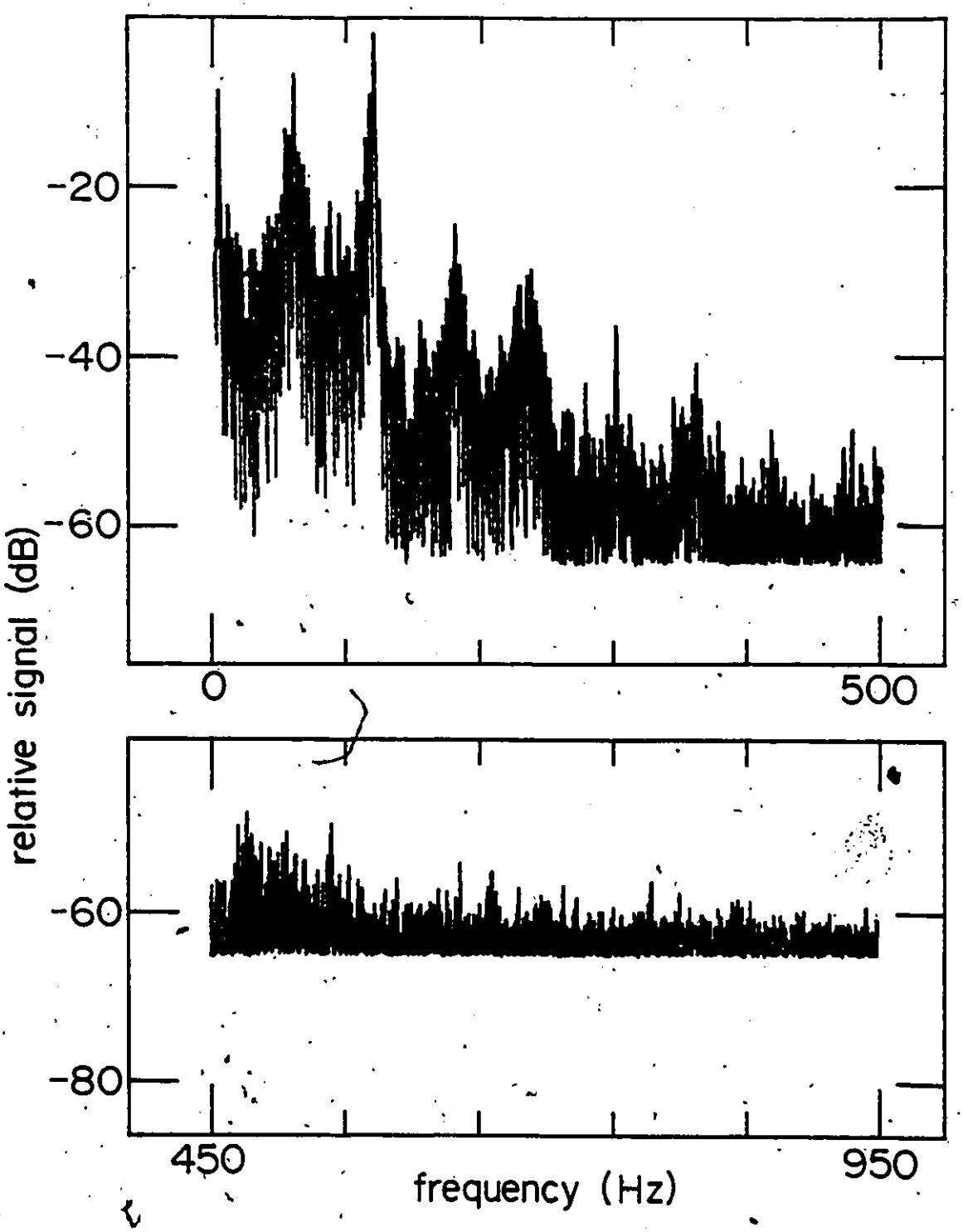
-20
-40
-60
0
500
relative signal (dB)
-60
-80
450
950
frequency (Hz)

Figure 6.10

Beam noise for the cooler on and off. All three traces are plotted on a linear scale. The cooler was on for the upper trace, and off for the recording of the middle trace. A bandwidth of 1 Hz was used for the upper trace and a 3 Hz bandwidth for the middle trace. The sine wave is the 120 Hz ripple on the detected power due to the action of the cooler. The peak-to-peak signal is ~1% of the total power. The sidebands are caused by the action of the cold head piston.

135b

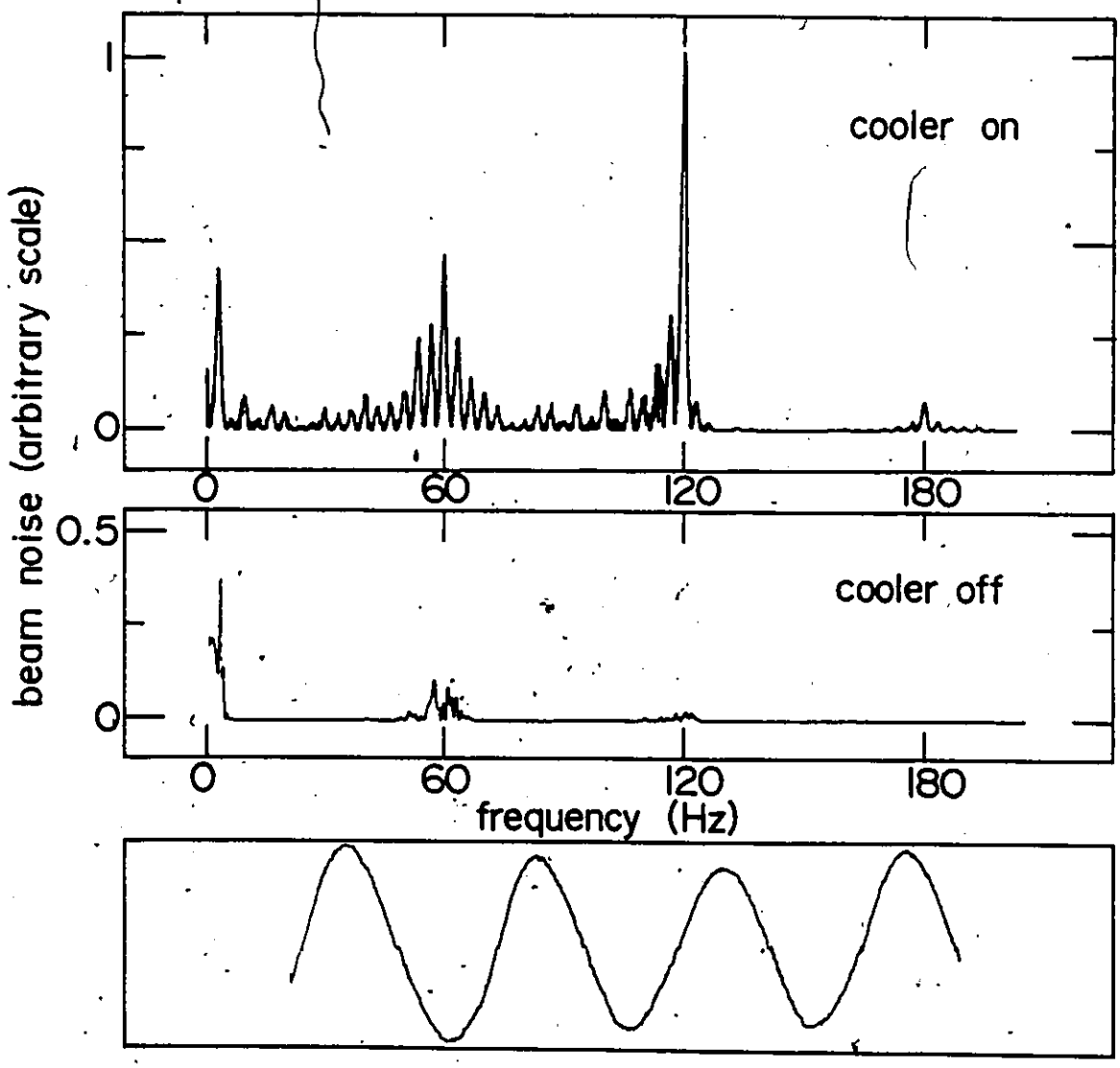
beam noise (arbitrary scale)
1
0
cooler on
0
60
120
180
0.5
0
cooler off
0
60
120
180
frequency (Hz)

the beam, the noise is multiplicative. This fact is demonstrated in Fig. 6.11. A sinusoidal modulation at 1 kHz was applied to the injection current of the laser, and the spectrum of the detected signal in the range 780-1280 Hz recorded. Sidelobes at integral multiples of 3.3 Hz, 60 Hz and 120 Hz are easily distinguished. Switching off the cold head piston eliminates the 3.3 Hz component and reduces the 60 Hz and 120 Hz signals by $\lesssim$ 20 dB. Switching off the compressor (with the cold head off) reduces the 120 Hz component by a further ≈ 20 dB while leaving the 60 Hz noise unaffected.

The magnitude of the beam noise determines the minimum time constant required to make a measurement at a specified sensitivity. Apertures placed in the beam and complicated optical arrangements can greatly increase the beam noise. A fraction of the beam noise is due to the motion of the laser beam, thus any apertures in the path result in a time-dependent transmission. For harmonic detection, the effect of beam noise can be reduced by detecting at frequencies $\gtrsim$ 1 kHz and at harmonics where the background is neglible (compare Fig. 6.9 and Fig. 4.4). Sweep integration is more sensitive to the beam noise. In sweep integration one would like to subtract two independent measurements of the power to within ~0.01%. To achieve this result the dominant noise at 3.3, 60 and 120 Hz must be reduced to $\lesssim$ 0.005% by time averaging. Elimination of the vibrations associated with the operation of the cooler would result in enhanced sensitivities and resolution. For very high-sensitivity work it may be advantageous to place the diode in a dewar containing liquid He. The difficulty of dealing with liquid He

Figure 6.11

The multiplicative nature of the beam noise is shown in this figure. The dominant components at 3.3, 60, and 120 Hz are easily identified. The large component at 1033 Hz is due to a modulation applied to the laser diode. The intensity modulation for this signal corresponds to ~2% of the total laser power.

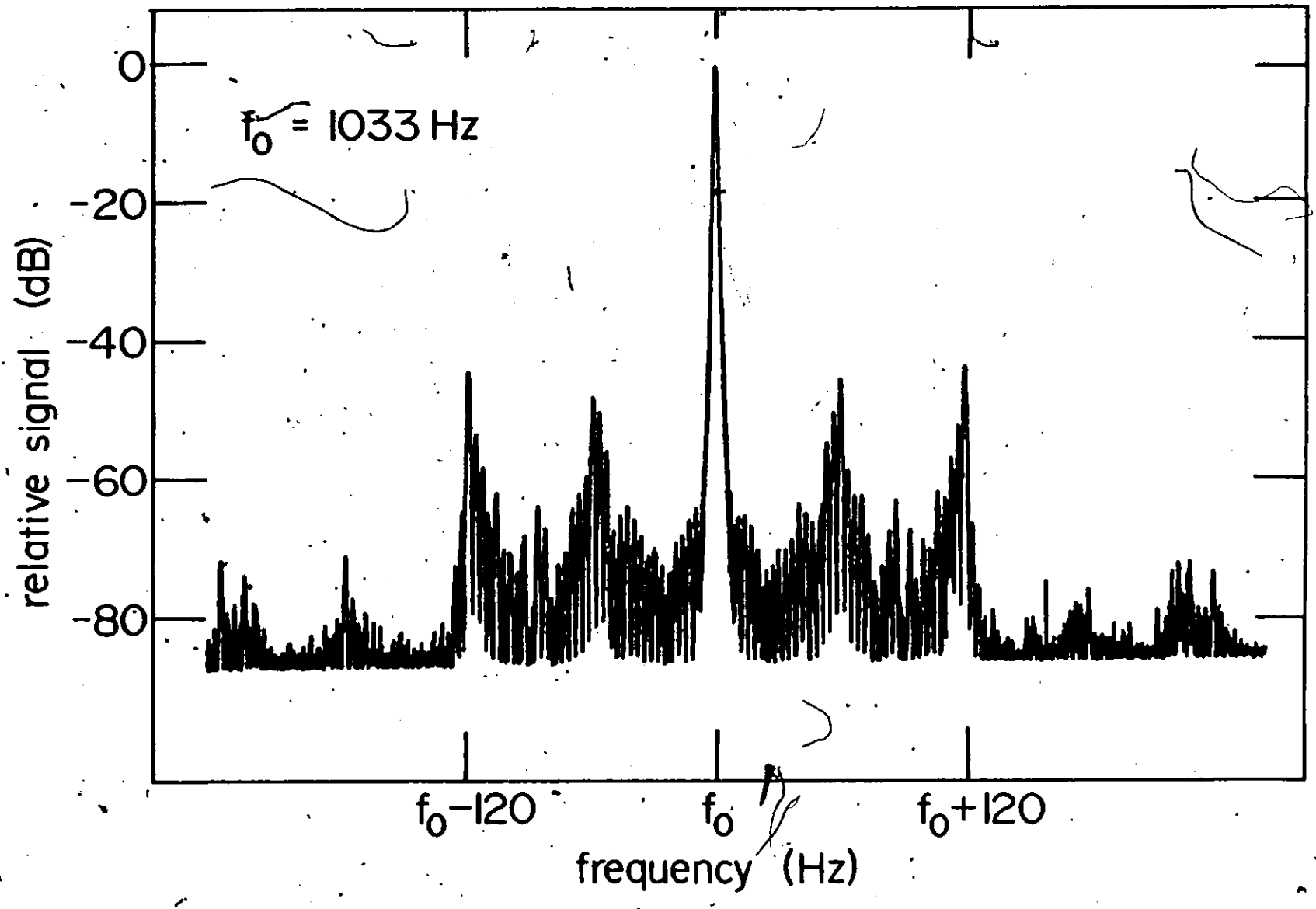
f_0 = 1033 Hz
0
-20
-40
-60
-80
relative signal (dB)
f_0−120
f_0
f_0+120
frequency (Hz)

may be more than compensated for by reduced beam noise and laser linewidth.

6.4 Discussion and Summary

Linewidth measurements made on several Pb-salt tunable diode lasers illustrate the difficulty in predicting the linewidth behaviour of these devices. The measured linewidth varies dramatically from laser to laser, and for any particular laser the linewidth depends strongly upon junction temperature and injection current. In general, linewidths are considerably broadened by the shock waves produced by the operation of closed-cycle coolers. Even in the absence of these vibrations, the minimum linewidth observed was ~1 MHz FWHM. We have made no attempt to determine the source of this residual linewidth [86,87], but did observe that the linewidth generally appeared independent of laser power.

The simple technique of measuring the linewidth of the laser presented in this chapter allows rapid and easy identification of the lasing modes which possess a minimum linewidth. Measurements performed with narrow linewidth modes will exhibit higher resolution, and possibly better sensitivity than measurements made with wider linewidth modes.

It is demonstrated in this chapter that vibrations due to the operation of closed-cycle coolers significantly affect the linewidth and output power of lead-salt diode lasers. The achievable sensitivity of a tunable diode laser spectrometer is intimately related to the noise carried on the beam. Efforts to improve the stability of the laser and associated optical components will lead to sensitivity limits which are

closer to the theoretical limit discussed by Shimoda [75].

The next chapter summarizes the achievements realized in the work reported in this thesis.

CHAPTER 7

CONCLUSION

Methods for high-sensitivity, resonance absorption detection of trace gases using tunable diode lasers are described in Chapters 3-6. These techniques were applied to the detection of gases over a wide range of pressures; from atmospheric to low pressures of a few Torr. The careful investigation and identification of the mechanisms which limit the sensitivity of a tunable diode laser absorption spectrometer that we performed and report in this thesis have provided us with the insight to implement detection schemes which permit significant advances to be made in the achievable sensitivity. The purpose of this chapter is to summarize the contributions of this work to the field of high-sensitivity detection of trace gases and to suggest possible system improvements. The material will be discussed, to a large extent, in the same order as it is presented in the main body of the thesis. Chapter 1 lists the reasons for undertaking a study of the sensitivity which can be attained using a tunable diode laser absorption spectrometer. Chapter 2 provides the background material necessary for the understanding of the chapters to follow. The summary commences with the material of Chapter 3.

Reid et al. [15] reported that the best technique for reducing the effect of optical interference fringes, and hence increase the sensitivity, was to use a second or jitter modulation. They

(erroneously) suggested that the fringes were minimized when the jitter modulation amplitude was equal to exactly one-half a fringe or integral multiples thereof. They also stated that typically the second harmonic absorption signal was decreased by $\lesssim$ 10% upon addition of the jitter. We developed a mathematical analysis of the harmonic response to optical interference fringes and of the two-tone harmonic response to fringes and Lorentzian absorptions. This analysis is developed and compared to experimental measurements in Chapter 3. Excellent agreement is found between the theory and experiment. A simple analytic expression for the two-tone harmonic line shape is derived in Chapter 3. This expression allows one to evaluate easily the effects of the jitter modulation on the shape and width of the detected signal. For a specific choice of the jitter frequency and phase we find that it is possible to enhance the harmonic signal by as much as 50% while simultaneously minimizing the optical fringes. The calculations and expressions presented in Chapter 3 provide a detailed understanding of two-tone harmonic detection. This understanding should assist in improving the detectivity of weak absorptions.

Atmospheric-pressure monitoring of trace gases using harmonic techniques is discussed in Chapter 4. We achieved a sensitivity limit equivalent to detecting an absorption of 0.01% over path lengths up to 250 m long. This represents an order of magnitude increase in sensitivity over results previously published. Ku et al. [16] reported a noise level equivalent to an absorption of 0.7% over a path length of 600 m in the first demonstration of open-path atmospheric-pressure

monitoring using tunable diode lasers. Ku et al. [16] reported their work in 1975, and there have been no major improvements in sensitivity of open-path monitors in recent years. Chaney et al. [17] in 1979 added frequency stabilization and mode selecting optics, but did not improve the sensitivity. Eng et al. [18] studied the low-frequency noise of tunable diode lasers and characterized atmospheric turbulence over laboratory paths. They estimated their sensitivity to be 0.1% over path lengths of ~100 m. Eng et al. [18] modified the optic set-up by employing a 30 cm diameter retroreflector and attributed the decreased noise to aperture averaging. Aperture averaging reduces the beam noise due to atmospheric turbulence [88]. We did not find beam noise to be a dominant noise source. We identified the nonreproducibility of the background and optical feedback as the dominant sources of noise. Oversize collection optics as employed by Eng et al. [18] would reduce the amount of aperturing which takes place, thus stabilizing the background and potentially accounting for the observed reduction in noise.

We increased the sensitivity of open-path monitors by minimizing the effects of the background and optical feedback. The background can be reduced to a negligible level by detecting at the higher harmonics. Feedback was reduced for the optical arrangement used (compare Fig. 4.1) by inserting apertures and attenuators in the beam path. This method of reducing feedback has the unfortunate consequence of drastically reducing the detected power level, thus increasing the detector noise relative to the signal and requiring longer integration times for a

given sensitivity. A noncoaxial transmit-receive optical arrangement should increase the sensitivity of open-path monitors by eliminating feedback.

The detection of band structure absorptions by harmonic techniques and the reduction of interferences are also considered in Chapter 4. The data presented indicate that there should be no loss in sensitivity for the detection of band structure absorption provided that a significant change in absorption takes place over a ~0.1 cm^{-1} region. It is shown that interferences from neighbouring lines may be reduced by decreasing the depth of modulation m. The detection of molecules which possess overlapping absorptions and the potential influence of interferences are areas which must be considered in any practical open-path monitoring system.

Measurements of low pressure absorptions by harmonic techniques are reported in Sec. 5.5. We achieved a sensitivity of ~3 x 10^{-8} m^{-1}, the same as the best previously reported [15], but in one-tenth the integration time. Optical feedback from the White cell is identified as a factor which limits the sensitivity of low-pressure detection. The role of feedback, and the amount of feedback from White cells, had not been appreciated in previous work. Methods to eliminate feedback, such as employing very-good quality optics to minimize the scattering of light and the use of polarizing optics to provide isolation, are potential improvements which should lead to increased sensitivities.

The development of an alternative technique for high-sensitivity detection of trace gases is described in Chapter 5. Data accumulation

by sweep integration using presubtraction permits absorptions as small as 10^{-3}% to be detected over path lengths up to 200 m long for low-pressure gases. The sensitivity of 5×10^{-8} m^{-1} achieved is significantly better than that reported by Jennings [19]. Using the sweep integration technique, the recorded absorptions appear the same as the actual absorption profile. There is no complicated mathematical transform linking the measured absorption shape and the actual profile as there is in harmonic spectroscopy. Data accumulation by the sweep integration technique will be of use in studies of line shape, line position, linewidth, and in rapid searches of ~0.4 cm^{-1} spectral regions for weak absorption features.

The technique of sweep integration is not as robust as harmonic detection; a stable optical alignment is required for sweep integration. We believe that the sensitivity of sweep integration may be improved by interfacing the detection electronics to a computer system. With a computer system the residual background could be removed by a mathematical manipulation of the recorded data. This would eliminate the need for a separate measurement of the residual background, thus relaxing the requirements on the optical stability and reduce the time spent recording the data. The reduction of the residual background by an appropriate computer code would not work for atmospheric pressure measurements. For atmospheric-pressure lines it is difficult to distinguish between the gently sloping background and the lines themselves. Techniques to reduce feedback, as discussed earlier, should also result in improved sensitivities for both low- and high-pressure

work.

A study of the effects of the operation of the closed-cycle coolers on the laser linewidth and the beam noise is presented in Chapter 6. A new method for measuring the linewidth of any tunable laser is reported. The new technique, which requires only a Fabry-Perot etalon and rms voltmeter, avoids the complexity and limited wavelength range of heterodyne measurements. We find that the operation of the closed-cycle cooler significantly affects the laser linewidth and beam noise. Our conclusions regarding the beam noise and operation of the cooler are in agreement with those of Eng et al. [18,71]. For high-sensitivity, high-resolution measurements it may be advantageous to place the diode laser in a liquid helium dewar.

This thesis describes the development of methods for the high-sensitivity detection of trace gases using resonance absorption and lead-salt diode lasers. Tunable diode laser absorption spectrometers have already been used in a wide variety of applications which require high-sensitivity and high-resolution. The techniques described in this thesis will undoubtedly lead to further experiments of a similar nature but with significantly increased sensitivities.

APPENDIX A

DERIVATION OF THE TWO-TONE HARMONIC ABSORPTION LINE SHAPE

We wish to derive an expression for the two-tone harmonic line shape obtained by modulating over a Lorentzian absorption profile. The procedure is a generalisation of Arndt's calculation [45].

The detector signal S(x) due to modulating over a Lorentzian line shape L(x,0,1) is

$$S(x) = L(x + m_1\cos\omega_1 t + m_2\cos\omega_2 t, 0, 1) \quad . \tag{A-1}$$

The harmonic components may be evaluated as follows:

Let s(y) and g(y) be the Fourier transforms of S(x) and L(x,0,1) respectively.

Then,

$$s(y) = g(y)\exp(im_1 y\cos\omega_1 t)\exp(im_2 y\cos\omega_2 t) \tag{A-2}$$

and using the Jacobi-Anger relations [51]

$$s(y) = g(y) \sum_{p,q=0}^{\infty} \varepsilon_p \varepsilon_q \, i^{p+q} \cos(p\omega_1 t)\cos(q\omega_2 t)$$

$$\times J_p(m_1 y) J_q(m_2 y) \quad . \tag{A-3}$$

The integral representations for the Bessel functions [51]

$$J_n(z) = \frac{i^{-n}}{2\pi} \int_0^{2\pi} \exp[i(z\cos\theta + n\theta)]d\theta \tag{A-4}$$

permit S(x) to be calculated. The desired result is found by inverse Fourier transforming, performing the angular integration which defines

$J_q(m_2y)$, and then integrating for $J_p(m_1y)$. The steps are performed below.

$$S(x) = \sum_{p,q=0}^{\infty} S_{pq}(x) \cos(p\omega_1 t) \cos(q\omega_2 t) \tag{22}$$

where

$$S_{pq}(x) = \varepsilon_p\varepsilon_q \int_0^{2\pi} \frac{d\theta_1}{2\pi} \int_0^{2\pi} \frac{d\theta_2}{2\pi} \int_{-\infty}^{+\infty} \exp-|y| \exp[ixy]$$

$$x \exp[i(m_1 y\cos\theta_1 + p\theta_1)] \exp[i(m_2 y\cos\theta_2 + q\theta_2)] \frac{dy}{2}$$

$$= \varepsilon_p\varepsilon_q \int_0^{2\pi} \frac{d\theta_1}{2\pi} e^{ip\theta_1} \int_0^{2\pi} \frac{d\theta_2}{2\pi} \frac{e^{ip\theta_2}}{1+(x + m_1\cos\theta_2 + m_2\cos\theta_2)^2} \tag{A-5}$$

The integral over θ_2 can be performed analytically by using contour integration around the unit circle in the complex plane. After some algebraic manipulation,

$$S_{pq}(x) = \varepsilon_p \int_0^{2\pi} S_q(x+m_1\cos\theta) \cos p\theta \frac{d\theta}{2\pi} \tag{A-6}$$

where

$$S_q(x) = \varepsilon_q R_e \left[\frac{i^q\{[(1 - ix)^2 + m_2^2]^{1/2} - (1 - ix)\}^q}{m_2^q [(1 - ix)^2 + m_2^2]^{1/2}} \right] . \tag{14}$$

If $m_1 = 0$, then

$$\int_0^{2\pi} e^{ip\theta_1} S_q(x) \frac{d\theta_1}{2\pi} = S_q(x) \delta_{p0} \tag{A-7}$$

where δ is the kronecker delta

and

$$S(x) = \sum_{q=0}^{\infty} \varepsilon_q \, S_q(x) \cos(q\omega_2 t) \quad , \tag{A-8}$$

which is the harmonic line shape for single-frequency modulation derived by Arndt [45].

For small m_2 the denominator of Eq. (14) can be made a rational function by expressing the radical in a binomial series and ignoring terms of second order.

$$[(1 - ix)^2 + m_2^2]^{1/2} \simeq (1 - ix) \left[1 + \frac{m_2^2}{2(1 - ix)^2}\right] \tag{A-9}$$

The integral of Eq. (22) can be performed analytically when Eq. (A-9) is used. The result for q = 0 is

$$S_{p0}(x) = \frac{1}{2} \left[S_p\left(x + \frac{m_2}{\sqrt{2}}\right) + S_p\left(x - \frac{m_2}{\sqrt{2}}\right)\right] . \tag{23}$$

$S_{p0}(x)$ is the pth harmonic line shape in the presence of a jitter modulation. It is possible to detect a (p+q)th harmonic line shape by detecting at a frequency of $|p\omega_1 \pm q\omega_2|$. The harmonic line shape for q = 1 is given by

$$S_{p_1}(x) = \frac{1}{2} \left[S_p\left(x + \frac{m_2}{\sqrt{2}}\right) - S_p\left(x - \frac{m_2}{\sqrt{2}}\right)\right] \tag{A-10}$$

which, not surprisingly, is just the first forward difference of the appropriate single-frequency harmonic line shape.

APPENDIX B

SUM AND DIFFERENCE CONTRIBUTIONS TO THE TWO-TONE HARMONIC SIGNAL

Two-tone modulation increases the number of frequencies at which detection for a specific harmonic line shape may be carried out. As an example, consider fourth harmonic detection while modulating at two non-related frequencies ω_1 and ω_2. A fourth harmonic line shape signal may be observed at $4\omega_1$, $4\omega_2$, $|3\omega_1 \pm \omega_2|$, $|3\omega_2 \pm \omega_1|$, $|2\omega_1 \pm 2\omega_2|$, a fact which we have experimentally verified. The additional contributions account for the modification of the second harmonic absorption signal when the jitter modulation $\omega_2 = 3\omega_1$.

Table B.1 illustrates the contributions of the various sum and difference combinations to the second harmonic line centre signal. The entries in Table B.1 are normalised to the maximum value of the second harmonic (single-frequency modulation) line centre signal $S_2(0)$. Experimentally we observe an enhancement of 50%, which compares favourably with the calculated enhancement including all the significant terms, of 54.2% for $3\omega_1 = \omega_2$, $m_1 = 2m_2 = 2.2$ linewidths, and the cosinusoidal modulations in phase. The parity column of Table B.1 indicates the parity of $S_{pq}(x)$ under the transformation $m_i \to -m_i$; $i = 1$ or 2. If the fundamental and jitter modulation are 180° out of phase, then the negative parity entries are added to the sum column with the opposite sign. The enhancement is fairly insensitive to choices of m_1 and m_2; for $m_1 = 2.2$ linewidths, an enhancement of 50% is obtained for

Table B.1

Calculated contributions to the second harmonic line centre signal for $3\omega_1 = \omega_2$, $m_1 = 2m_2 = 2.2$ linewidths, and the cosinusoidal modulations in phase.

Combination	p,q	$S_{pq}(0)/S_2(0)$	Sum	Parity
$2\omega_1$	2,0	0.670	0.670	+
$\omega_2 - \omega_1$	1,1	0.501	1.197	-
$2\omega_2 - 4\omega_1$	4,2	0.147	1.344	+
$5\omega_1 - \omega_2$	5,1	0.117	1.461	-
$3\omega_2 - 7\omega_1$	3,7	0.039	1.500	-
$8\omega_2 - 2\omega_1$	8,2	0.023	1.523	+

m_2 in the range 0.75 to 1.25 linewidths. For m_1 and m_2 180° out of phase, the calculated decrease in line centre signal is 50% at m_2 = 0.75 linewidths and 90% at m_2 = 1.25, in excellent agreement with experimental results.

The second harmonic contribution from modulating over Fabry-Perot fringes with harmonically related signals is much more complicated than for incoherent (ie, not harmonically related) signals. For second harmonic detection at $2\omega_1$, $\omega_2 = 3\omega_1$ and the modulations in phase, the fringe response varies as

$$J_2(2\pi m_1')J_0(2\pi m_2')$$

$$+ 2\sum_{p=1}^{\infty} J_{2p}(2\pi m_2')[J_{6p-2}(2\pi m_1') + J_{6p+2}(2\pi m_1')]$$

$$+ 2\sum_{p=0}^{\infty} J_{2p+1}(2\pi m_2')[J_{6p+1}(2\pi m_1') + J_{6p+5}(2\pi m_1')] \quad \text{(B-1)}$$

The parity, $J_n(-x) = (-)^n J_n(x)$, of the Bessel functions is required to calculate the second harmonic fringe signal in the event m_1 and m_2 are 180° out of phase.

REFERENCES

1. J. F. Butler, A. R. Calawa, R. J. Phelan, Jr., T. C. Harman, A. J. Strauss, and R. H. Rediker, Appl. Phys. Lett. 5, 75 (1964).

2. E. D. Hinkley, Appl. Phys. Lett. 16, 351 (1970).

3. R. J. Saykally and R. C. Woods, Ann. Rev. Phys. Chem. 32, 403 (1981).

4. K. Kawaguchi, Y. Endo, and E. Hirota, J. Mol. Spectrosc. 93, 381 (1982).

5. R. N. Zare and R. B. Bernstein, Physics Today, November 1980, p. 43.

6. E. D. Hinkley, Ed., Laser Monitoring of the Atmosphere (Springer, Berlin, 1976).

7. H. Kildal and R. L. Byer, Proc. IEEE 59, 1644 (1971).

8. R. M. Measures and G. Pilon, Opto-electron. 4, 141 (1972).

9. W. M. Fairbank, Jr. and C. Y. She, Opt. News, Spring 1979, p. 4.

10. G. S. Hurst, M. G. Payne, S. D. Kramer, and C. H. Chen, Physics Today, September 1980, p. 24.

11. H. Inaba in Laser Monitoring of the Atmosphere, E. D. Hinkley, Ed. (Springer, Berlin, 1976), p. 154.

12. C. K. N. Patel and R. J. Kerl, Appl. Phys. Lett. 30, 578 (1977).

13. Y. Ueda and K. Shimoda in Laser Spectroscopy, J. Ehlers, K. Hepp, H.A. Weidenmuller, and J. Zittartz, Eds., (Springer, Berlin, 1975), pp. 186-197.

14. K. M. Evenson, R. J. Saykally, D. A. Jennings, R. F. Curl, Jr., and J. M. Brown, in Chemical and Biochemical Applications of Lasers, C. B. Moore, Ed. (Academic, New York, 1980).

15. J. Reid, M. El-Sherbiny, B. K. Garside and E. A. Ballik, Appl. Opt. 19, 3349 (1980).

16. R. T. Ku, E. D. Hinkley, and J. O. Sample, Appl. Opt. 14, 854 (1975).

17. L. W. Chaney, D. G. Rickel, G. M. Russwurm, and W. A. McClenny, Appl. Opt. 18, 3004 (1979).

18. R. S. Eng, A. W. Mantz and T. R. Todd, Appl. Opt. 18, 3438 (1979).

19. D. E. Jennings, Appl. Opt. 19, 2695 (1980).

20. D. T. Cassidy and J. Reid, Appl. Opt. 21, 1185 (1982).

21. D. T. Cassidy and J. Reid in Technical Digest, Cleo'82, Pheonix, Arizona, April 1982, p. 146.

22. D. T. Cassidy and J. Reid, Appl. Opt. 21, 2465 (1982).

23. D. T. Cassidy and J. Reid, submitted to Appl. Phys., June (1982).

24. J. Reid, D. T. Cassidy, and R. T. Menzies, submitted to Appl. Opt. July (1982).

25. D. Kasemset and C. G. Fonstad, Jr., IEEE J. Quant. Electron., QE-18, 1078 (1982).

26. E. D. Hinkley, K. W. Nill, and F. A. Blum in Laser Spectroscopy of Atoms and Molecules, H. Walther, Ed. (Springer, Berlin, 1976), p. 130.

27. H. Prier, Appl. Phys. 20, 189 (1979).

28. R. S. Eng, J. F. Butler, and K. L. Linden, Opt. Eng. 19, 945 (1980).

29. H. Flicker and N. Nereson, IEEE J. Quant. Electron. QE-12, 326 (1976).

30. A. R. Calawa, J. O. Dimmock, T. C. Harman, and I. Melngailis, Phys. Rev. Lett. 23, 7 (1969).

31. J. M. Besson, J. F. Butler, A. R. Calawa, W. Paul, and R. H. Rediker, Appl. Phys. Lett. 7, 206 (1965).

32. I. I. Zasavitskii, A. I. Likhter, E. G. Pehl', and A. P. Shotov, Sov. Phys. Semicond. 6, 1859 (1973).

33. I. I. Zasavitskii, B. N. Matsonashvili, V. I. Pogodin, and A. P. Shotov, Sov. Phys. Semicond. 8, 467 (1974).

34. Spectra Physics, Laser Analytics Division, 25 Wiggins Ave., Bedford, Massachesetts, 01730, USA.

35. H.-H. Hsieh and C. G. Fonstad, IEEE J. Quant. Electron. QE-16, 1039 (1980).

36. E. Kapon, A. Hardy, and A. Katzir, IEEE J. Quant. Electron. QE-17, 391 (1981).

37. R. Grisar, W. J. Riedel, and H. M. Prier, IEEE J. Quant. Electron. QE-17, 586 (1981).

38. W. S. Benedict, R. Herman, G. E. Moore, and S. Silverman, Can. J. Phys., 34, 830 (1956).

39. D. W. Posener, Austral. J. Phys. 12, 184 (1959).

40. J. U. White, J. Opt. Soc. Am. 32, 285 (1942).

41. T. H. Edwards, J. Opt. Soc. Am. 51, 98 (1961).

42. J. Shewchun, B. K. Garside, E. A. Ballik, C. C. Y. Kwan, M. M. El-Sherbiny, G. Hogenkamp, and A. Kazandjian, Appl. Opt. 15, 340 (1976).

43. J. Reid, J. Shewchun, B. K. Garside and E. A. Ballik, Appl. Opt. 17, 300 (1978).

44. R. J. Hanisch, G. P. Hughes, and J. R. Merrill, Rev. Sci. Instrum. 46, 1262 (1975).

45. R. Arndt, J. Appl. Phys. 36, 2522 (1965).

46. H. Walquist, J. Chem. Phys. 35, 1708 (1961).

47. J. Reid and D. Labrie, Appl. Phys. B26, 203 (1981).

48. J. Reid, B. K. Garside, J. Shewchun, M. El-Sherbiny, and E. A. Ballik, Appl. Opt. 17, 1806 (1978).

49. M. D. Miller, A. Pires, D. Chen, S. K. Poultney: Poster paper presented at the conference on High-Resolution Infrared Applications and Developments, National Bureau of Standards, Gaithersburg, Maryland, June 23-25 (1980).

50. R. S. Longhurst, Geometrical and Physical Optics, 3rd ed. (John Wiley and Sons Inc., New York, 1973), p. 180.

51. G. Arfken, Mathematical Methods for Physicists, 2nd ed. (Academic Press, New York, 1970), Chapter 11.

52. W. A. McClenny and G. M. Russwurm, Atmos. Environ. 12, 1443 (1978).

53. E. D. Hinkley, R. T. Ku, K. W. Nill, and J. F. Butler, Appl. Opt. 15, 1653 (1976).

54. E. D. Hinkley, Opt. Quant. Electron. 8, 155 (1976).

55. E. Max and S. T. Eng, Opt. Quant. Electron. 11, 97 (1979).

56. N. Menyuk, D. K. Killinger, and W. E. DeFeo, Appl. Opt. 19, 3282 (1980).

57. J. Altmann, W. Lahmann, and C. Weitkamp, Appl. Opt. 19, 3453 (1980).

58. J. Altmann and P. Pokrowsky, Appl. Opt. 19, 3449 (1980).

59. J. W. Strohbehn, Ed., Laser Beam Propagation in the Atmosphere (Springer, Berlin, 1978).

60. H. C. Casey, Jr. and M. B. Panish, Heterostructure Lasers (Academic, New York, 1978).

61. T. L. Paoli and J. F. Svacek, Rev. Sci. Instrum. 47, 1016 (1976).

62. M. Menyuk and D. K. Killinger, Opt. Lett. 6, 301 (1981).

63. C. N. Harward and J. M. Hoell, Appl. Opt. 18, 3978 (1979).

64. L. S. Rothman, Appl. Opt. 20, 791 (1981).

65. P. D. Goldan, W. C. Kuster, D. L. Albritton, and A. L. Schmeltekopf, J. Geophys. Res. 85, 413 (1980).

66. L. S. Rothman, A. Goldman, J. R. Gillis, R. H. Tipping, L. R. Brown, J. S. Margolis, A. G. Maki, and L. D. G. Young, Appl. Opt. 20, 1323 (1980).

67. M. L. Olson, D. L. Grieble, and P. R. Griffiths, Appl. Spectrosc. 34, 50 (1980).

68. J. J. Hillman, D. E. Jennings, and J. L. Faris, Appl. Opt. 18, 1808 (1979).

69. J. N-P. Sun, M. L. Olson, D. L. Grieble, and P. R. Griffiths, Appl. Opt. 19, 2762 (1980).

70. Princeton Applied Research Model 4202 Digital Signal Averager.

71. R. S. Eng, A. W. Mantz, and T. R. Todd, Appl. Opt. 18, 1088 (1979).

72. J. Reid and A. R. W. McKellar, Phys. Rev. A18, 224 (1978).

73. J. Reid, R. L. Sinclair, A. M. Robinson, and A. R. W. McKellar, Phys. Rev. A24, 1944 (1981).

74. L. S. Rothman and W. S. Benedict, Appl. Opt. 17, 2605 (1978).

75. K. Shimoda, Appl. Phys. 1, 77 (1973).

76. S. Lundqvist, J. Margolis, and J. Reid, Appl. Opt. 21, 3501 (1982).

77. D. E. Jennings, Appl. Phys. Lett. 33, 493 (1978).

78. M. Takami, Appl. Phys. lett. 34, 682 (1979).

79. W. H. Weber and R. W. Terhune, Opt. Lett. 6, 455 (1981).

80. T. L. Worchesky, K. L. Ritter, J. P. Sattler, and W. A. Riessler, Opt. Lett. 2, 70 (1978); see also Opt. Lett., 5, 21 (1980).

81. E. D. Hinkley and C. Freed, Phys. Rev. Lett. 23, 277 (1979).

82. G. N. Steinberg, Rev. Sci. Instrum. 50, 1622 (1979).

83. D. E. Jennings and J. J. Hillman, Rev. Sci. Instrum. 48, 1568 (1977).

84. C. Freed, IEEE J. Quant. Electron. QE-4, 404 (1968).

85. B. Fridovich, V. Maalthy Devi, and P, P. Das, J. Mol. Spec. 81, 269 (1980).

86. D. Welford and A. Moordain, Appl. Phys. Lett. 40, 865 (1982).

87. C. H. Henry, IEEE J. Quant. Electron., QE-18, 259 (1982).

88. D. L. Fried, J. Opt. Soc. Am. 57, 169 (1967).